**Epithelial Oncogenic KRAS Drives Immunosuppression in Pancreatic Cancer**

by

Ashley Velez

A dissertation submitted in partial fulfillment
of the requirements for the degree of
Doctor of Philosophy
(Cell and Developmental Biology)
in the University of Michigan
2022

Doctoral Committee:

Associate Professor Qing Li, Chair
Adjunct Professor Howard Crawford
Associate Professor Timothy Frankel
Professor James Moon
Professor Marina Pasca di Magliano

Ashley Velez

veleza@umich.edu

ORCID iD:  0000-0002-1506-9305

## Dedication

To my mom Ida, a cancer survivor. You worked hard to give us the best life you could while we were growing up. You are my motivation for continuing achieving great things in life. To my grandma Chiry, who is another cancer survivor and honestly a survivor of so many other things. Eres una guerrera! And to the people I have unfortunately lost, my grandpa Pio (rest in peace) and my aunt Rosin, who lost her fight with cancer.

**Acknowledgements**

I would not be here today if it was not for the help of my lab members, my friends, and my amazing family. I have met so many great people that have been pivotal for my success through my Ph.D. training. First, I want to thank my mentor, Dr. Marina Pasca di Magliano, for providing me with the opportunity to work in her laboratory and for being a supportive mentor. Marina, thank you for being very supportive in each step of my process, I came with no knowledge in most of the things that we do in lab, and you were patient with me, believed in me and supported everything I wanted to do for my career and for the DEI efforts. I really value that you believe in work/life balance, you let us be independent, but you are there when we start to freak out because experiments are not working. You are definitely an inspiring woman that taught me that women need to be in more positions of power and leadership.

I would also like to thank my committee members Dr. Qing Li, Dr. Howard Crawford, Dr. Timothy Frankel, and Dr. James Moon for their time and all the advice given over the course of the years to move my project forward.

Huge thanks to my lab members, especially Dr. Yaqing Zhang, who has been my guidance in lab, she taught me most of the techniques I know now, and she was patient with me during my early years when I was learning. I really appreciate that we can talk about our research and help each other with ideas and at the end you treat me as a colleague which I much appreciate. I couldn't be where I am today without your mentoring. Rosa Menjivar, you were the first graduate student I mentored, and after you joined the lab, we basically grew in the lab together, you have helped me so much in the lab but also by being a friend outside the lab. Kristee Brown, you have been

pivotal in moving my research forward by helping me with my mice colonies and with tissue staining. But not just that, you have been more than a friend in life, you became my sister! Thank you for all your support in so many different ways. Big thanks to the amazing postdocs, Wenting and Joyce, they have always been very honest, gave good advice and are always willing to help in anything. Joyce, thank you for all the food you made for us! Katelyn, thank you for your bioinformatics skills and your willingness to help. I know you became the person that helped everyone in lab but that will pay forward. You will receive more than you give. Carlos Espinoza thank you for managing the lab, keeping us organized, helping with some treatments and for all the sweets you shared with us. Nina Steele, thanks for your advice and the CyTOF help. Also, I want to thank to other lab members that were helpful in different ways: Mike Scales, Eileen Carpenter, Emily, Zeribe Nwosu, Wei Yan and Padma Kadiyala. Lastly, thanks to the former Pasca Lab members: Heather, Arthur, Paloma, Valerie, Maeva, Sam and Veerin.

Next, I want to thank the Pancreatic Tumor Eradication Alliance (PanTErA) group for been a supportive group and for giving me plenty of feedback. It was always fun and informative to get together, eat bagels and listen to great advances in pancreatic cancer research.

Special thanks to my collaborators: Dr. Shaomeng Shang, Dr. James Moon, Dr. Costas Lyssiotis and Dr. Joerg Lahann for providing me with reagents, and necessary materials for my experiments.

I also want to thank the graduate program that opened the doors for me: The Cell and Developmental Biology (CDB) program. I want to thank the administrative crew for the assistant and aid, you have been amazing and very helpful (Thank you Lori Mirabitur and Karen Lang!). Thank you the CDB faculty especially Dr. Scott Barolo (PIBS director), Dr. Ben Allen, Dr. Kristen Verhey, Dr. Diane Fingar and Dr. Roman Giger for their support. Lastly, I want to thank the current

CDB DEI committee (Jackie Graniel, Emily Freeburn, Hannah Hafner, Jun Park, Karen Wang, and Dr. Mara Duncan) and former members (Flor and Nick). We have accomplished so much for improving the climate and CDB culture. I'm proud of every single person that is part of this, many people don't realize the amount of work that requires to do all this as a graduate student. You are all amazing for giving the extra mile.

My CDB besties: Jackie Graniel, since the day I met you I have learned so much from you, you taught me skills that only great leaders possess, and you are a natural in this! But not only you taught me leadership skills, you have also been an amazing friend and a great support during all these years. For that and more I thank you. Love you! Fatima, I met you during my 1st year and although and we have kept our friendship with our usual 'Hopcat' and 'Blank slate' dates, in those we vent so much about everything happening in our life that after going home I felt relieved. Thank you for always been there for me. Jeff, you have help me in so many ways that you probably don't even realize, and Seth have always been someone that pump you when you fell the worst. Thank you to both of you!

My Puerto Rican crew: First, thanks to Valerie Irizarry, you arrived as a summer undergraduate student to our lab, we quickly became friends but always keeping a good mentor/mentee relationship in the lab. Then you returned a year later as a PREP student. Years later you parted to go a be an amazing PhD student at UPenn and I am so proud of you. I'm still your friend and mentor in the distance and I love that! Desiree, you were my first roommate ever and the first person I met when I got to Ann Arbor. Thank for all your support over the years, I have learned a lot from you. Lyanne, you were my second roommate, and that allowed us to become friends and I'm so grateful for your friendship. Even though life have distanced of a bit, I know our friendship will remain strong. Thank you for providing me with your great friendship.

Candilianne, you were my third roommate and that made us be closer friends. During the year we lived together our friendship grew so much. Thank you for all the support, you are my cheerleader and a person to vent to. Thank you for listening. I'm happy that we could become this close and help each other the way we do. Attabey, you were not my roommate (haha) but I appreciate how helpful you have been in multiple situations, you have always been there for me. Huge thanks to the rest of my friends: Jaime, Francisco, Ricardo, Francisco, Nestor, Bryant and Alvin. You are all part of the amazing group of people that have been a huge part to keep my sanity during my PhD training. I'm so glad for having all of you in my life, we have our little niche; we speak the same language in every sense. I have seen so many of you grow and become doctors, other have left to continue with their careers, but it has been amazing meeting you, going camping with you, helping moving people and celebrating our accomplishments together. And even those who I don't see any more I thank you because you were important in my life during the time in my PhD training.

Frances, Brenda, Neike and Rosa (again), my other little group of empowered women. We talk about so many topics in a day, we talk about silly stuff and complex topics. I have learned so much from our conversations. It's always fun to have trips with all of you (we have made plenty of trips together). Thanks for existing in my life and empowering me.

Finally, the biggest thanks to my family. First, my mom (Ida) you gave me my life, you have been supportive and always took care of me. I appreciate every effort you made as a single mom, you had us young and you never stopped fighting for us. You sacrificed most of your youthful years for us and all I can give you right now if making you proud. Te amo mucho! My grandma (Chiry), you took care of me when my mom was working, you fed us and still do. You took us to school and that is why you are a second mother to me, and I call you Mami. Te amo mucho mami! My sister Andrea, thank you for being the first one to celebrate my

accomplishments. I'm proud of everything you have accomplished too. My brother Alexander, we barely talk but when we do you always makes me laugh and you always opened the doors of your home to me. My stepdad (Gardy) has been a father to me, always proud of every accomplishment I achieve. My cousin (Keishla) we have always been close and me leaving PR distance us a bit, but you are always waiting for me to go for Christmas to have some fun and share some quality time. My sister-in-law (Dianed) you have been supportive and even though we don't talk a lot you have always had the doors open when I come to visit, and it feels like time never passed. Moreover, you and my brother gave me the greatest gift to be an aunt for the first time (of baby Leah)! Unfortunately, cancer and other diseases took away some amazing people in my family, including my aunt Rosin and my grandpa Pio, rest in peace. Pio was such a great leader and an intellectual, you were so kind, and anyone would want to aspire to be like you. Fortunately, life have also brought a new blessing into my life, my niece Leah, which brought joy to our family.

## Table of Contents

## List of Tables

## List of Figures

## Abstract

Pancreatic ductal adenocarcinoma (PDAC) is the most common type of pancreatic cancer. PDAC is one of the deadliest malignancies with a poor 5-year survival rate of 11%. The high metastatic capability and its late detection are among the reasons why it is so lethal. The best treatment is surgical resection but unfortunately most patients have unresectable tumors or metastatic disease. The current chemotherapies for PDAC have a moderate improvement in overall survival and unfortunately most patients develop resistance. Therefore, it is critical to have a better understanding of this disease to discover potential therapeutic avenues.

$KRAS^{G12D}$ is the main mutation found in over 90% of human pancreatic tumor samples. One of the hallmarks of PDAC is the extensive fibroinflammatory response. Most of the tumor volume in humans is composed by stroma, particularly fibroblasts and immune cells. Despite of the abundant infiltration of immune cells, PDAC tumors are known as "cold tumors" because most of the cells are immunosuppressive. These immunosuppressive cells [tumor associated macrophages (TAMs), myeloid derived suppressor cells (MDSCs) or regulatory T cells (T regs)] interrupt T cell anti-tumor immunity. In fact, $CD8^+$ T cells are very scarce in murine and human PDAC tumors.

Most of the efforts now are trying to understand the immunosuppressive environment and how to reverse it. In our lab, we have published abundantly about different immunosuppressive mechanisms involving the crosstalk of multiple cell types. We have mainly used a multi-modality approach by using a combination of methods: genetically engineered mouse models,

immunohistochemistry, flow cytometry, CyTOF, single cell RNA sequencing and bulk RNA sequencing to dissect the crosstalk between immune cells, fibroblasts, and tumor cells.

In my dissertation, I first described in chapter 2, the initial events in the establishment of the precursor lesion microenvironment (PME) using a mouse model in which the expression of epithelial-specific oncogenic *Kras* can be activated or inactivated at will. We found that oncogenic KRAS drives the reprogramming of fibroblasts early during pancreatic carcinogenesis to an inflammatory phenotype. The cytokines produced by fibroblasts (IL6, IL33, CXCL1 and SAA3) have receptors in myeloid cells, including macrophages. Both, fibroblasts, and macrophages activate the JAK/STAT3 pathway which is downregulated upon oncogenic *Kras* inactivation. Furthermore, macrophages in the PME are modulated by oncogenic KRAS by having an immunosuppressive phenotype when oncogenic *Kras* is activated and a tumor repair phenotype upon oncogenic *Kras* inactivation.

Secondly, I described a project that focused on understanding the mechanism by which myeloid cells are immunosuppressive. We specifically targeted the JAK/STAT3 pathway in the myeloid compartment and used a syngeneic tumor transplantation model to study the effect of deleting myeloid-STAT3 in pancreatic cancer progression. We found that STAT3 was a major player in driving immunosuppression by myeloid cells and deleting it from myeloid cells decreased immunosuppressive cells and increased the number of T cells.

All together we found that oncogenic KRAS drives immunosuppression early during carcinogenesis and identified the JAK/STAT3 pathway as a main pathway driving immunosuppression in myeloid cells.

# Chapter 1 Introduction

## 1.1 Pancreas physiology

The pancreas is an organ localized behind the stomach with the head of the pancreas attached to the duodenum and the tail attached to the spleen. It has two main functions: exocrine (ducts) and endocrine (glands). The acinar and ductal cells are both part of the exocrine compartment and they compose most of the pancreas mass. The acinar cells' main function is to produce the digestive enzymes such as lipase, protease, amylase, trypsin, etc, that are delivered as zymogens (except for lipase and amylase) to the duodenum for digestion. The ducts, that are formed by ductal cells, deliver these enzymes to the duodenum. The duodenum stimulates the release of digestive enzymes by producing the hormone Cholecystokinin. The endocrine compartment consists of the islets of Langerhans which produce hormones for sugar metabolism including insulin and glucagon. (Longnecker, 2021) The pancreas, as other organs, is susceptible to different diseases including diabetes, chronic pancreatitis, and different types of cancers (adenocarcinoma, squamous cell carcinoma, neuroendocrine, etc) (MedlinePlus, 2021).

## 1.2 Pancreatic cancer statistics and treatments

The most common and deadly type of pancreatic cancer is pancreatic ductal adenocarcinoma (PDAC). PDAC has several risk factors, including: obesity, diabetes, chronic pancreatitis, excessive alcohol consumption, and others (Capasso et al., 2018). A myriad number of factors contribute to the lethality of this disease, including its late detection and fast metastatic capability to the liver and lungs, which occurs early in disease progression (Kamisawa, Isawa,

Koike, Tsuruta, & Okamoto, 1995) (Disibio & French, 2008). The current 5-year survival rate for all stages combined increased to barely 11% in 2022 (Society, 2022). Surgery is the best treatment, and it increases the 5-year survival rate to 25% but only 10-20% of patients have resectable tumors (Bilimoria et al., 2007). Unfortunately, most patients are diagnosed with locally advance or metastatic disease preventing them from having resection surgery (Orth et al., 2019). Gemcitabine has been the standard of care for these patients since 1977, yet its use as a single therapeutic only offers a moderate increase in overall survival by a few weeks (3rd et al., 1997). As such, it is now given in combination with albumin-bound paclitaxel (nab-paclitaxel) with a better outcome (Von Hoff et al., 2013). In 2011, FOLFIRINOX was observed to produce better outcomes and soon became the first line of treatment in patients that can tolerate it well. Currently, both Gemcitabine/Nab-paclitaxel and FOLFIRINOX are the best and most prescribed treatments for metastatic PDAC (Conroy et al., 2011) (Conroy et al., 2018) (Thierry Conroy 2018 and Daniel D. Von Hoff 2013) (Principe et al., 2021). These therapies are also given as neoadjuvant to the small percentage of patients that have borderline resectable/locally advance PDAC to increase the chances for tumor resection. In these cases, FOLFIRINOX provides the highest rates of resectability (60.8%) when compare to other therapies (Hackert et al., 2016) (Scheufele, Hartmann, & Friess, 2019) (Principe et al., 2021). Unfortunately, many patients develop resistance to these chemotherapeutics and even when tumors are resected, a large number of patients relapse with metastatic disease (Sarabi et al., 2017) (Jones et al., 2019). Given the lethality of this disease and the lack of treatments, we need to understand the biology of this disease to improve future treatments.

### 1.3 Oncogenic KRAS and PDAC initiation

The main mutation found in human PDAC is oncogenic KRAS, which is found in over 90% of human tumor samples (Almoguera et al., 1988) (Smit et al., 1988). KRAS is a small GTPase that is required for the activation of the mitogen-activated protein kinase (MAPK) pathway and is involved in the transactivation of the phosphatidylinositol-3-kinase (PI3K)/AKT signaling pathway. Activation of these pathways promote transcription of genes involved in cell proliferation, survival, differentiation, etc (Young et al., 2009) (di Magliano & Logsdon, 2013). In pancreatic cancer, it was found that both, the MAPK and PI3K pathways, are activated and required for cancer progression (Christine M. Ardito et al., 2012; Collisson et al., 2012) (Eser et al., 2013). However, it is important to mention that the findings of the requirement of PI3K activation for PDAC development have been contradicting in two independent studies. In one study the use of PI3K (H1047R) allele in a mouse model did not lead to precancerous lesions development. In the other study, expression of PI3K (H1047R) led to precancerous lesions formation. These results could be contradicting due to the use of different mouse models with different Cre drivers (Collisson et al., 2012) (Eser et al., 2013).

The most common KRAS mutation in PDAC is a single amino acid substitution of glycine for aspartic acid (G12D) in codon 12. This single amino acid substitution causes the enzyme to get locked in the guanosine triphosphate (GTP) bound active conformation instead of hydrolyzing GTP to guanosine diphosphate (GDP). As a result, the enzyme remains active for a longer time and is insensitive to Guanoside activating proteins (GAPs) which are important for the conversion of GTP to GDP (for review, see Wittinghofer et al. 1997; McCormick 1998). The use of genetically engineered mouse models has allowed us to better understand the role of $KRAS^{G12D}$ in the initiation of PDAC. The first and most popular murine models express endogenous $Kras^{G12D}$ in

the pancreas through the expression of Cre recombinases under the pancreas specific promoters, *Ptf1a* or *Pdx1*. *Ptf1a* is expressed mainly in the pancreas (at E9.5), but *Pdx1* is expressed earlier during development (E8.5) in the foregut endothelium, hence it also gets recombined in the duodenum, as well as in the brain and other sites (Hingorani et al., 2003; Kawaguchi et al., 2002). *Pdx1*-Cre;LSL-*Kras*$^{G12D}$ or *Ptf1a*-Cre;LSL-*Kras*$^{G12D}$ mice are both referred to as KC. The KC mouse model recapitulates the different stages of the human precursor lesions to PDAC, known as pancreatic intraepithelial neoplasia (PanIN). These mice develop PanINs with high penetrance that keep progressing through all PanIN stages and occasionally develops into invasive and metastatic cancer. Two of the caveats of these models is that (1) *Kras*$^{G12D}$ is expressed embryonically, and (2) that the expression is not inducible and/or reversible. In 2012, our group and the DePinho group published a mouse model (referred to as iKras*) that expresses *Kras*$^{G12D}$ specifically in the pancreas through the *Ptf1a* promoter and the expression is inducible by giving doxycycline and reversible by removing doxycycline (Collins, Bednar, et al., 2012) (Ying et al., 2012). This model allowed us to activate *Kras*$^{G12D}$ expression in adult mice and observe the consequences of *Kras*$^{G12D}$ inactivation during PanIN and invasive cancer stages (iKras*P53* model).

In all these mouse models, expression of *Kras*$^{G12D}$ lead to the transdifferentiating of the acinar cells into duct-like structure through a process known as Acinar-to-ductal metaplasia (ADM). ADM is a reversible mechanism of protection that acinar cells have upon stress, which was studied in a model with TGF$\alpha$ overexpression (Jhappan et al., 1990) (Sandgren, Luetteke, Palmiter, Brinster, & Lee, 1990). During ADM, acinar cells downregulate acinar specific genes such as *Ptf1a*, *Mist1* and *Nr5a2* and upregulate ductal specific genes such as *Krt19* and *Muc1* (Krah et al., 2019) (Krah et al., 2015) (Cobo et al., 2018) (G. Shi et al., 2013) (Tuveson et al., 2006) (von Figura, Morris, Wright, & Hebrok, 2014). In the presence of KRAS$^{G12D}$, ADM

progresses to PanIN ((Hingorani et al., 2003) (Collins, Bednar, et al., 2012)) and our lab showed that $KRAS^{G12D}$ was required for the formation and maintenance of PanINs in mice (Collins, Bednar, et al., 2012).

Despite $KRAS^{G12D}$ being the initiator, this mutation by itself is not sufficient to progress to cancer (Tuveson et al., 2004). Loss of tumor suppressor genes through point mutations in the *TP53* tumor suppressor gene (75% of cases) and inactivating mutations of *CDKN2A* (30% of cases) and *SMAD4* (32% of cases) are also found in human tumors (Cancer Genome Atlas Research Network. Electronic address & Cancer Genome Atlas Research, 2017). To study metastatic PDAC, researchers generated engineered mouse models carrying some of these mutations. For instance, the KC was crossed to a mouse that had an *Ink4a* mutation (Aguirre et al., 2003) or to a P53 loss of function mouse (KPC) (Hingorani et al., 2005). Both models accelerated the formation of PanINs and resulted in invasive and metastatic disease. Today, the KPC model remains the best preclinical model of pancreatic cancer.

Unfortunately, there are no inhibitors or therapies targeting $KRAS^{G12D}$. Although there is a G12C inhibitor, this mutation is rare in pancreatic cancer (Canon et al., 2019; Janes et al., 2018) (Hallin et al., 2020). Thus, understanding different manners in which $KRAS^{G12D}$ downstream effects can be targeted is critical.

### 1.4 Pancreatitis and PDAC initiation

Chronic pancreatitis is a risk factor for developing pancreatic cancer in humans. Pancreatitis is inflammation of the pancreas, that is associated with zymogen proteolysis that lead to acinar cell death, edema and inflammation (Grady et al., 1998). Acute pancreatitis is sudden and short whereas chronic pancreatitis is ongoing inflammation (clinic, 2020). In mouse models, pancreatitis has been widely used to study the impact of inflammation on pancreatic cancer. To

induce pancreatitis in mouse models, caerulein, a cholecystokinin analog, is used since it mimics human pancreatitis (Lampel & Kern, 1977). In healthy mice, the induction of pancreatitis causes the acinar cells to go through the reversible process of ADM to protect themselves and the pancreas can recover in a few days post pancreatitis induction.

In the context of pancreatic cancer, it has been shown that both acute and chronic pancreatitis synergize with $KRAS^{G12D}$ to promote pancreatic cancer. For example, using a model expressing $KRAS^{G12V}$ in the pancreas, chronic pancreatitis was essential for PDAC development (Guerra et al., 2007). Furthermore, using the popular murine pancreatic cancer model (KC), acute pancreatitis accelerated pancreatic cancer progression (Carrière, Young, Gunn, Longnecker, & Korc, 2009). These results were also true in our iKras* mouse model, in which caerulein treatment accelerated PanIN formation (Collins, Bednar, et al., 2012). Recently, it was shown that pancreatitis causes epigenetic changes in the acinar cells even after the pancreas seems fully recovered. These epigenetic changes make the pancreas more susceptible to $KRAS^{G12D}$ and mice develop PanINs faster even after apparent full recovery from pancreatitis (Del Poggetto et al., 2021).

### 1.5 PDAC tumor microenvironment

One of the hallmarks of PDAC is the extensive fibroinflammatory response, composed mainly of immune cells, fibroblasts, and extracellular matrix (ECM). The extensive stroma accumulation is recapitulated in the KC, KPC, iKras* and iKras*P53* mouse models (Hingorani et al., 2003) (Aguirre et al., 2003) (Hingorani et al., 2005) (Collins, Bednar, et al., 2012) (Collins, Brisset, et al., 2012). These components of the tumor microenvironment (TME) are characterized by having complex interactions that are poorly understood and that start early during

carcinogenesis (Clark et al., 2007). In the past years, immune cells have been extensively studied in the TME because they possess anti-tumorigenic abilities.

It has been shown that activation of cytotoxic T lymphocytes (CTLs) can elicit an anti-tumor immune response through expression of interferon gamma (IFN$\gamma$), perforin, and other molecules (Dighe, Richards, Old, & Schreiber, 1994) (van den Broek et al., 1996). It has also been shown that in some tumors, IFN$\gamma$ signaling by CTLs can even prevent the development of spontaneous tumors (Kaplan et al., 1998) (Shankaran et al., 2001). However, other studies have shown that other components of the immune system can have opposing roles by being pro-tumorigenic. Myeloid cells, in particular macrophages and immature myeloid derived suppressor cells (MDSCs), and regulatory T cells (Tregs) can express molecules such as Arginase 1 (ARG1), Nitric Oxide (NO) and Transforming growth factor beta (TGF$\beta$) that exclude T cells from the tumor, completely preventing the anti-tumor immunity from T cells (Bronte et al., 2003; S. A. Kusmartsev, Li, & Chen, 2000) (Almand et al., 2001) (Gabrilovich, Velders, Sotomayor, & Kast, 2001) (Polanczyk, Walker, Haley, Guerrouahen, & Akporiaye, 2019). PDAC is one of the cancers that is recognized as a "cold tumor" because most of the immune cells are immunosuppressive and it lacks immune responses by T cells (Clark et al., 2007). The recruitment of these immunosuppressive cells has been associated with signaling coming from tumor cells but also from fibroblasts. In this section, I will describe three main components of the TME: T cells, myeloid cells, and fibroblasts.

### *1.5.1 T cells*

T cells are part of the adaptative immune system, and they are known as lymphocytes. T cells ($CD3^+$) are divided in different groups that possess different gene expression and functions: (1) $CD8^+$ T cells, (2) $CD4^+$ T cells (T helpers and T regs), and (3) $\gamma\delta$TCR T cells. The most well

studied are the $CD4^+$ T cells and $CD8^+$ T cells. In the iKras* model, it was shown that $CD4^+$ T cells were pro-tumorigenic since the use of a CD4 deficient mice prevented carcinogenesis by increasing the numbers of CTLs (Zhang et al., 2014). $CD4^+$ T cells are divided in two groups: helper T cells (Th) and Tregs. Th cells are further divided in different types depending on the cytokine expression (Th1, Th2 and Th17). Th1 cells produce proinflammatory cytokines such as IFN$\gamma$ and IL2, considered to be anti-tumor. Th2 produce anti-inflammatory cytokines such as IL-4, IL-5 and IL-13. Finally, Th17 produce IL-17 and IL-22 (Chraa, Naim, Olive, & Badou, 2019). Th2 and Th17 are mostly pro-tumor, except for Th2 in breast cancer and Th17 in esophageal cancer. T regs ($FoxP3^+$) are immunosuppressive in nature and produce cytokines such as IL-10 and TFG$\beta$. T regs correlate with poor prognosis in pancreatic cancer (Hiraoka, Onozato, Kosuge, & Hirohashi, 2006). In a mouse model of transplanted pancreatic tumor, depletion of T regs in the cancer stage decreased tumor growth, a process mediated by $CD8^+$ T cells (Jang et al., 2017). However, deletion of T regs in a spontaneous mouse model led to accelerated progression, a process that involved crosstalk between T regs and fibroblasts (Zhang, 2020, 31911451). Finally, the $CD8^+$ T cell (also known as CTLs) are known for their killing abilities, and in cancer, high numbers of $CD8^+$ T cells is associated with good prognosis. $CD8^+$ T cells are the cytotoxic T cells that recognize antigens presented by the major histocompability complex (MHC) class I in cells, including tumor cells. In pancreatic cancer the presence of $CD8^+$ T cells is rare, and it is associated with the presence of immunosuppressive cells and to the lack of antigen presentation by tumor cells. Recently, it was shown that pancreatic tumor cells do not present antigens because they degrade MHC I (HLA-I in humans) through autophagy (Yamamoto et al., 2020). The few T cells that are present are dysfunctional and express immune checkpoint markers such as TIGIT, programmed death-1 (PD-1) and LAG-3 (Masugi et al., 2019) (Nina G. Steele et al., 2020). All

these markers are receptors that once activated by the ligand, have an inhibitory effect on T cells (apoptosis, anergy and T cell exhaustion). The ligands for these receptors, such as poliovirus receptor (PVR) and programmed cell death ligand-1 (PD-L1) are enriched in the myeloid population (Shi, Chen, Yang, & Li, 2013) (Nina G. Steele et al., 2020). Hence, many studies are focusing in understanding the mechanism by which myeloid cells suppress $CD8^+$ T cells.

### *1.5.2 Myeloid cells*

Myeloid cells ($CD45^+CD11b^+$) are a group of immune cells that include monocytes ($Ly6C^+$), macrophages ($F4/80^+$), neutrophils ($Ly6G^+$), dendritic cells ($CD11c^+$) and MDSCs ($Ly6C^+Ly6G^+$). Myeloid cells have been implicated in many different cancers including pancreatic cancer for the ability to induce immunosuppression and inhibiting the anti-tumor immunity of T cells. For instance, in pancreatic cancer, myeloid cell depletion, using mouse model, resulted in decrease tumor growth, albeit dependent on $CD8^+$ T cells (Y. Zhang, A. Velez-Delgado, et al., 2017). In the context of pancreatic cancer, the most studied myeloid populations are macrophages and immature myeloid cells.

#### *1.5.2.1 Macrophages*

The largest and most studied myeloid cell population are the macrophages. The macrophages, as the word suggest, are phagocytic cells important in maintaining tissue homeostasis by clearing away debris and engulfing foreign substances. They are also one of the primary responders of the body against pathogens (Jiawei Zhou et al., 2020). Macrophages respond to stimulants from other cells and in turn they are highly plastic. During inflammation, macrophages are known to have two main polarization states: M-1 and M-2 (Mills, Kincaid, Alt, Heilman, & Hill, 2000; Verreck et al., 2004). The classical activated macrophages (M-1) are known to be proinflammatory and to produce IFN$\gamma$ and nitric oxide (NO); these have been associated with strong killing abilities, tissue

destruction and anti-tumor capabilities. The alternative activated macrophages (M-2) are known to produce interleukin 4 (IL4), interleukin 10 (IL10), Arginase 1 (ARG1), etc (Orecchioni, Ghosheh, Pramod, & Ley, 2019); these are associated with tissue remodeling and pro-tumor capabilities (Mills et al., 2000; Verreck et al., 2004). However, these classifications, are now changing since deeper assessments in the role of the macrophages have determined that they are heterogeneous and extremely plastic, and continuously changing phenotypes (DeNardo & Ruffell, 2019).

In the TME, macrophages are known as tumor associated macrophages (TAMs) and they do not fall into the typical M-1 or M-2 classifications, but their immunosuppressive nature makes them to resemble more the M-2 phenotype. In pancreatic cancer, TAMs have two origins: tissue resident-embryonically derived macrophages or monocyte derived macrophages (Zhu et al., 2017). They were also found to have different roles: the embryonically derived TAMs are more pro-fibrotic whereas monocytes derived TAMs are involved in antigen presentation. TAMs have been shown to promote tumor growth in different ways. For instance, TAMs are a source of EGFR ligands which maintain high MAPK activity in epithelial cells, promoting PanIN progression (Y. Zhang, W. Yan, et al., 2017). Nevertheless, one of the most studied mechanisms of tumor promotion is the immunosuppressive function that TAMs possess. Some common immunosuppressive molecules include ARG1, IL4 and IL10. ARG1 depletes L-arginine, that is an essential amino acid for T cell fitness and survival capacity (Geiger et al., 2016). Inhibition of ARG1 in tumor bearing mice suppressed alloreactive T cells (Bronte et al., 2003). Also, it was shown that ARG1 is required for CD3ζ and CD3ε expression in T cells as well as T cell proliferation (Rodriguez et al., 2003) (Rodriguez et al., 2004). IL-4 is another cytokine with pro-tumor roles, IL4 is known to induce Th2 cells (immunosuppressive cells), it also induces ARG1

expression in TAMs and it has been shown to enhance proliferation of human PDAC cells (Rengarajan, Szabo, & Glimcher, 2000) (Bronte et al., 2003) (Prokopchuk, Liu, Henne-Bruns, & Kornmann, 2005). Finally, IL10 was shown to suppress $CD8^+$ T cell activation by reducing CD8 protein colocalization with the T cell receptor (TCR), hence reducing antigen sensitivity (Smith et al., 2018). Also, it was shown that M-2 TAMs promoted epithelial to mesenchymal transition (EMT) in pancreatic tumor cells through toll like receptor-4 (TLR4)/IL10 signaling (Liu et al., 2013).

Antigen presenting cells (APCs), including TAMs, and tumor cells can express immune checkpoint molecules that downregulate immune responses. APCs express PD-L1, which is the ligand that binds to PD-1, a well-known immune checkpoint receptor found in T cells. Also, APCs express B7-1 and B7-2 which are ligands that interact with cytotoxic T-lymphocyte-associated protein 4 (CTLA-4) expressed on T cells and is another immune checkpoint. The PD-1/PD-L1 and CTLA4/B7-1/2 axis are known to send inhibitory signals to T cells. PD-1/PD-L1 blockade using the anti-PD1(Nivolumab and Lambrolizumab) or anti-PD-L1 in non-small-cell lung cancer, melanoma or renal cancer were successful (Brahmer et al., 2010) (Topalian et al., 2012) (Brahmer et al., 2012) (Hamid et al., 2013). Similarly, CTLA-4 blockade (Ipilimumab) is effective in metastatic melanoma and renal cancer (Downey et al., 2007) (Yang et al., 2007). However, in PDAC these checkpoint inhibitors have been unsuccessful (Royal et al., 2010) (Brahmer et al., 2012).

Due to all the immunosuppressive signaling that macrophages have, they present as great therapeutic targets to reverse immunosuppression. One of the targets that have been exploited and had great results in combination with gemcitabine was the use of CD40 agonist. CD40 agonist in combination with gemcitabine led to tumor regression in a murine model and in a few PDAC

patients. Interestingly this process was mediated by macrophages and not T cells (Beatty et al., 2011). To this combination of anti-CD40 and Gemcitabine was later added Nab/paclitaxel, together regression of tumor was dependent on T cells. Gemcitabine and Nab/Paclitaxel was required for a greater functionality of T cells (Byrne & Vonderheide, 2016). Unfortunately, preliminary results of anti-CD40 combined with checkpoint inhibitors and Gemcitabine/Nab-paclitaxel in clinical trial do not have promising results (O'Hara et al., 2021).

Overall, TAMs are a major source of immunosuppressive molecules that regulate T cells. However, they are not the only myeloid population mediating immunosuppression in PDAC.

*1.5.2.2 Immature myeloid cells*

MDSCs are a heterogenous population of immature myeloid cells known from their immunosuppressive abilities through ARG1, NO and reactive oxygen species (ROS) (Bronte et al., 2003) (S. Kusmartsev, Nefedova, Yoder, & Gabrilovich, 2004) (Sinha, Clements, & Ostrand-Rosenberg, 2005). They are divided into granulocytic (Gr-MDSCs $Ly6G^{hi}$) or monocytic MDSCs (Mo-MDSCs, $Ly6C^{hi}$). Gr-MDSCs inhibit $CD8^+$ T cells by activation of STAT3 and increase in ROS. However, Mo-MDSCs inhibit $CD8^+$ T cells by activation of STAT1 and increase in the expression of iNOS and NO. In pancreatic cancer, MDSCs are recruited early during carcinogenesis by expression of GM-CSF derived mainly from tumor cells (Clark et al., 2007) (Bayne et al., 2012). Furthermore, it was shown that depletion of a subset of MDSCS (Gr-MDSCs) unmask tumor cells to T cell antitumor immunity by increasing $CD8^+$ T cells (Stromnes et al., 2014). Similarly, inhibition of CXCR2 signaling improved survival in a PDA murine model ($Kras+Tgfbr2^{KO}$) (Ijichi et al., 2011). CXCR2 is the receptor for the CXC chemokines such as CXCL1 and CXCL2, and it is expressed by neutrophils and MDSCs and was shown to be

important for their migration (Thyagarajan et al., 2019). Another study, using the KPC, showed that CXCR2 inhibition or $Ly6G^+$ cells depletion led to decrease in metastasis and also enhancement of immunotherapy since it increased the number of T cells in the tumor (C. W. Steele et al., 2016b). Overall, these results concluded that TAMs and MDSCs are populations that need to be targeted to reverse immunosuppression in pancreatic cancer.

### 1.6 Fibroblasts

Fibroblasts are a major component of the PDAC TME [for review see (Helms, Onate, & Sherman, 2020)]. In PDAC, the role of cancer associated fibroblasts (CAFs) have been controversial with both pro-tumor and anti-tumor capabilities (Helms et al., 2020). CAFs are a very heterogeneous population that come from different origins. Several subpopulations of CAFs have been found including: myofribroblasts (myCAFs), inflammatory fibroblasts (iCAFs) and antigen presenting fibroblasts (ApCAFs) [(Ohlund, 2017, 28232471) (Elyada et al., 2019)]. myCAFs (spatially closer to tumor cells) are induced by TGF$\beta$/SMAD2/3 and are characterized by the expression of $\alpha$SMA and TGF$\beta$ responsive genes such as *Ctgf* and *Col1a1*. iCAFs (distant to tumor cells) are induced by IL1/JAK/STAT3 and express *Pdgfra*, *Il6*, *Cxcl1* and *Cxcl2* (Ohlund, 2017, 28232471) (Biffi, 2019, 30366930). Recently, ApCAFs were identified as fibroblasts with abilities to present antigen to T cells (Elyada et al., 2019).

CAF different subtypes could be explained by their different origins from the healthy pancreas. Pancreatic stellate cells (PSCs) for a long time have been thought to be the primary source of CAFs, but recently it was shown that PSCs compose a very small fraction of the CAF's population. Two other populations of fibroblasts were found in the healthy pancreas, $Gli^+$ and $Hoxb6^+$ fibroblasts. Both were found in similar levels in the healthy pancreas, but they contributed

differently to carcinogenesis. Hoxb6$^{+}$ fibroblasts do not expand during carcinogenesis, on the other hand, Gli$^{+}$ fibroblasts comprised most of the fibroblasts in the tumor ((Garcia et al., 2020) (E. J. Helms et al., 2021)).

CAFs promote tumor growth by production of ECM and immunomodulatory factors. ECM gives physical and chemical cues that influence cancer progression and in PDAC it has been shown that it provides nutrients for the tumor (Olivares et al., 2017). CAFs' ECM production acts as a physical barrier to exclude cytotoxic T cells from the tumor and in this way promoting tumor growth. CAFs immunomodulatory factors also promote tumor growth, for example, CXCL12 expression by CAFs exclude T cells (Feig et al., 2013) (Hartmann et al., 2014) (Jiang et al., 2016). CAFs have also been found to promote resistance to Gemcitabine treatment by acting as a physical barrier and releasing deoxycytidine (Dalin et al., 2019). On the contrary, many other studies have shown the tumor restricting capabilities of CAFs. For example, targeting of the ECM by Collagen 1 deletion in myCAFs accelerated PanINs and PDAC and decreased overall survival (Y. Chen et al., 2021). Similarly, depletion of $\alpha$SMA$^{+}$ fibroblasts (myCAFs) (Ozdemir et al., 2014) causes tumor to progress faster and more undifferentiated. Furthermore, genetically ablation of epithelial sonic hedgehog (SHH), which is a ligand that binds to smoothened (SMO), a receptor found in CAFs, led to accelerated tumor progression. In the same study, they used a pharmacological inhibitor of SMO and found that tumors progressed faster (Rhim et al., 2014). However, targeting SHH has been controversial due to the dosage dependent effect of SHH in which a reduced amount of HH activity promotes tumor vascularity and growth, and complete inhibition of HH impairs tumor growth (Mathew, Zhang, et al., 2014 ). In 2009, it was shown that inhibition of hedgehog (HH) using IPI-926 improved delivery of gemcitabine in a murine PDAC and the combination led to a transient stabilization of the disease (K. P. Olive et al., 2009). Recently, in 2021, a study from

our lab found that SHH deletion (previously found to be tumor promoter, Rhim, 2014, 24856585) increases Indian hedgehog (IHH), which was found to be tumor promoter (N. G. Steele et al., 2021). Adding a potential explanation on why so many studies have contradicting results. Previous use of pharmacological inhibition of SMO [Vismodegib (Genentech) and IPI-926 (Infinity Pharmaceuticals)] showed disappointing results in clinical trials (Kenneth P Olive et al., 2009) (Kim et al., 2014) (Ko et al., 2016). However, the use of the SMO LDE2245 (Sonidegib, Novartis, (Pan, 2010 #31)) currently in clinical trials had good results in mice (N. G. Steele et al., 2021). The use of different inhibitors could have different results due to the different degrees of hedgehog inhibition.

With all the new insights in the mechanisms of immune evasion driven by CAFs it is important to continue to understand the different populations and how they interact with the distinct components of the TME.

### 1.7 Tumor cells signaling to the TME

The tumor cells in different cancers are known to produce a myriad number of factors with different effects in the TME. However, some of the factors that are secreted by tumor cells aid in the creation of an immunosuppressive microenvironment. At the onset of pancreatic carcinogenesis, during ADM, it was shown that intercellular adhesion molecule-1 (ICAM) expression is induced by *Kras*$^{G12D}$ activation in acinar cells. ICAM serves as an attractant for macrophages which contributed to ADM by macrophage-TNF secretion (Liou et al., 2015). Another known secreted molecule by tumor cells is CCL2. The CCL2/CCR2 axis is important for attracting inflammatory monocytes to sites of inflammation. Expression of epithelial-CCL2 recruits CCR2$^{+}$ infiltrating macrophages to the tumor site. CCR2 blockade depletes monocytes

and macrophages and enhances antitumor immunity (Sanford et al., 2013). It was also reported that genetic ablation of CCL2 in murine models decreased tumor growth, improve angiogenesis and enhanced radiotherapy efficacy (Kalbasi et al., 2017). Macrophages are also recruited by tumor cells by expression of colony stimulating factor-1 (CSF-1). In pancreatic cancer, CSF1R inhibition decreases the number of $CD206^{+}$ macrophages and monocytes and increases the expression of genes related to CTL activation (such as *Ifng* and *Prf1*) and T cell recruitment (*Cxcl10*). In this study they also show that macrophages that persisted in the pancreas after CSF1R inhibition were less immunosuppressive. Additionally, it was found that CSF1/CSF1R inhibition enhanced immunotherapy in PDAC murine models (Yu Zhu et al., 2014). Pancreatic tumor cells were shown to express IL13 as well, which was demonstrated to promote $YM1^{+}$ macrophages (another immunosuppressive molecule) and bolster fibrosis and carcinogenesis (Liou et al., 2017). Further, tumor cells were shown to recruit and drive the development of MDSCs by expression of GM-CSF. MDSCs were shown to cause immunosuppression in pancreatic cancer (Bayne et al., 2012).

Pancreatic tumor cells do not only communicate with immune cells, but they also express molecules that recruit and/or promote the expansion of fibroblasts. One of the most studied and controversial signaling between tumor cells and fibroblasts is the HH pathway. SHH and IHH have been shown to be expressed by tumor cells, both activate the GLI transcription factors in CAFs which increases desmoplasia by expanding fibroblasts (Bailey et al., 2008) (N. G. Steele et al., 2021). Furthermore, tumor cells secrete factors that shape the heterogeneity in CAF subtypes. For example, IL1$\alpha$ is secreted by tumor cells and drives the iCAFs phenotype by activating the JAK/STAT pathway. Interestingly, tumor cells also express TGF$\beta$ which signals in a juxtracrine manner to the fibroblasts in proximity. The TGF$\beta$ signaling antagonizes the IL1$\alpha$-induced

JAK/STAT activation by downregulating the IL1$\alpha$ receptor (IL1R1) to promote the myCAFs subtype instead of iCAF (Biffi, 2019, 30366930). All these signals make fibroblasts important cell types that release many molecules in the TME.

### 1.8 Fibroblasts immunomodulatory capacity in pancreatic cancer

Fibroblasts are one of the major components in human PDAC. Besides communicating with tumor cells and producing supporting ECM, they also possess immunomodulatory functions in the TME. CAFs expressing the fibroblast activating protein (FAP) have been shown to interact with T cells. $FAP^+$ CAFs express CXCL12 with the receptor, CXCR4, on T cells. Depletion of CXCL12 induces T cell accumulation and improves efficacy of PD-L1 treatment in a murine PDAC model (Feig, 2013, 24277834). Additionally, the CAF subtype ApCAF, directly interacts with T cells by presenting antigens to $CD4^+$ T cell through their MHC class II molecules (Elyada et al., 2019). CAFs also communicate with myeloid cells, including macrophages and MDSCs. Using a co-culture of CAFs with PBMCs (or using CAF conditioned media (CM) on PBMCs), it was demonstrated that CAFs express M-CSF, and they enhanced ROS production by monocytes. This induced an M-2 phenotype in TAMs (CD206 and CD163) (A. Zhang et al., 2017). Another molecule involved in the fibroblast-macrophage interaction is IL33. Using a pancreatic cancer cell line injected into the mouse pancreata it was shown that $PDGFR^+$ fibroblasts express IL33 and deletion of IL33 receptor (ST2) decreases M-2 polarization in macrophages. In this study, it was shown that TAMs activated by IL33 produced MMP9 which facilitated metastasis (Andersson et al., 2018). CAFs have also been shown to have a role in MDSCs differentiation from PBMCs *in vitro* through CAF expression of IL6, VEGF, M-CSF, and MDSC chemoattracting molecules such

as monocyte chemoattractant protein-1 (MCP-1) and CXCL12. Blocking of IL6 led to a decrease in STAT3 activation which prevented the differentiation of PBMCs to MDSCs (Mace et al., 2013).

### 1.9 The JAK/STAT pathway

The JAK/STAT3 pathway plays a critical role in controlling the immunosuppressing function of myeloid cells. The Janus Kinases (JAKs) are a type of tyrosine kinases that are bound to the cytoplasmic portion of some cytokine receptors. Ligand binding to these receptors causes dimerization, which is critical for JAK transphosphorylation and recruitment of signal transducer and activator of transcription (STAT) for phosphorylation. Once STATs are phosphorylated, they enter the nucleus for activation or suppression of target genes. There are 4 JAKs (JAK1, JAK2, JAK3 and TYK2) and 7 STATs (STAT1, STAT2, STAT3, STAT4, STAT5A, STAT5B and STAT6) (Seif et al., 2017). In pancreatic cancer the JAK/STAT3 is frequently found activated in epithelial and stromal cells compared to other STATs proteins. Hence, STAT3 has also been the most studied of all STATs proteins in pancreatic cancer. A knockout of STAT3 in the epithelial compartment decreases the formation of PanINs and hence invasive disease (Corcoran et al., 2011) (Fukuda et al., 2011). Similarly, another group found that when knocking down *Stat3* from pancreatic tumor cells in a murine xenograft, these tumors grew at a slower rate and were smaller (H. Li et al., 2011). Recently, targeting the STAT3 using a small molecule that binds to the SH2 domain of STAT3 caused decrease in tumor growth and decrease in macrophages and $SMA^{+}$ fibroblasts (H. Chen et al., 2021). STAT3 has been shown to be critical in the development of MDSCS and it makes them more immunosuppressive by increasing ARG1 levels (Mace et al., 2013) (Trovato et al., 2019). JAK/STAT inhibition using Ruxolitinib, a JAK1/2 inhibitor, decreases tumor growth and increase CTL infiltration which improve efficacy of immunotherapies

(Lu, Talukder, Savage, Singh, & Liu, 2017). Although the JAK/STAT inhibitor Ruxolitinib has been successful in mouse models, it has been unsuccessful in improving survival in clinical trials (Lu et al., 2017) (H. Hurwitz et al., 2018) (Bauer et al., 2018). The targeting of STAT3 still has great potential in pancreatic cancer, thus more extensive studies are required to understand how to best target the pathway.

My dissertation work aims to understand two questions: (1) How epithelial oncogenic KRAS drives the recruitment and establishment of the tumor microenvironment? And (2) Does the JAK/STAT3 pathway drives immunosuppression by myeloid cells in PDAC? I studied these two independent but related projects mainly using genetically engineered mouse models. In chapter 2, I present a story of the role of $KRAS^{G12D}$ in signaling to fibroblasts to reprogram them into a different phenotype that is more immunomodulatory. In chapter 3, I share a story of the assessment of the role of the JAK/STAT3 pathway specifically in the myeloid compartment during pancreatic cancer. Finally, in chapter 4, I discuss my findings and future directions for each project.

# Chapter 2 Extrinsic KRAS Signaling Shapes the Pancreatic Microenvironment Through Fibroblast Reprogramming[1]

## 2.1 Abstract

**Background and aims:** Oncogenic KRAS is the hallmark mutation of human pancreatic cancer and a driver of tumorigenesis in genetically engineered mouse models of the disease. While the tumor cell-intrinsic effects of oncogenic KRAS expression have been widely studied, its role in regulating the extensive pancreatic tumor microenvironment is less understood.

**Methods:** Using a genetically engineered mouse model of inducible and reversible oncogenic *Kras* expression and a combination of approaches that include mass cytometry and single cell RNA sequencing we studied the effect of epithelial oncogenic KRAS in the tumor microenvironment.

**Results:** We have discovered that non-cell autonomous (i.e., extrinsic) oncogenic KRAS signaling reprograms pancreatic fibroblasts, activating an inflammatory gene expression program. As a result, fibroblasts become a hub of extracellular signaling, and the main source of cytokines mediating the polarization of pro-tumorigenic macrophages while also preventing tissue repair.

**Conclusions:** Our study provides fundamental new knowledge on the mechanisms underlying the formation of the fibroinflammatory stroma in pancreatic cancer and highlights stromal pathways with the potential to be exploited therapeutically.

[1] Data in Chapter 2 has been published in Cellular and Molecular Gastroenterology and Hepatology (CMGH) in a manuscript entitled: “Extrinsic KRAS signaling shapes the pancreatic microenvironment through fibroblast reprogramming” (2022).

## 2.2 Introduction

Pancreatic ductal adenocarcinoma (PDA) is the third leading cause of cancer-related death in the United States and is among the most lethal malignancies, with an expected 5-year survival of about 10% (Society, 2020). Over 90% of PDA instances harbor an oncogenic mutation in the *KRAS* gene, most commonly $KRAS^{G12D}$ (Almoguera et al., 1988; Smit et al., 1988). Autopsy studies have revealed that over 75% of the population harbors pre-neoplastic lesions in the pancreas linked to mutations in *KRAS*, yet pancreatic cancer is relatively rare (Matsuda et al., 2017; Pour, Sayed, & Sayed, 1982). This finding is reproduced in mouse models of the disease, where widespread epithelial expression of oncogenic KRAS leads to cancer with long latency. Why some KRAS-mutant lesions maintain an indolent pre-neoplastic state while others progress to deadly invasive cancer is a fundamental gap in knowledge.

A longstanding question has been the identity of the cell of origin to pancreatic cancer. The most frequently utilized genetically engineered mouse models of pancreatic cancer express $Kras^{G12D}$ broadly across the pancreas epithelium upon Cre recombination. Two of the most common Cre drivers include the Pdx1 promoter (Pdx1-Cre;$Kras^{LSL\text{-}G12D/+}$) and insertion into the Ptf1a locus ($Ptf1a^{Cre/+}$;$Kras^{LSL\text{-}G12D/+}$); both of these models are commonly referred to as KC (Hingorani et al., 2003) (Aguirre et al., 2003). Different precursor lesions to pancreatic cancer have been described in human patients (Ying et al., 2016}), of which Pancreatic Intraepithelial Neoplasia (PanIN) is the most common. KC mice undergo a stepwise carcinogenesis process that mimics the progression of human disease, including PanIN formation (Hingorani et al., 2003) (Aguirre et al., 2003). While in mouse models both acinar cells and ductal cells can give rise to pancreatic cancer, acinar cell origin is the most frequent (De La et al., 2008), (Kopp et al., 2012), (Habbe et al., 2008), (von Figura, Fukuda, et al., 2014).

Acinar cells are highly plastic: upon tissue damage, they downregulate expression of digestive enzymes and acquire a duct-like differentiation status through a process known as acinar-to-ductal metaplasia (ADM). Acinar cells that have undergone ADM can be distinguished from ductal cells due to their unique expression of acinar progenitor factors (Roy et al., 2016). In the context of acute injury, ADM is reversible, and the acinar parenchyma is re-established over time. However, expression of oncogenic KRAS prevents ADM reversal and the duct-like cells instead undergo neoplastic transformation (Morris, Wang, & Hebrok, 2010). The cell intrinsic mechanisms regulating the balance between cellular plasticity and carcinogenesis have been extensively studied. ADM is driven by fundamental changes in the transcriptional regulation of acinar cells, with acinar transcription factors restraining and ductal transcription factors promoting this process (for review see (Krah & Murtaugh, 2016)). For example, reduction of expression of the acinar transcription factors PTF1a, MIST1 or NR5A2 promote transformation, while forced expression of MIST1 and PTF1a protect acinar cells from de-differentiation (Cobo et al., 2018; Krah et al., 2015; Krah et al., 2019; G. Shi et al., 2013; Tuveson et al., 2006; von Figura, Morris, et al., 2014). ADM is also regulated by intracellular signaling, including a requirement for epithelial MAPK activation (Collins, Yan, Sebolt-Leopold, & Pasca di Magliano, 2014; Collisson et al., 2012). Recently, epigenetic reprogramming driven by oncogenic KRAS has emerged as a key determinant of progression/redifferentiation of acinar cells upon injury (Alonso-Curbelo et al., 2021).

While the cell autonomous (i.e., intrinsic) effects of oncogenic KRAS activation have been extensively studied, the non-cell autonomous effects are less understood. Here, we set out to investigate how oncogenic KRAS -expressing cells affect the microenvironment, which we refer to as “extrinsic” KRAS signaling. To understand the role of oncogenic KRAS in established PanINs, we take advantage of a unique model of pancreatic cancer, the iKras mouse, that allows

inducible and reversible expression of the oncogene (Collins, Bednar, et al., 2012; Ying et al., 2012). PanIN formation is accompanied by accumulation of a precursor lesion microenvironment (PME), with activation of fibroblasts (for review see (Helms et al., 2020)) and infiltration of immune cells. The latter are largely immune suppressive (Clark et al., 2007), and include myeloid cells that both suppress T cell responses and directly promote pancreatic cancer progression (Mitchem et al., 2013; Y. Zhang, A. Velez-Delgado, et al., 2017). Myeloid cells support ADM (Liou et al., 2013) and are required for sustaining ADM and promoting progression to PanIN (Y. Zhang, W. Yan, et al., 2017). Conversely, myeloid cells are also required for tissue repair both in the setting of injury and redifferentiation (Criscimanna, Coudriet, Gittes, Piganelli, & Esni, 2014; Y. Zhang, W. Yan, et al., 2017). Further, experimental induction of acute pancreatitis with its associated inflammation synergizes with oncogenic KRAS to accelerate the formation of ADM and PanIN (Carriere, Young, Gunn, Longnecker, & Korc, 2009; Guerra et al., 2011). Thus, inflammation both accompanies and promotes carcinogenesis, but the relationship between epithelial cells and surrounding stroma in this process remains unclear.

In this study, we dissected the role of oncogenic KRAS in driving the formation and maintenance of the PME. We discovered that fibroblast reprogramming occurs during the earliest stages of carcinogenesis in a JAK/STAT3 signaling-dependent manner, resulting in the activation of an inflammatory gene expression program that includes multiple cytokines known to drive the tumor-promoting functional status of myeloid cells infiltrating the pancreas. Consequently, approaches to inhibit fibroblasts reprogramming during carcinogenesis should be explored to prevent, and possibly reverse, KRAS-driven carcinogenesis.

## 2.3 Results

### Extrinsic signaling by oncogenic Kras reprograms the pancreas microenvironment

To study the recruitment of immune cells by oncogenic Kras-expressing tumor cells, we used Ptf1a$^{Cre/+}$;R26$^{rtTa\text{-}ires\text{-}EGFP/rtTa\text{-}ires\text{-}EGFP}$;TetO-Kras$^{G12D}$ mice (hereby **iKras**) that express oncogenic Kras$^{G12D}$ in pancreatic epithelial cells in an inducible and reversible manner upon Doxycycline (DOX) administration (Collins, Bednar, et al., 2012). Initially, we activated Kras$^{G12D}$ in adult mice (6-12 weeks old) by feeding iKras mice or littermate controls (lacking either Cre or Kras$^{G12D}$ expression) DOX chow for 3 days, 1 week or 2 weeks (See scheme in **Fig. 2.1A**). Pancreata from iKras mice appeared largely histopathologically normal 3 days following Kras$^{G12D}$ activation, with the parenchyma largely composed of acinar cells and CK19 expression confined to the ducts (**Fig. 2.1B-2.1D**). One week after Kras$^{G12D}$ induction, although the pancreas is largely histologically normal, we observed focal ADM accompanied by an increase in the proliferation marker Ki67 that became more widespread by 2 weeks (**Fig. 2.1B, 2.1C** and **2.1E**). Three days after Kras$^{G12D}$ induction, we observed patchy epithelial expression of phosphorylated ERK (p-ERK), indicating activation of the MAPK pathway (**Fig. 2.1F)** in otherwise histologically normal areas. At later time points (1 and 1 weeks), areas of apparent ADM had elevated p-ERK staining (**Fig. 2.1F**), while the remainder of the pancreas had patchy expression of p-ERK. The limited expression of p-ERK even as all pancreas epithelium expresses Kras$^{G12D}$ in this model is consistent with the known requirement of stimulation by various upstream factors to fully activate Kras$^{G12D}$ signaling, including myeloid-derived EGFR ligands (Wen et al., 2019) (C. M. Ardito et al., 2012; Navas et al., 2012).

Next, we investigated the dynamics of immune infiltration and the presence of activated fibroblasts (as marked by expression of smooth muscle actin, SMA). Co-immunofluorescence and

immunohistochemistry analysis revealed the presence of macrophages surrounding untransformed p-ERK-expressing acinar cells as early as 3 days post-Kras$^{G12D}$ activation (**Fig. 2.1F** and **2.2A**), while T cells were rare at this stage (**Fig. 2.1D and 2.2B**). Macrophages increased by 1 and 2 weeks post-Kras$^{G12D}$ activation, and T cells, including CD8$^{+}$ T cells, were easily detected at these timepoints, at least in the ADM areas **(Fig. 2.1D, 2.1F, 2.2A and 2.2B)**. Infiltrating macrophages were largely negative for the immunosuppressive marker ARG1 (**Fig. 2.2C**). ADM clusters at this stage were also surrounded by SMA$^{+}$ fibroblasts (**Fig. 2.1D-2.1F**). We then examined the areas of the pancreas that were morphologically normal at the 1-week timepoint (majority of the pancreas) (**Fig. 2.2D**). Interestingly, high-magnification images revealed morphologically normal clusters of acini with elevated p-ERK surrounded by both macrophages and a thin layer of SMA$^{+}$ fibroblasts, indicating that changes in the microenvironment precede acinar transdifferentiation. Careful analysis of the tissue from the 3-day timepoint also revealed some p-ERK-expressing acini with surrounding macrophages but without SMA$^{+}$ fibroblasts (**Fig. 2.1F**), but these instances were rare, and we cannot exclude that fibroblasts were present outside the plane of the section. Of note, the fibroblasts had no expression of p-ERK at this stage (**Fig. 2.2E**). Taken together, our findings are consistent with a model whereby epithelial activation of p-ERK, downstream of oncogenic Kras, is accompanied by fibroblast activation and macrophage infiltration, which precede acinar transdifferentiation.

**Epithelial Kras$^{G12D}$ is required to maintain acinar transdifferentiation and fibroblast accumulation but not immune infiltration**

Acute pancreatitis synergizes with oncogenic Kras to drive neoplastic transformation (Carriere et al., 2009; Collins, Bednar, et al., 2012; Guerra et al., 2011). Previously, we have shown that

iKras mice on DOX ($Kras^{G12D}$ ON) develop widespread early PanIN lesions at three weeks post-pancreatitis induced by Caerulein, and withdrawal of DOX ($Kras^{G12D}$ OFF) at this stage leads to PanIN regression and tissue repair (Collins, Bednar, et al., 2012). Thus, epithelial oncogenic $Kras^{G12D}$ is required to maintain acinar transdifferentiation. Here, using the same experimental strategy we sought to study the potential role of $Kras^{G12D}$ in regulating the precursor lesion microenvironment (PME). Accordingly, we placed iKras and control mice on DOX and then induced acute pancreatitis and harvested the pancreata 3 weeks post pancreatitis (see scheme in **Fig. 2.3A**). Pancreata in iKras mice presented with widespread ADM and low grade PanINs (with intracellular mucin accumulation as shown by PAS staining) and accumulation of fibrotic stroma (**Fig. 2.3B and 2.3C**). Expression of p-ERK was confined to the epithelium when $Kras^{G12D}$ was ON as previously shown (**Fig. 2.3D**) (Collins, Bednar, et al., 2012). In contrast, control mice treated in parallel had normal pancreas architecture. iKras pancreata were also marked by extensive collagen deposition, fibroblast expansion (as detected by Podoplanin) and activation (by SMA expression) (**Fig. 2.3C-2.3H**). To study the effect of $Kras^{G12D}$ inactivation on the PME, we replaced DOX chow with DOX-free chow to inactivate $Kras^{G12D}$ expression in iKras mice (for 3 days or 1 week) 3 weeks post-administration of caerulein (see scheme in **Fig. 2.3A**). The 3-day and 1-week timepoints were chosen to coincide with the early and mid-phases of the pancreatic remodeling process (Collins, Bednar, et al., 2012). As previously described, $Kras^{G12D}$ inactivation led to a drastic reduction in epithelial p-ERK and redifferentiation of acinar cells progressively over time (**Fig.2.3B, 2.3C and 2.3D**) (Y. Zhang, W. Yan, et al., 2017) (Y. Zhang, W. Yan, et al., 2017) (Y. Zhang, W. Yan, et al., 2017) (Y. Zhang, W. Yan, et al., 2017) (Y. Zhang, W. Yan, et al., 2017). We then investigated changes in the stroma following inactivation of $Kras^{G12D}$. We observed a reduction in both total fibroblasts ($podoplanin^+$ cells) and activated, $SMA^+$ fibroblasts

(**Fig. 2.3D, 2.3E, 2.3F** and quantification in **2.3G, 2.3H**), as well as a reduction in collagen deposition (**Fig. 2.3C**). These results are consistent with a requirement for continued oncogenic $Kras^{G12D}$ activity to maintain fibroblast expansion and pancreatic fibrosis.

Myeloid cells, including abundant macrophages, infiltrate early during pancreatic carcinogenesis and are required for sustained ADM and progression to PanIN (Liou et al., 2013; Storz, 2017; Y. Zhang, W. Yan, et al., 2017). Therefore, we endeavored to study the effect of $Kras^{G12D}$ inactivation on macrophages and other myeloid cell infiltration in the pancreas. We performed a combination of flow cytometry (gating strategy in **Fig. 2.4A**) and immunostaining, including multiplex immunofluorescent staining (Opal multiplex IHC, Akoya). As expected, we observed an increase in $CD45^+$ immune cells in the iKras mice at 3w ON compared to control mice (**Fig. 2.4B and 2.4C**). This increase included total myeloid cells ($CD45^+CD11b^+$) as well as macrophages ($CD45^+CD11b^+F4/80^+$) and immature myeloid cells ($CD45^+CD11b^+F4/80^-Ly6C^+Ly6G^+$, often referred to as MDSCs), with the majority being macrophages (**Fig. 2.4B and 2.4D-2.4F**), consistent with the increase in leukocyte infiltration observed in KC mice (Clark et al., 2007). Surprisingly, $Kras^{G12D}$ inactivation resulted in little to no reduction in total immune infiltration, total myeloid cells, or macrophages (**Fig. 2.4B-2.4F**). These results are consistent with the role of myeloid cells during the pancreatic tissue repair process (Y. Zhang, W. Yan, et al., 2017).

**Extrinsic signaling from $Kras^{G12D}$ transformed cells drives myeloid polarization**

As myeloid cell numbers did not change upon $Kras^{G12D}$ inactivation, we sought to determine whether their polarization status was affected. For this purpose, we used mass cytometry (CyTOF) with a panel of ~20 antibodies (Table 2-3). We limited the scope of the CyTOF experiment to the

3 weeks Kras* ON (N=2) and 3 days OFF (N=3) timepoints (See scheme in **Fig. 2.5A**) in order to highlight the short-term effect of Kras* inactivation, prior to extensive tissue remodeling. We visualized the multi-dimensional CyTOF data using tSNE plots (t-distributed stochastics neighbor embedding) and identified 17 distinct immune cell clusters (**Fig. 2.5B-2.5D**). Among T cells, we observed a trend towards increase upon $Kras^{G12D}$ inactivation, but no statistical difference (**Fig. 2.5E**). The myeloid immune landscape was complex, with multiple populations, including heterogeneous macrophage subtypes (**Fig. 2.5B, 2.5C** and **2.5E**). While some populations did not change or trended towards an increase when we compared $Kras^{G12D}$ OFF to $Kras^{G12D}$ ON samples, other populations drastically decreased (**Fig. 2.5E**). Notably, immunosuppressive $ARG1^{+}$ $Ly6C^{+}$ macrophages, granulocytic myeloid derived suppressor cells Gr-MDSCs — defined as $CD45^{+}CD11b^{+}F4/80^{-}Ly6C^{lo}Ly6G^{hi}$, and $CCR1^{+}CD206^{+}$ macrophages, decreased significantly upon $Kras^{G12D}$ inactivation (**Fig. 2.5E and 2.5F**). Down-regulation of $ARG1^{+}$ macrophages was validated by co-immunofluorescent and multiplex immunofluorescent staining (**Fig. 2.6A and 2.6B**). Furthermore, we discovered that p-STAT3, indicating activation of JAK/STAT3 signaling and known to promote the immune-suppressive function of macrophages (Yu, Kortylewski, & Pardoll, 2007)[43], was similarly down-regulated in macrophages and other stromal cells, as well as in epithelial cells, by inactivation of epithelial oncogenic $Kras^{G12D}$ (**Fig. 2.6C**).

As CyTOF and immunostaining are limited by available antibodies, and to identify the differential transcriptional regulations in the stromal cells induced by oncogenic Kras expression in epithelial cells, we performed single cell RNA sequencing (scRNAseq) to elucidate how epithelial $Kras^{G12D}$ expression alters the microenvironment, and in particular, macrophage polarization. We harvested pancreata from mice with $Kras^{G12D}$ ON for 3 weeks plus 3 days (N=2, pooled for submission) or ON for 3 weeks and then OFF for 3 days (N=3, pooled for submission).

The experiment was designed such that pancreata were harvested and processed at the same time to avoid batch effects. The multidimensional scRNAseq data included a total of 5,073 cells overall, with 1,984 cells from the 3w ON sample and 3,089 cells from the 3d OFF sample. The data was analyzed using the Seurat package in R (version 3.2.2) and visualized by UMAP (uniform and manifold approximation and projection) (**Fig. 2.6D**). By comparing the transcriptome of each cluster to known markers of epithelial, immune, and stromal cell types (**Fig. 2.6E**), we identified acinar cells, $CK19^{+}$ epithelial cells (PanIN or ducts), fibroblasts, endothelial cells, and 16 distinct immune cell populations. Similar cell populations were present in both the ON and OFF condition, allowing us to compare gene expression changes upon inactivation of $Kras^{G12D}$ within each. We first assessed gene expression changes in macrophages (**Fig. 2.6F**). Notably, tumor-associated macrophage (Vasquez-Dunddel et al.) markers such as *Arg1* and *Ccr1* were downregulated upon $Kras^{G12D}$ inactivation. We also observed downregulation of Apolipoprotein E (*Apoe*) – a secreted protein that our group recently described as highly expressed in TAMs and as promoting immune suppression in invasive pancreatic cancer (Kemp, Carpenter, et al., 2021). Additionally, we observed downregulation of the complement genes *C1qa*, *C1qb, C1qc* and the transcription factor *Trem2*, which together define TAMs in several malignancies including, as described by our group, primary and metastatic pancreatic cancer (Katzenelenbogen et al., 2020; Kemp, Steele, et al., 2021). These findings are consistent $Kras^{G12D}$ being required to maintain TAM-like macrophage polarization. Conversely, inactivation of $Kras^{G12D}$ induced a "repair-associated" gene expression program, including *Tgfb, Il10*, *Il4*, *Pdgfb* and *Mmps* (**Fig. 2.6F**). While oncogenic Kras is not required to maintain immune infiltration, it extrinsically (non-cell autonomously) regulates macrophage gene expression in PanIN.

**Epithelial Kras$^{G12D}$ drives inflammatory reprogramming of pancreatic fibroblasts.**

We next sought to understand how Kras$^{G12D}$ expression in epithelial cells directed cellular crosstalk to account for the changes in macrophage polarization. To achieve this, we filtered the single cell RNA sequencing data for expression of known ligand and receptor pairs using a published list further curated in our laboratory (Ramilowski et al., 2015; Nina G. Steele et al., 2020). We thus identified potential predicted interactions within the tissue (**Fig. 2.7A**). We then plotted interactions that were induced by oncogenic Kras (hence downregulated upon Kras$^{G12D}$ inactivation). Strikingly, most Kras-driven interactions connected fibroblast expressed ligands with receptors on epithelial cells and immune cells (**Fig. 2.7B, 2.7C**). We then queried the fibroblast gene expression data to identify cytokines specifically expressed in an epithelial Kras$^{G12D}$-dependent manner **(Fig. 2.7D)**. Finally, we selected from that list the genes encoding for cytokines mainly, or exclusively, expressed by fibroblasts, including *Il33, Il6, Cxcl1* and the inflammatory mediators *Saa1* and *Saa3* (the ortholog of human *SAA1*) (**Fig. 2.7E** and **2.8**). Intriguingly, these aforementioned cytokines all have known roles in pancreatic cancer (Djurec et al., 2018; Lesina et al., 2011; J. Li et al., 2018; Mace et al., 2016; Y. Zhang et al., 2013). Conversely, the respective receptors for these secreted factors were expressed by immune cells, including *Cxcr2* (CXCL1 receptor) on immature myeloid cells, *Il6r* (IL6 receptor)*, P2rx7 and Scarb1* (SAA3 and SAA1 receptors) on several myeloid populations*,* and *Il1rl1* (IL33 receptor also known as ST2) on macrophages, regulatory T cells (Tregs), mast cells, and innate lymphoid cells type 2 (ILC2). Thus, fibroblasts are extrinsically reprogrammed by Kras$^{G12D}$ epithelial cells to activate a gene expression profile that includes cytokines with cognate receptors expressed by myeloid cells, and with a known role in driving myeloid cell/macrophage mediated immune suppression.

To investigate the mechanism of fibroblast reprogramming, we used an *in vitro* approach. We harvested conditioned media (CM) from iKras cells derived from a Ptf1a$^{Cre/+}$;R26$^{rtTa\text{-}ires\text{-}EGFP/rtTa\text{-}ires\text{-}EGFP}$;TetO-Kras$^{G12D}$;Trp53$^{R172H/+}$ (iKras;P53) mouse tumor (Collins, Brisset, et al., 2012); the inclusion of mutant *Trp53* being required for growth in cell culture. In brief, iKras cells (Collins, Brisset, et al., 2012) were grown in the presence of DOX, thus expressing Kras$^{G12D}$. Then, media was changed to either DOX-containing or DOX-free media, thus maintaining Kras$^{G12D}$ expression or inactivating it, respectively. After 48-72 hours, we harvested CM from each condition and boiled half of it to denature heat-labile components. CM was then administered to cultured primary mouse fibroblasts (CD1WT and B6318) derived from healthy adult pancreata as previously described (Mathew, Collins, et al., 2014) (Kemp, Carpenter, et al., 2021) (**Fig. 2.9A**). Compared to control DMEM media, CM from iKras cells induced expression of *Cxcl1, Il6, Il33* and *Saa3* in fibroblasts in a Kras$^{G12D}$ dependent manner (**Fig. 2.9B**), recapitulating the *in vivo* results. To distinguish between a Kras$^{G12D}$-dependent protein factor or metabolite signaling to fibroblasts, we compared intact CM with boiled CM, and found that the latter induced *Il6* but none of the genes encoding the other cytokines of interest (**Fig. 2.9B**). Thus, a combination of cancer cell-derived, Kras$^{G12D}$-dependent heat-labile factors such as proteins and metabolites mediated fibroblast reprogramming. Oncogenic Kras regulates the intracellular metabolome of pancreatic cancer cells (Ying et al., 2012). We enquired whether the extracellular metabolome is similarly dependent on expression of oncogenic Kras. Indeed, mass spectrometry-based metabolomics profiling revealed numerous extracellular metabolites whose abundance changed depending on Kras$^{G12D}$ expression (**Fig. 2.9C and 2.9D**). Among these, several released metabolites have been reported to act as direct extracellular signaling molecules (e.g. pyruvate, lactate, alpha-ketoglutarate) while, alternatively, the decreased abundance of other metabolites may impact signaling downstream of

mTOR (e.g. arginine, isoleucine, cystine, glutamine) (**Fig. 2.9D**) (Colegio et al., 2014; Hooftman & O'Neill, 2019; Saxton & Sabatini, 2017; Wu et al., 2020). We then interrogated the extracellular metabolite composition following incubation of the iKras$^{G12D}$ conditioned medium from the various conditions described above. We observed that the lactate concentration was not affected while pyruvate was depleted upon culturing with fibroblasts (**Fig. 2.9E**). Thus, it appears that fibroblasts consume pyruvate from the medium, an intriguing finding given that fibroblasts serve as a source of pyruvate in breast cancer (Becker et al., 2020).

We then interrogated the list of secreted factors expressed by Kras$^{G12D}$ expressing epithelial cells in the single-cell sequencing data. We noted, among others, expression of *Hbegf, Tnf, Pdgfa, Pdgfb, Hgf* and *Il6* (**Fig. 9F**). Expression of *Hbegf*, *Tnf* and *Pdgfa* was higher in epithelial cells, whereas *Hgf*, *Il6* and *Pdgfb* were higher in fibroblasts. Given the multitude of factors, we reasoned that we were unlikely to identify a single factor driving fibroblast reprogramming. We focused instead on signaling pathways that might be activated in fibroblasts. *In vivo*, we observed expression of p-STAT3, but not p-ERK, in PDGFR$^{+}$ or SMA$^{+}$ fibroblasts when Kras$^{G12D}$ is ON in iKras mice (**Fig. 2.10A and 2.10B**). Similar to the p-STAT3 expression within macrophages (**Fig. 2.6C)**, p-STAT3 expression in fibroblasts was downregulated upon Kras$^{G12D}$ inactivation, identifying it as a potential mediator of fibroblast reprogramming (**Fig. 2.10A**). In contrast, p-ERK was upregulated in fibroblasts upon Kras$^{G12D}$ inactivation (**Fig. 2.10B**), consistent with its role during tissue repair (Collins et al., 2014; Y. Zhang, W. Yan, et al., 2017). We then repeated the *in vitro* experiment described above, this time inhibiting JAK/STAT signaling using Ruxolitinib (JAKi) (**Fig. 2.10C** and **2.10D**). CM-induced fibroblast expression of *Cxcl1*, *Il33, Saa3* and *Il6* was inhibited by JAKi (**Fig. 2.10E** and **2.10F**). Thus, *in vitro*, activation of fibroblast JAK/STAT3 signaling is required for epithelial cell induced reprogramming.

We then studied the effect of JAK/STAT inhibition *in vivo*. We administered DOX to iKras mice and induced acute pancreatitis; three weeks later, the mice were randomized Ruxolitinib (JAKi, 180mg/kg) or vehicle daily for 3 days (**Fig. 2.11A**). As expected, pSTAT3 was reduced upon JAKi treatment (**Fig. 2.11B and 2.11C**). Intriguingly, histology analysis showed that the pancreata of mice treated with the JAKi had fewer PanIN lesions and more acini areas when compared to vehicle treated mice (**Fig. 2.11B, 2.11D and 2.11E).** We also observed reduction on $SMA^+$ fibroblasts (**Fig. 2.11F**). Although the number of $F4/80^+$ macrophages did not change in JAKi treated mice, the number of $ARG1^+$ macrophages tended towards decreasing (**Fig. 2.11G and 2.11H**). Thus, inhibition of JAK/STAT in early PanINs partially reversed tumorigenesis and drove stromal remodeling.

## 2.4 Discussion

In summary, our results showed that oncogenic $Kras^{G12D}$ in epithelial cells drives the recruitment of macrophages and activates fibroblasts prior to ADM formation. Further, continuous $Kras^{G12D}$ expression is required for fibroblast reprogramming, including expression of an inflammatory gene expression panel with cytokines known to be key mediators of macrophage polarization in pancreatic cancer. Thus, $Kras^{G12D}$ signaling drives formation and maintenance of an immune suppressive stroma from early stages of carcinogenesis in an extrinsic manner.

Mutations in the *KRAS* gene are present in most human pancreatic cancers (Biankin et al., 2012) and have a high prevalence in PanINs (Kanda et al., 2012). To date, the only clinically available KRAS inhibitor targets the $KRAS^{G12C}$ mutant form (Canon et al., 2019; Wilhelm et al., 2006), which is exceedingly rare in pancreatic cancer (Ying et al., 2016). Thus, understanding the downstream effects of oncogenic KRAS signaling is essential to design alternative targeting strategies. Further, even when/if inhibitors of the more common $KRAS^{G12D}$ and $KRAD^{G12V}$

mutations become available, resistance to single agent targeting is to be expected, and understanding what agents might synergize with KRAS inhibition essential. Oncogenic Kras expression in pancreatic cancer has been associated with immune evasion (Irene Ischenko et al., 2021); in lung cancer, KRAS and MYC cooperate to shape the immune microenvironment (Kortlever et al., 2017).

Pancreatic cancer is characterized by an extensive tumor microenvironment (TME) rich in fibroblasts and suppressive immune cells. PanIN formation is similarly accompanied by accumulation of a fibroinflammatory stroma, which we refer to as PME, precursor lesion microenvironment (Clark et al., 2007). The mechanisms underlying the formation of the PME are poorly understood. In the current study, we set out to understand how the interplay between epithelial cells expressing oncogenic Kras and the surrounding components of the pancreatic microenvironment regulate the balance between tissue repair and carcinogenesis. We exploited the iKras genetically engineered mouse model (Collins, Bednar, et al., 2012) where oncogenic Kras can be activated and inactivated at will, to understand how inactivation of oncogenic Kras affects the precursor lesion microenvironment. Our results show that immune infiltration is not reduced upon $Kras^{G12D}$ inactivation, but polarization of macrophages and other myeloid cells is, with epithelial Kras respectively inducing genes expressed in tumor associated macrophages and inhibiting expression of repair promoting factors, consistent with previous findings by our group (Y. Zhang, W. Yan, et al., 2017). When we investigated the mechanism of this polarity change, we discovered that cytokines known to regulate macrophage polarization are prevalently expressed by fibroblasts and extrinsically regulated by oncogenic Kras. Thus, our work supports the notion to target fibroblasts to reverse their reprogramming and block the activation of inflammatory

pathways in the pancreas. Mechanistically, we show that a combination of epithelial factors drives fibroblast reprogramming, and that reprogramming can be inhibited by blocking the JAK/STAT3 signaling pathway.

Our work is complementary with studies in later stages of carcinogenesis, where oncogenic KRAS blocks anti-tumor immune responses (I. Ischenko et al., 2021). Further, changes in the microenvironment can mediate escape from oncogenic Kras dependence (Hou et al., 2020). Here, we identify fibroblasts as a key mediator of the extrinsic role of oncogenic KRAS and identify JAK/STAT3 signaling as required for fibroblast reprogramming and a potential target to reverse this process.

Based on our data, fibroblasts are a source of multiple cytokines that are dependent on epithelial $Kras^{G12D}$ expression: some are expressed by other cell types (*Il33* and *Il6*), while others are uniquely fibroblast specific (*Cxcl1, Saa1* and *Saa3*). Recently, IL33 has been described as expressed by epithelial cells during the early stages of carcinogenesis and noted to promote neoplastic progression (Alonso-Curbelo et al., 2021); interestingly, we found that IL33 is also highly expressed by fibroblasts in early tumorigenesis stages, while its receptor is expressed by multiple immune cell populations. Fibroblasts are also a source of IL6, with a known role in pancreatic cancer progression (Fukuda et al., 2011; Lesina et al., 2011; Y. Zhang et al., 2013); Saa3 (ortholog to human SAA1), an apolipoprotein required for neoplastic progression (Djurec et al., 2018) and CXCL1, which has been studied in epithelial cells, and shown to be a key moderator of T cell exclusion in malignant disease (J. Li et al., 2018). In our study, fibroblasts emerged as mediators of epithelial/immune cell crosstalk during the onset of pancreatic carcinogenesis. We found that fibroblasts are reprogrammed when exposed to CM from oncogenic Kras-expressing epithelial cells, supporting direct communication between these cell types. Interestingly, while the

majority of cytokines we assessed in fibroblasts required a heat-labile component of the conditioned media, *Il6* did not, implying that a combination of Kras $^{G12D}$-dependent signals are required for establishing a complete reprogramming of pancreatic fibroblasts, potentially including both peptide and metabolic secreted factors (See Scheme in **Fig. 2.12**).

The role and origin of fibroblasts in pancreatic cancer remains poorly understood. Fibroblasts secrete a number of cytokines that influence the immune milieu (for example, CXCL12, which has been shown to reduce T cell infiltration in pancreatic cancer), and as such they promote cancer growth (Feig et al., 2013). However, in other models, fibroblast depletion promotes carcinogenesis (Ozdemir et al., 2014). These contradictory findings might be explained by the heterogeneity of fibroblast populations. In recent years, the nature and origin of fibroblasts in advanced disease have been addressed by several studies, and previous assumptions regarding these cell populations have been challenged. Cancer-associated fibroblasts (CAFs) have been long assumed to derive from a pancreatic stellate cell (PSC) population in the pancreas (similar to hepatic stellate cells), but recent lineage tracing work by our group has revealed that a substantial proportion of CAFs derive from perivascular fibroblasts present in the normal pancreas (Garcia et al., 2020). Accordingly, a lineage tracing study following PSCs in pancreatic cancer showed that they only contribute to a small subset of CAFs (Erin J. Helms et al., 2021). *In vitro* characterization and, more recently, scRNAseq studies have identified CAF subsets with specific transcriptional signatures and functional roles (Biffi et al., 2019; Elyada et al., 2019; Ohlund et al., 2017).

In advanced disease, fibroblasts have been classified as myCAFs, expressing high levels of SMA and genes encoding for extracellular matrix components, and iCAF, inflammatory fibroblasts secreting cytokines such as IL6 (Biffi & Tuveson, 2021; Ohlund et al., 2017). Formation of iCAFs is dependent on IL1 and JAK/STAT3 signaling (Biffi et al., 2019). While

fibroblast heterogeneity has been described in precursor lesions (Hosein et al., 2019), whether the biological function of different fibroblast subsets is similar in early and advanced disease is not known. Here, we show that fibroblasts activated during the earliest stages of carcinogenesis have elevated SMA, but are also source of inflammatory cytokines such as IL6; further, fibroblast activation, including SMA expression, requires JAK/STAT3 signaling. This suggests that the reported iCAF/myCAF dichotomy in established tumors is not as distinct in premalignant lesions. Whether other populations, such as the antigen presenting apCAFs (Elyada et al., 2019), are recapitulated in early lesions remains to be determined. Analysis of the myeloid cells revealed other differences in the PME compared to the TME. In the earliest stages of Kras activation, macrophages have low/no expression of Arginase 1, while expression is elevated in established PanINs and in pancreatic cancer. This observation recapitulates earlier functional studies on the role of macrophages in pancreatic carcinogenesis. In the PME, macrophages promote PanIN formation/progression independently from their ability to inhibit $CD8^+$ T cell responses, likely through direct signaling to epithelial cells (Y. Zhang, W. Yan, et al., 2017). In contrast, in advanced disease, the main role of macrophages is to inhibit anti-tumor immunity (Mitchem et al., 2013; C. W. Steele et al., 2016a; Y. Zhang, A. Velez-Delgado, et al., 2017). Our findings thus highlight profound differences between the PME and the TME, and raise the question as to whether fibroblasts are equally required to regulate production of inflammatory cytokines in the TME, or whether they become dispensable at later stages. It is also possible that different tumor types, such as basal and classical, have different reliance on fibroblasts, an area of future exploration.

In this study, we close the loop on communication between epithelial cells, fibroblasts and immune cells. Reprogramming of myeloid cells to alleviate the profound immune suppression of pancreatic cancer is a key concept in potential therapeutic approaches (Beatty et al., 2011; Y. Zhu

et al., 2014). Unfortunately, the initial results from clinical trial testing of a CD40 agonist administered to reprogram myeloid cells combined with immune checkpoint inhibition and chemotherapy did not benefit the majority of patients (O'Hara et al., 2021), pointing to the need for yet additional avenues by which to target the microenvironment. Our current work suggests that fibroblast reprogramming should be considered in high-risk patients to prevent malignant progression and could also be explored to prevent tumor relapse in surgical patients. Finally, our study provides another piece of the puzzle in our understanding of the events that lead to the onset and progression of pancreatic cancer, and as such contribute to our fundamental knowledge of this deadly disease.

## 2.5 Methods

### *Mice*

Mice were housed in the specific pathogen-free animal facility at the Rogel Cancer Center, University of Michigan, and overseen by the unit for laboratory animal medicine (ULAM). Ptf1a(p48)-Cre;Rosa26$^{rtTa/rtTa}$ mice were crossed to TRE-Kras$^{G12D}$;R26$^{rtTa/rtTa}$ to generate the p48-Cre;TRE-Kras$^{G12D}$;R26$^{rtTa/rtTa}$ (iKras*), as described (Collins, Bednar, et al., 2012). Expression of Kras $^{G12D}$ was induced in adult mice (8-14 weeks old) by replacing regular chow with Doxycycline chow (Bio-Serv, 1gm/kg). Acute pancreatitis was induced by administering eight hourly doses of caerulein (75$\mu$g/kg, Sigma-Aldrich) intraperitoneally for two consecutive days. For JAK/STAT pathway inhibition, the JAK1/2 inhibitor Ruxolitinib (INCB18424, MedChemExpress) was administered orally once a day for total four doses at 180mg/kg in 100$\mu$l of 10% DMSO in corn oil. Control mice received vehicle in parallel. All animal studies were conducted in compliance with the guidelines of the Institutional Animal Care & Use Committee (IACUC) at the University of Michigan.

***Histology and Immunohistochemistry***

Pancreatic tissue samples from experimental and control mice were fixed in 10% neutral-buffered formalin (FisherBrand) overnight and then embedded in paraffin and sectioned into slides. Hematoxylin and Eosin (H&E), Gomori's Trichome, Periodic Acid-Schiff (PAS) and Immunofluorescence (IF) staining were performed as previously described (Collins, Bednar, et al., 2012). For immunohistochemistry, fresh cut paraffin sections were re-hydrated using 2 series of xylene, 2 series of 100% ethanol and then 2 series of 95% ethanol. Water was used to wash all residues from previous washes. Antigen retrieval was performed using Antigen Retrieval CITRA Plus (BioGenex) and microwaved for total 8 minutes. Upon cool down, sections were blocked using 1% BSA in PBS for 30 minutes and then primary antibodies (for details see Table 2.1) were used at their corresponding dilutions. Primary antibody incubation was performed at 4°C overnight. Biotinylated secondary antibodies were used in 1:300 dilution and applied to sections for 45 minutes at room temperature. Following secondary antibody incubation, sections were incubated for 30 minutes with the ABC reagent from Vectastain Elite ABC Kit (Peroxidase), followed by DAB (Vector). For immunofluorescence (IF), Alexa fluor secondary antibodies (Invitrogen) were used, then slides were mounted with Prolong Diamond Antifade Mountant with DAPI (Invitrogen). TSA Plus Fluorescein system (PerkinElmer) was used in IF for mouse primary antibodies. Olympus BX53F microscope, Olympus DP80 digital camera, and CellSens Standard software were used for imaging. Quantification of positive cell number or area was done by ImageJ using 3-5 images/slide (200x or 400x magnification) taken from 2-4 samples per group. We also use the Leica STELLARIS 8 FALCON Confocal Microscopy System and the LAS X software to acquire and visualize images.

### *Multiplex IHC Staining and Analysis*

Multiplex immunohistochemistry staining was performed on paraffin embedded pancreatic tissue sections as follows. Slides were baked in a hybridization oven for one hour at 60 degrees Celsius, cooled for 10 minutes at room temperature, then dipped sequentially (x3) into xylene for 10 minutes each for removal of paraffin. Slides were then rehydrated in alcohol with dilutions of 100%, 95%, then 70% for 10 minutes each, followed by a wash in deionized water for 2 minutes. Slides were then placed in neutral buffered formalin for 30 minutes. The slides were then washed for 2 minutes in deionized water then microwaved at 100% power in Rodent Decloaker (Biocare Medical) for 30 seconds, the power level was reduced to 20% and microwaving continued for an additional 10 minutes followed by a resting step of 15 minutes at room temperature. Microwaving continued at 10% power for an additional 10 minutes. Prior to microwaving with Rodent Decloaker, plastic wrap was secured on top of the microwave-proof slide box with rubber bands and a partial opening for steam escape to prevent loss of solution. After the last microwaving step, slides were left to cool until slides and solution achieved room temperature. The multiplex staining was performed for each primary-color combination. Slides were placed in a deionized water wash for two minutes followed by a TBST wash for 2 minutes. Slides were placed in a slide incubation chamber and Bloxall was applied for 10 minutes followed by an additional blocking step of 1% BSA (in TBST) for 20 minutes, primary antibody was applied after tapping slide to remove the primary antibody and was left to incubate for 1 hour, slides were washed in TBST (x3) for 2 minutes each, secondary antibody was applied, followed by TBST wash (x3) for 2 minutes each, Opal color was applied for 10 minutes and a TBST wash (x3) for 2 minutes each was performed. The slides were then microwaved with either AR6 or AR9 for 45 seconds at 100% followed by 15

minutes at 20%. The previous steps were then repeated for each of the following antibodies and Opal colors in exact listed order: 1) F4/80 at 1:600 (abcam ab6640), 2) CD3 at 1:400 (Dako A0452)-TSA 520, 3) CD8 at 1:400 (Cell Signaling 98941), 4) Arginase 1 (ARG1) at 1:100 (Cell Signaling 93668), 5) CK19 at 1:400 (Max Plank Institute Troma III). After the last application of multiplex was completed, slides were washed as above and placed in AR6, then microwaved. After cooling the slides were washed in deionized water followed by TBST for 2 minutes each. Opal spectral DAPI solution was applied (3 drops diluted in 1mL of TBST for 10 minutes followed by a wash in TBST for 30 seconds. Coverslips were mounted with Prolong Diamond, slides were left to lie flat overnight away from light. If the entire multiplex could not be completed without interruption, the slides were left in AR6 or AR9 after a microwaving step, covered from light until the next day. All primary antibodies were diluted in 1% BSA and all TSA Opal colors were diluted in TSA diluent at 1:50.

The Mantra Quantitative Pathology Work Station was used to image sections of each of the slides. One to three images per slide was captured at ×20 magnification. Cube filters (DAPI, CY3, CY5, CY7, Texas Red, Qdot) were used in taking each image capture. All images were analyzed using inForm Cell Analysis software (Akoya Biosciences). Sixty-three images of encompassing the 26 different control and experimental slides were batched analyzed after using a mouse formulated library consisting of each single TSA fluorophore listed above. Unmixing was performed and no spectral overlap was found between fluorophores. Using inForm version 2.3.0 training software, cell compartments were segmented into nucleus, cytoplasm, and membrane. DAPI was used to identify the nucleus of the cells and determine their shape and size. The cytoplasm was segmented using ARG1 (Opal 650), F4/80 (Opal 540), and CD3 (Opal 520). The inner distance to the nucleus was set at zero pixels and the outer distance of the nucleus was set at

6 pixels. The membrane was segmented using CK19 (Opal 690) with the max cell size set at 25 pixels from nucleus to the membrane, each pixel is 0.496 microns. X and Y coordinates were assigned to each identified cell in each image. Cell phenotypes (T cell, macrophage, epithelial cell, acinar cell, other cell) were manually selected at random throughout the 63 images. T cell, macrophage, and epithelial cells were selected based on single staining of CD3 (Opal 520), F4/80 (Opal 540), and CK19 (Opal 690) respectfully. Other cells were manually selected based on the lack of staining of the above listed fluorophores and acinar cells were labeled based on the lack of listed fluorophores and tissue morphology. Fluorescent intensity of ARG1 (Opal 650) in the nucleus at a max threshold of 200 and a positivity threshold level of 13 was used to identify $ARG1^+$ cells. R programs were used to make complex phenotypes by combining the primary cell phenotypes (T cell, macrophage, epithelial cell, acinar cell, and other cell) and the positivity thresholds for $CD8^+$ and $ARG1^+$ (Table 2.5).

***Flow cytometry***

Pancreata were harvested and dissociated to single cells by mincing the tissue finely using scissors followed by Collagenase IV (1 mg/ml, Sigma) digestion for 30 minutes at 37°C while shaking. A 40um mesh strainer was used to separate single cells. RBC lysis buffer (eBioscience) was used to lyse all the red blood cells. Live cells were stained for surface markers using the antibodies listed in Table 2.2. The cells were either fixed after the primary antibody staining and use for analysis or the cells were fixed and permeabilized before intracellular staining using antibodies in Table 2.2. Flow-cytometric analysis was performed on the Cyan ADP analyzer (Beckman coulter) and the ZE5 analyzer (Bio-Rad). Data were analyzed using the FlowJo v10 software.

### *CyTOF*

Pancreas was harvested and disrupted to single cells as described above. Three mesh strainers were used: 500um, 100um and 40um, to separate single cells. Cells were washed twice in PBS and incubated with Cell-ID cisplatin (1.67 umol/L) for 5 min at room temperature (RT), as a viability marker. Surface and intracellular staining was performed as detailed in manufacturer instructions (Fluidigm) with the antibodies listed in Table 2.3. Cells were shipped in intercalator buffer on ice overnight to the Flow Cytometry core at the University of Rochester Medical Center, where sample preparation was finalized, and CyTOF2 Mass Cytometer (Helios) analysis was performed. Data analysis was performed using the Premium CytoBank Software (cytobank.org) and R studio using the CyTOF workflow from Nowicka M. Et. al. (Nowicka et al., 2017).

### *Single-cell RNA sequencing*

Pancreatic tissues were mechanically minced and enzymatically digested with collagenase IV (1 mg/ml in RPMI). Cell suspensions were subsequently filtered through 500-μm, 100-μm, and 40-μm mesh to obtain single cells. Dead cells were removed using the MACS Dead Cell Removal Kit (Miltenyi Biotec). The resulting single cell suspensions were pooled by experimental group (Kras ON/Kras OFF). Single-cell complementary DNA libraries were prepared and sequenced at the University of Michigan Advanced Genomics Core using the 10× Genomics Platform (Raw and processed data are available at GSM4175981 and GSE179846). Samples were run using 50-cycle paired-end reads on the HiSeq 4000 (Illumina) to a depth of 100,000 reads. The raw data were processed and aligned by the University of Michigan DNA Sequencing Core. Cell Ranger count version 3.0.0 was used with default settings, with an initial expected cell count of 10,000. R version

3.6.2, RStudio version 1.2.5033, and R package Seurat version 3.2.2 were used for scRNA-seq data analysis (RStudio Team RStudio: Integrated Development for R (RStudio, 2015); http://www.rstudio.com/; R Core Development Team R: A Language and Environment for Statistical Computing (R Foundation for Statistical Computing, 2017); https://www.R-project.org/ (Stuart et al., 2019) (Butler, Hoffman, Smibert, Papalexi, & Satija, 2018) ). Data were initially filtered to only include cells with at least 100 genes and genes that appeared in more than three cells. Data were normalized using the NormalizeData function with a scale factor of 10,000 and the LogNormalize normalization method. Data were then manually filtered to include only cells with 1,000-60,000 transcripts and <15% mitochondrial genes. Variable genes were identified using the FindVariableFeatures function. Data were scaled and centered using linear regression of transcript counts. PCA was run with the RunPCA function using the previously defined variable genes. Cell clusters were identified via the FindNeighbors and FindClusters functions, using dimensions corresponding to approximately 90% variance as defined by PCA. UMAP clustering algorithms were performed with RunUMAP. Clusters were defined by user-defined criteria. The complete R script including figure-specific visualization methods is publicly available on GitHub (https://github.com/PascaDiMagliano-Lab/).

For Interactome analysis, ligand–receptor pairs were defined based on a curated literature-supported list in Ramilowski *et al.* (Ramilowski et al., 2015), further curated as described in (Nina G. Steele et al., 2020). The average expression values of ligands and receptors in each cell population for both experimental groups (Kras ON/Kras OFF) were calculated individually, and ligands and receptors expressed below a user-defined threshold (median average expression) were removed from analysis. Ligand–receptor pairs were also excluded if the ligands and receptors were not expressed in both experimental groups. Differences in the ligands and receptors between

groups were determined using the Wilcoxon ranked test, and P values were adjusted for multiple comparisons using the Bonferroni correction method. Ligands and receptors were considered significantly different if $P < 0.05$. The resulting data table was visualized using Cytoscape (version 3.7.2) software (Shannon et al., 2003). The complete R script is publicly available on GitHub (https://github.com/PascaDiMagliano-Lab/). The Circos plot was built with the Circos software (version 0.69-9) and the heatmap values within the circus plot displays the average expression of each fibroblast ligand and their corresponding receptor across the iKras pancreatic tissue.

***Cell culture***

All cell lines were cultured in DMEM with 10% Fetal Bovine Serum and 1% Penicillin Streptomycin. The tumor cell line (9805) was derived from an iKras$^{G12D}$P53$^{R172H}$(ptf1a-Cre; TetO-Kras$^{G12D}$;Rosa26$^{rtTa/+;}$ p53$^{R172H/+)}$ pancreatic cancer (Collins, Brisset, et al., 2012). The fibroblasts cell lines, CD1WT and B6318, were derived from wild type pancreata of a mixed or C57BL/6J background, respectively. The 9805 cell line was maintained in Doxycycline-containing (1ug/mL) medium. To generate conditioned media, fresh medium containing Doxycycline (Kras $^{G12D}$ ON) or without Doxycycline (Kras $^{G12D}$ OFF) was replaced and harvested after 2-3 days based on cell confluency. The media were then centrifuged (300G, 10 minutes at 4ºC) to remove contaminating cancer cells. The CM was used to culture fibroblasts with a 1:1 ratio of CM to normal DMEM for 2-3 days. An aliquot of the conditioned media before and after culturing fibroblasts was collected for metabolomics analysis (described below). To test the effect of heat labile factors, media were boiled for 10 mins to denature secondary and tertiary peptide structures. For inhibitor experiments, Ruxolitinib (INCB018424, Selleckchem) at 0.1$\mu$M, 0.5 $\mu$M and 5 $\mu$M or Trametinib

(GSK1120212, Selleckchem) 0.1 $\mu$M, 0.5 $\mu$M and 2 $\mu$M or vehicle control were added to the medium.

### *Quantitative RT-PCR*

RNA was extracted using the QIAGEN kit. RNA samples went through Reverse Transcription-PCR (RT-PCR) using the cDNA kit (Applied Biosystems). cDNA samples for quantitative Real Time PCR were prepared using a mix of 1X Fast-SYBR Green PCR Master Mix (Applied Biosystems) and the primers listed in Table 2.4. The reaction conditions were used as previously described (Collins et al. 2012). Cyclophilin A (*Ppia*) was used as housekeeping control.

### *Western Blot*

Cells were lysed using RIPA buffer (Sigma-Aldrich) with protease and phosphatase inhibitors (Sigma-Aldrich). Protein levels were quantified and the same amount of protein was loaded to the wells in a 4-15% SDS-PAGE gel (BioRad). Protein was transferred to a PVDF membrane (BioRad), that was blocked with milk and then incubated with primary antibodies listed in Table 2.1 overnight. HRP-conjugated secondary anti- rabbit and anti-mouse (1:5000) were used and detected by using the enhance Chemiluminescent Substrate (PerkinElmer). The bands were visualized using the ChemiDoc Imaging System (BioRad).

### *Metabolomics analysis*

The conditioned medium from tumor cells and fibroblasts (described above) was aspirated and 1 ml of 80% methanol -cooled in dry ice- was added per well. The plates were incubated on dry ice for 10 min, then scraped and transferred to sample tubes. The samples were vortexed and

centrifuged for 10 min at 13,000 x *g*, 4 °C. Then, 1 ml of the supernatant was aspirated from each tube, transferred to a tightly capped sample tube, and stored at -80 °C until analysis.

Samples were run on an Agilent 1290 Infinity II LC -6470 Triple Quadrupole (QqQ) tandem mass spectrometer (MS/MS) system with the following components: Agilent Technologies Triple Quad 6470 LC-MS/MS system with a 1290 Infinity II LC Flexible Pump (Quaternary Pump), Multisampler and Multicolumn Thermostat with 6 port valves. Agilent Masshunter Workstation Software LC/MS Data Acquisition for 6400 Series Triple Quadrupole MS with Version B.08.02 was used for compound optimization, calibration, and data acquisition.

The following solvents were employed for LC analysis. Solvent A (97% water and 3% methanol 15 mM acetic acid and 10 mM tributylamine, pH of 5), solvent B (15 mM acetic acid and 10 mM tributylamine in methanol) and washing solvent C (acetonitrile). LC system seal washing solvent (90% water and 10% isopropanol) and needle wash solvent (75% methanol, 25% water) were used. Solvents were purchased from the following vendors: GC-grade tributylamine 99% (ACROS ORGANICS), LC/MS grade acetic acid Optima (Fisher Chemical), InfinityLab deactivator additive, ESI –L Low concentration Tuning mix (Agilent Technologies), LC-MS grade water, acetonitrile, methanol (Millipore) and isopropanol (Fisher Chemical).

For LC analysis, 2 µl of sample was injected into an Agilent ZORBAX RRHD Extend-C18 column (2.1 × 150 mm, 1.8 µm) with ZORBAX Extend Fast Guards. The LC gradient profile was: flow rate: 0.25 ml/min, 0-2.5 min, 100% A; 2.5-7.5 min, 80% A and 20% B; 7.5-13 min 55% A and 45% B; 13-24 min, 1% A and 99% B; 24-27min, 1% A and 99% C; 27-27.5min, 1% A and 99% C. Then, at 0.8 ml/min, 27.5-31.5 min, 1% A and 99% C; at 0.6 ml/min, 31.5-32.25 min, 1% A and 99% C; at 0.4 ml/min, 32.25-39.9 min, 100% A; at 0.25 ml/min, 40 min, 100% A. Column temp was maintained at 35℃ while the samples were at 4℃.

For MS analysis, a 6470 Triple Quad MS calibrated with the Agilent ESI-L low concentration tuning mix was used. Source parameters: Gas temp 150℃, gas flow 10 l/min, nebulizer 45 psi, sheath gas temp 325℃, sheath gas flow 12 l/min, capillary -2000 V, Delta EMV -200 V. Dynamic MRM scan type was used with 0.07 min peak width and 24 min acquisition time. Delta retention time of ± 1 min, fragmentor of 40 eV and cell accelerator of 5 eV were incorporated in the method.

The MassHunter Metabolomics Dynamic MRM Database and Method was used for target identification. Key parameters of AJS ESI were Gas Temp: 150℃, Gas Flow 13 l/min, Nebulizer 45 psi, Sheath Gas Temp 325℃, Sheath Gas Flow 12 l/min, Capillary 2000 V, Nozzle 500 V. Detector Delta EMV (-) 200.The QqQ data were pre-processed with an Agilent MassHunter Workstation QqQ Quantitative Analysis Software (B0700). The abundance level of each metabolite in every sample was divided by the median of all abundance levels across all samples for proper comparisons, statistical analyses, and visualization. The statistical significance test was done by a two-tailed t-test with a significance threshold level of 0.05.

Heatmaps were generated with Morpheus, https://software.broadinstitute.org/morpheus.

***Statistics***

We used GraphPad Prism Version 8 software for most of our analysis. The normality was checked in all data sets and either T-test or Mann Whitney was performed for statistical analysis, statistically significant when $p<0.05$. qRT-PCR data were analyzed using multiple comparison ANOVA and considered statistically significant when $p<0.05$.

## 2.6 Acknowledgements

We thank Daniel Long for his histological services. This project was supported by NIH/NCI grants R01CA151588, R01CA198074, the University of Michigan Cancer Center Support Grant (NCI P30CA046592), the American Cancer Society to MPM and U01CA-224145 to MPM and HCC. YZ was funded by NCI-R50CA232985. AVD was supported by Rackham Merit Fellowship, Cellular Biotechnology Training Program (T32GM008353) and the NCI F31-CA247037. KLD, NGS and VRS were funded by the Cancer Biology Training Program T32-CA009676. NGS is also a recipient of the American Cancer Society Postdoctoral Award PF-19-096-01 and the Michigan Institute for Clinical and Healthy Research (MICHR) Postdoctoral Translational Scholar Program fellowship award. REM was supported by the NIH Cellular and Molecular Biology Training Grant T32-GM007315 and the Center for Organogenesis Training Program (NIH T32 HD007505). S.T & A.R were supported by institutional startup funds from the University of Michigan, NCI grants R37CA214955 & NCI P30CA046592 and a Research Scholar Grant from the American Cancer Society (RSG-16-005-01). SBK was supported by NIH T32-GM113900 and NCI F31-CA247076. SAK was supported by F31CA24745701. CAL was supported by the NCI (R37CA237421, R01CA248160) and UMCCC Core Grant (P30CA046592). FB was funded by the Association of Academic Surgery Joel Roslyn Award. TF was supported by (K08CA201581). Metabolomics studies performed at the University of Michigan were supported by NIH grant DK097153, the Charles Woodson Research Fund, and the UM Pediatric Brain Tumor Initiative. This project was also supported by the Tissue and Molecular Pathology and Flow Cytometry Shared Resources at the Rogel Cancer Center and the University of Michigan DNA Sequencing Core. CyTOF was performed at the University of Rochester University of Rochester Medical Center Flow Cytometry Shared Resource and at the

Indiana University Simon Cancer Center Flow Cytometry Service. This work used a Leica STELLARIS 8 FALCON Confocal Microscopy System that was purchased with funds from a National Institutes of Health SIG grant *NIH* S10OD28612-01-A1.

**Author list:**

Ashley Velez-Delgado[1], Katelyn L. Donahue[2], Kristee L. Brown[3], Wenting Du[3], Valerie Irizarry-Negron[3], Rosa E. Menjivar[4], Emily L. Lasse Opsahl[2], Nina G. Steele[1], Stephanie The[5#], Jenny Lazarus[3,##], Veerin R. Sirihorachai[2], Wei Yan[3], Samantha B. Kemp[6], Samuel A. Kerk[2], Murali Bollampally[7], Sion Yang[7], Michael K. Scales[1], Faith R. Avritt[7], Fatima Lima[3], Costas A. Lyssiotis[2,8,9,10], Arvind Rao[2,5,9,11,12], Howard C. Crawford[2,8,9,10###], Filip Bednar[3,9], Timothy L. Frankel[3,9,], Benjamin L. Allen[1], Yaqing Zhang[3,9*] and Marina Pasca di Magliano[1,2,3,4,9*]

[1]Department of Cell and Developmental Biology; [2]Cancer Biology Program; [3]Department of Surgery,

[4]Cellular and Molecular Biology Program; [5] Department of Computational Medicine and Bioinformatics; [6]Molecular and Cellular Pathology Program; [7]Life Sciences and Arts college; [8]Department of Molecular and Integrative Physiology; [9]Rogel Cancer Center; [10]Department of Internal Medicine, Division of Gastroenterology and Hepatology; [11]Michigan Institute of Data Science (MIDAS); [12]Department of Radiation Oncology

University of Michigan, Ann Arbor, MI 48109 USA

[#]current affiliation: Cancer Data Science Shared Resource, University of Michigan, Ann Arbor, MI 48109 USA

[##]current affiliation: Lazarus Medical Corporation, Stonyford, CA 95979 USA.

###current affiliation: Henry Ford Pancreatic Cancer Center, Henry Ford Health System, Detroit, MI 48202, USA.

*Corresponding authors

**Grant support**

This project was supported by NIH/NCI grants R01CA151588, R01CA198074, the University of Michigan Cancer Center Support Grant (NCI P30CA046592), the American Cancer Society to MPM and U01CA-224145 to MPM and HCC. YZ was funded by NCI-R50CA232985. AVD was supported by Rackham Merit Fellowship, Cellular Biotechnology Training Program (T32GM008353) and the NCI F31-CA247037. KLD, NGS and VRS were funded by the Cancer Biology Training Program T32-CA009676. NGS is also a recipient of the American Cancer Society Postdoctoral Award PF-19-096-01 and the Michigan Institute for Clinical and Healthy Research (MICHR) Postdoctoral Translational Scholar Program fellowship award. REM was supported by the NIH Cellular and Molecular Biology Training Grant T32-GM007315 and the Center for Organogenesis Training Program (NIH T32 HD007505). S.T & A.R were supported by institutional startup funds from the University of Michigan, NCI grants R37CA214955 & NCI P30CA046592 and a Research Scholar Grant from the American Cancer Society (RSG-16-005-01). SBK was supported by NIH T32-GM113900 and NCI F31-CA247076. SAK was supported by F31CA24745701. CAL was supported by the NCI (R37CA237421, R01CA248160) and UMCCC Core Grant (P30CA046592). FB was funded by the Association of Academic Surgery Joel Roslyn Award. TF was supported by (K08CA201581). Metabolomics studies performed at the University of Michigan were supported by NIH grant DK097153, the Charles Woodson Research Fund, and the UM Pediatric Brain

Tumor Initiative. This project was also supported by the Tissue and Molecular Pathology and Flow Cytometry Shared Resources at the Rogel Cancer Center and the University of Michigan DNA Sequencing Core. CyTOF was performed at the University of Rochester University of Rochester Medical Center Flow Cytometry Shared Resource and at the Indiana University Simon Cancer Center Flow Cytometry Service. This work used a Leica STELLARIS 8 FALCON Confocal Microscopy System that was purchased with funds from a National Institutes of Health SIG grant *NIH* S10OD28612-01-A1.

The study sponsors did not have a role in the study design, collection, analysis, or interpretation of data.

**CONFLICT OF INTEREST STATEMENT**

CAL has received consulting fees from Astellas Pharmaceuticals and is an inventor on patents pertaining to KRAS regulated metabolic pathways, redox control pathways in pancreatic cancer, and targeting the GOT1-pathway as a therapeutic approach.

**Data transparency:**

All the data and study material will be available. Codes can be found at:

https://github.com/PascaDiMagliano-Lab/Extrinsic-KRAS-signaling-shapes-the-pancreatic-microenvironment-through-fibroblast-reprogramming

iKras* ON: GEO Accession #: GSM4175981
iKras* OFF: GEO Accession #: GSE179846

**Author contributions**

MPM directed the study. AVD, YZ and MPM designed experiments. AVD, KLD, KLB, WD, VIN, REM, ELLO, JL, WY, SBK, MB, SY, FRA, FL, CAL, HCH performed the experiments and generated data. AVD, KLD, WD, NGS, ST, JL, VRS, SAK, ACN, FL, AR, FB, TLF, YZ and MPM analyzed and interpreted data. AVD, YZ and MPM wrote the manuscript, then all authors edited and approved the final version.

## 2.7 Figures

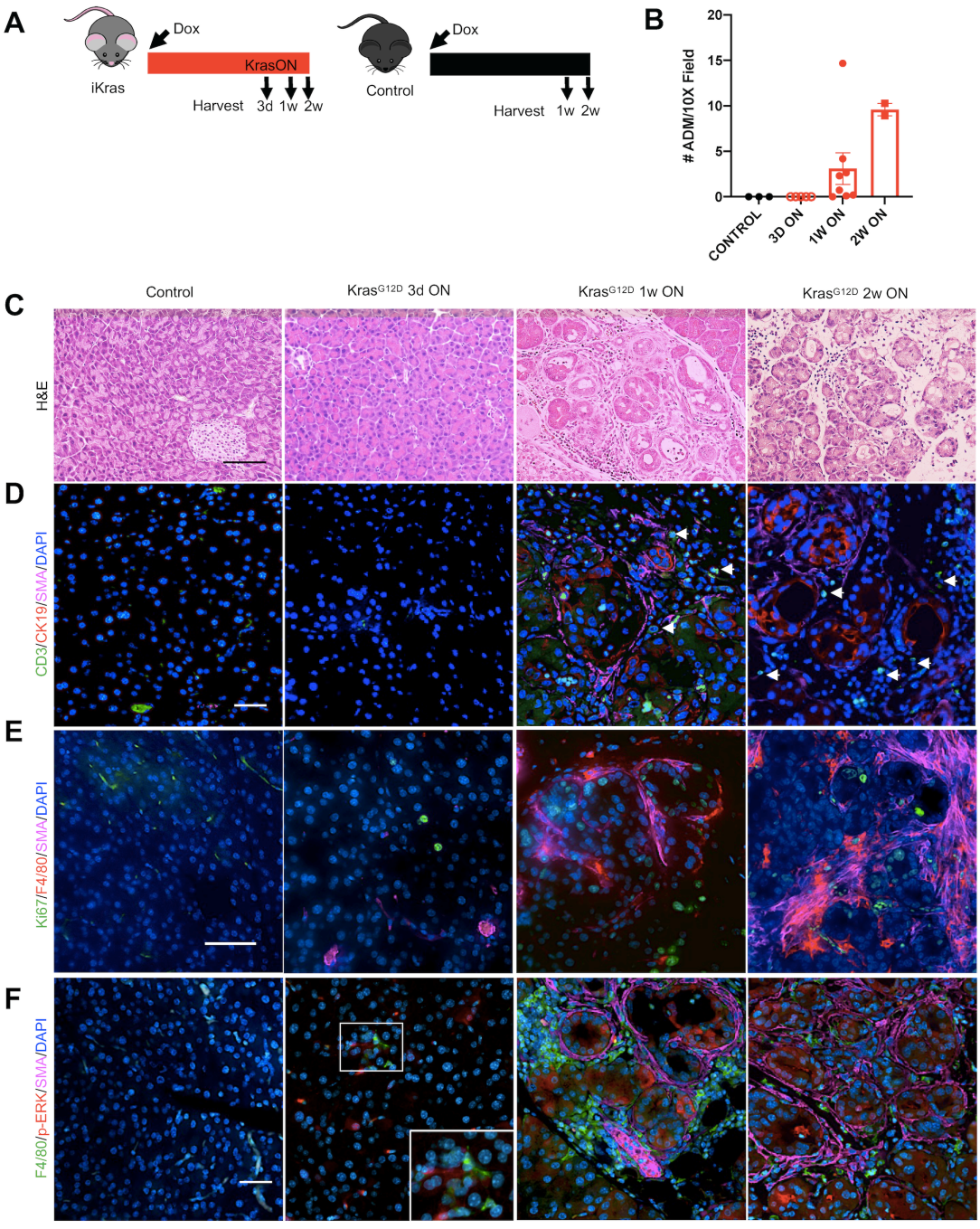
A
Dox
KrasON
iKras
Harvest 3d 1w 2w
Control
Dox
Harvest 1w 2w
B
# ADM/10X Field
20
15
10
5
0
CONTROL
3D ON
1W ON
2W ON
C
Control
KrasG12D 3d ON
KrasG12D 1w ON
KrasG12D 2w ON
H&E
D
CD3/CK19/SMA/DAPI
E
Ki67/F4/80/SMA/DAPI
F
F4/80/p-ERK/SMA/DAPI

**Figure 2-1:Oncogenic Kras drives immune cell recruitment during the onset of tumorigenesis.**

**A**, Experimental design. Control (lacking either the Kras or Ptf1a$^{Cre}$ allele) and iKras mice were given Doxycycline (DOX) chow to activate oncogenic Kras (Kras$^{G12D}$) and pancreata were harvested 3 days (3d), 1 week (1w) or 2 weeks (2w) after induction of Kras. N=3-5 mice per group**. B,** Quantification of acinar to ductal metaplasia (ADM) in pancreatic tissue from control or iKras mice that received DOX chow for 3 days, 1 week or 2 weeks. **C**, Representative images of Hematoxylin and Eosin (H&E) staining of control and iKras pancreata at the indicated time points. N=3-5 mice per group. Scale bar 100$\mu$m. **D**, Representative images of CD3 (green), CK19 (red) and SMA (magenta) co-immunofluorescent staining in control and iKras pancreata at the indicated time points, arrowheads pointing to CD3$^{+}$ T cells. N=3 mice per group. Scale bar 50$\mu$m. **E,** Immunostaining for Ki67 (green), F4/80 (red) and SMA (magenta). Scale bar 50$\mu$m. Scale bar 50$\mu$m. **F,** Representative images of F4/80 (green), p-ERK (red) and SMA (magenta) co-immunofluorescent staining in control and iKras pancreata at the indicated time points. N=3 mice per group. Scale bar 50$\mu$m.

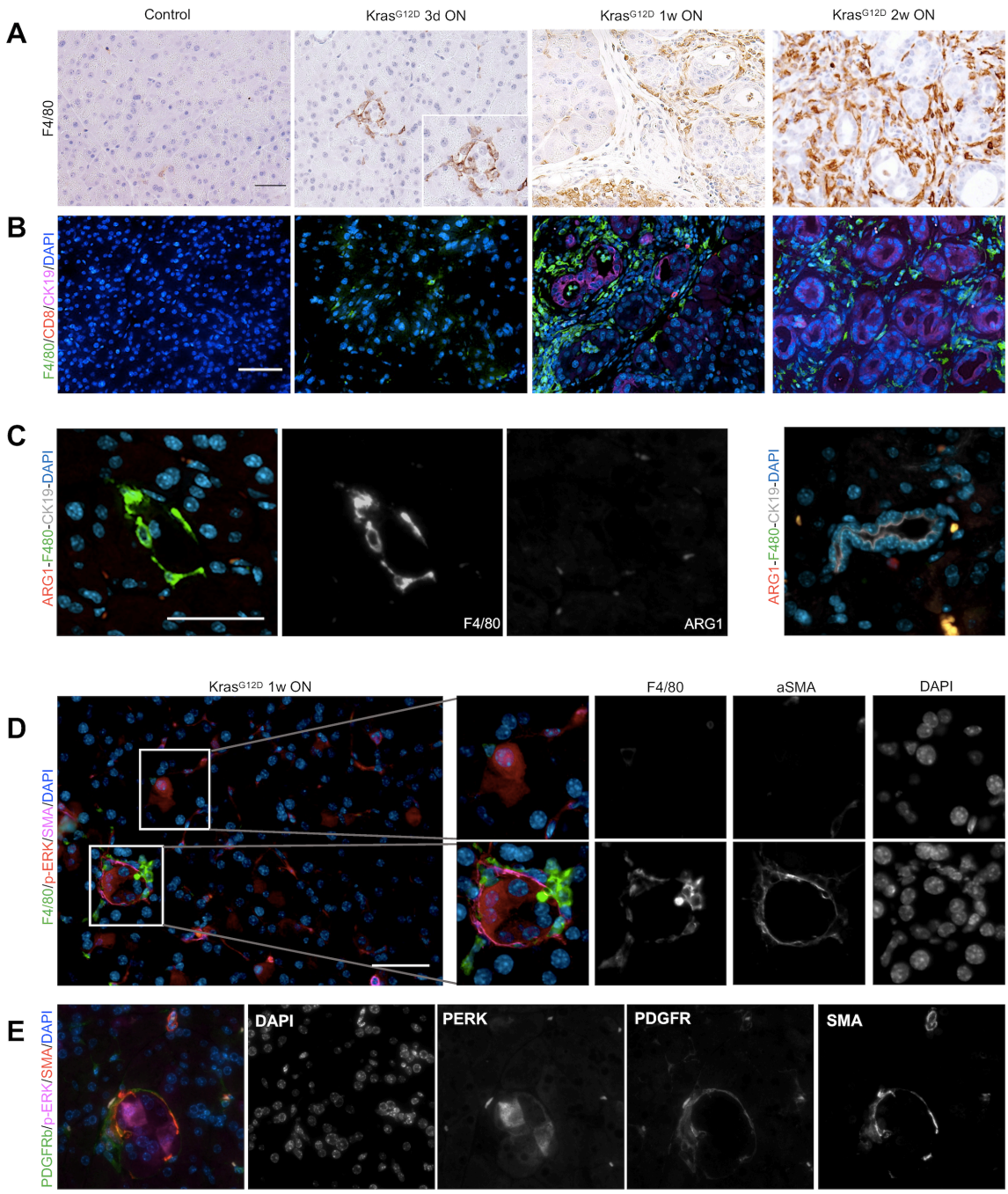


**Figure 2-2 Macrophage expansion precedes acinar transdifferentiation.**

**A,** Immunohistochemistry for F4/80. N=3 mice per group. **B,** Representative images of F4/80 (green), CD8 (red) and CK19 (magenta) co-immunofluorescent staining in control and iKras* pancreata. Scale bar 50$\mu$m. **C,** Co-immunostaining for F4/80 (green), ARG1 (red) and CK19 (Collisson et al.) in iKras* pancreata at 3 days ON. Note that macrophages surround CK19$^{-}$ acinar cells. The image on the right shows a CK19$^{+}$ duct in the same section. Scale bar 50$\mu$m. **D,** Representative images of F4/80 (green), p-ERK (red) and SMA (magenta) co-immunofluorescence staining of an iKras pancreas after activating Kras$^{G12D}$ for 1 week. Regions with high expression of p-ERK are enlarged and single channel images are included. N=3 mice. Scale bar 50$\mu$m. **E,** Representative images of PDGFRb (green), p-ERK (red) and SMA (magenta) co-immunofluorescence staining of an iKras pancreas after activating Kras$^{G12D}$ for 1 week. Single channel images are included. N=3 mice.

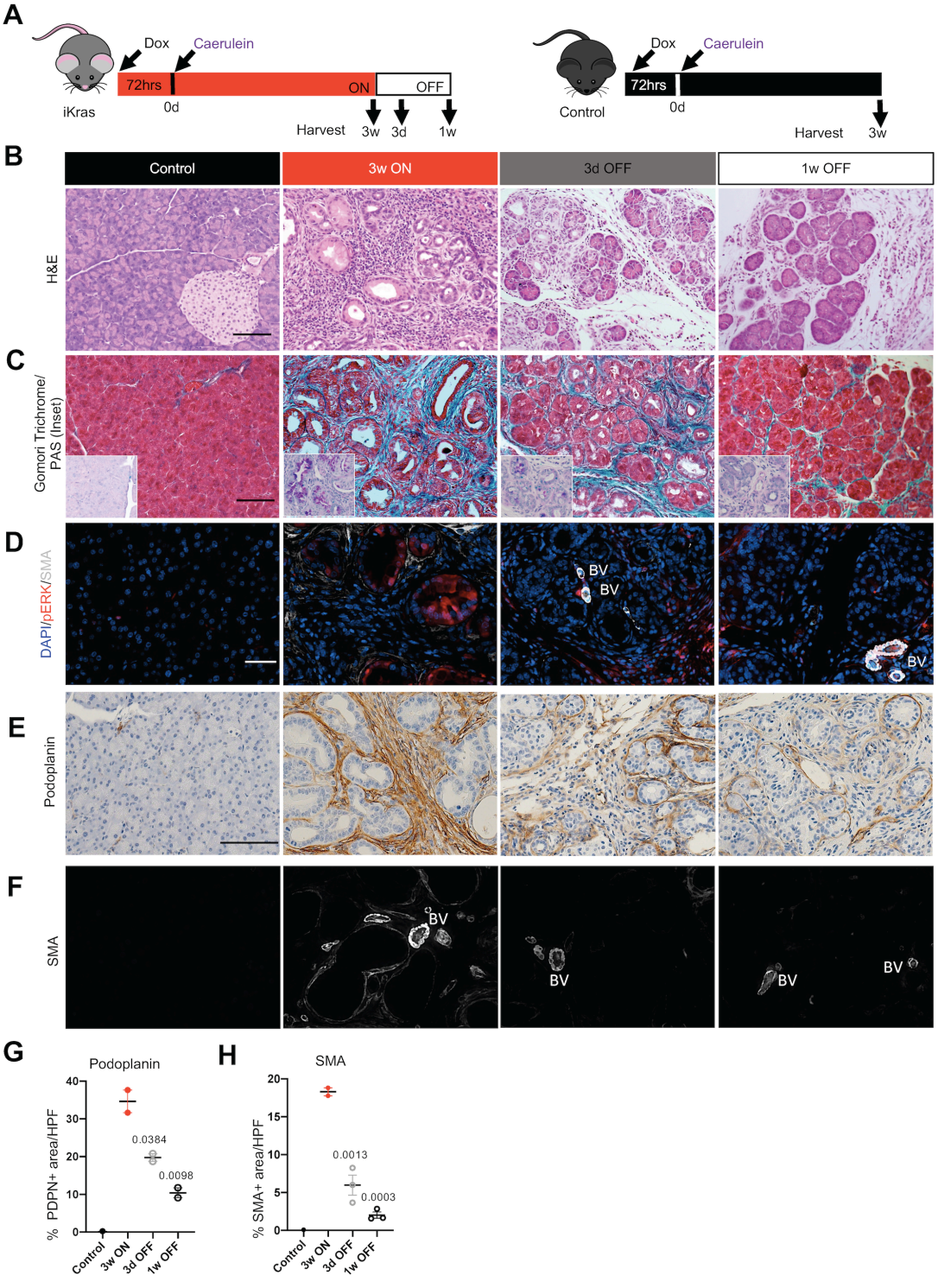
A
Dox
Caerulein
72hrs
ON
OFF
iKras
0d
Harvest
3w
3d
1w
Control
B
Control
3w ON
3d OFF
1w OFF
H&E
C
Gomori Trichrome/
PAS (Inset)
D
DAPI/pERK/SMA
BV
E
Podoplanin
F
SMA
G
Podoplanin
% PDPN+ area/HPF
0.0384
0.0098
H
SMA
% SMA+ area/HPF
0.0013
0.0003

**Figure 2-3 Sustained expression of KrasG12D is required to maintain PanIN and fibrosis.**

**A,** Experimental design. Wild type control and iKras mice were given DOX chow to activate $Kras^{G12D}$ followed by induction of acute pancreatitis. Mice either remained on DOX chow for three weeks, and pancreata were harvested (3w ON) or DOX chow was removed and the pancreata were harvested after 3 days or 1 week (labeled 3d OFF or 1w OFF respectively). N=8 mice per group. **B,** Representative images of H&E staining of control and iKras* pancreata at the indicated time points, N=8 mice per group. Scale bar 100$\mu$m. **C**, Representative images of Gomori Trichrome and Periodic Acid-Schiff Stain (PAS; inset) of control or iKras pancreata at the indicated time points, N=2-3 mice per group. Scale bar 100$\mu$m. **D,** Immunofluorescent staining for SMA (White) and p-ERK (red). BV= blood vessels. Scale bar 50$\mu$m. N=2-3 mice per group. **E,** Immunostaining for Podoplanin (Scale bar 100$\mu$m). **F,** Immunofluorescent staining for SMA (single channel) used for quantification. BV= Blood vessels. Scale bar 50$\mu$m. N=2-3 mice per group. Quantification of Podoplanin **(G)** and SMA staining **(H)**, shown as mean ± SEM. Statistical differences were determined by multiple ANOVA, all compared to 3w ON group.

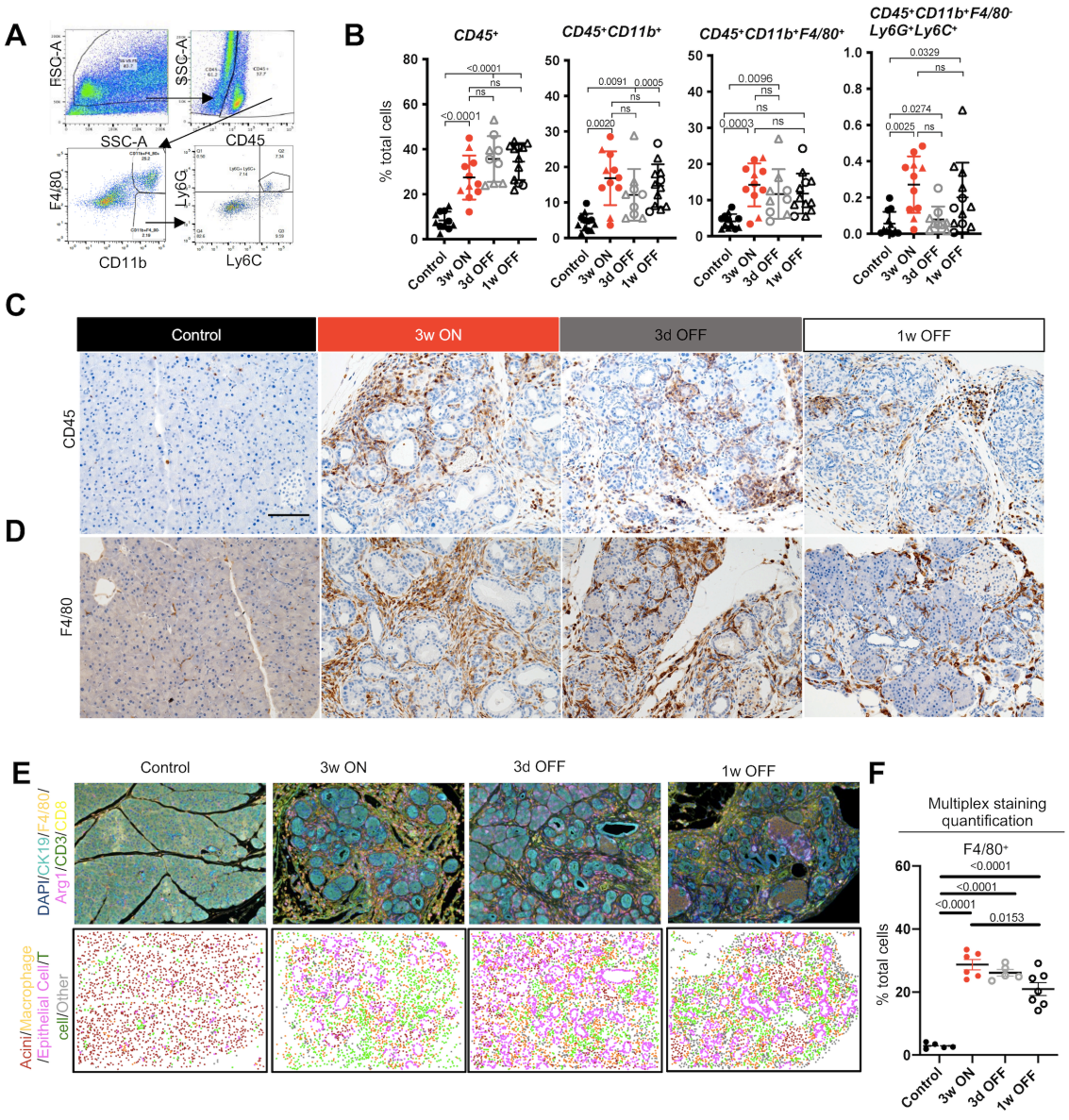


**Figure 2-4 Immune infiltration persists during tissue repair following epithelial-Kras inactivation**

**A,** Flow cytometry gating strategy for myeloid cells in FlowJo. **B,** Quantification of flow cytometry results. Immune cell populations are expressed as percentage of total cells in control or iKras pancreata at the indicated time points, shown as mean ± SD. N=9-11 mice per group. Statistical analysis by multiple comparison ANOVA and multiple comparison Kruskal Wallis. Triangles represent females and circle represent males. Representative immunohistochemistry images for CD45 (**C**) and F4/80 (**D**) in the pancreatic tissue of control or iKras* mice at the indicated time points, scale bar 100$\mu$m. N=3 mice per group. **E,** Top panel: Representative images of F4/80, Arg1, CD3, CD8 and CK19 immunofluorescent multiplex staining at the indicated time points. N=5-7 mice per group. Bottom panel: Identification of cell types using inForm Cell Analysis software. T cell, macrophage, and epithelial cells were selected based on single staining of CD3 (Opal 520), F480 (Opal 540), and CK19 (Opal 690) respectfully. Acinar cells were labeled based on the lack of listed fluorophores and by tissue morphology. **F,** OPAL staining quantification of the percentage of F4/80 positive cells from total cells in the pancreatic tissue of control or iKras mice at the indicated time points. Data is shown as mean ± SEM. N= 5-7 mice per group. Statistical analysis by two-tailed unpaired t-test.

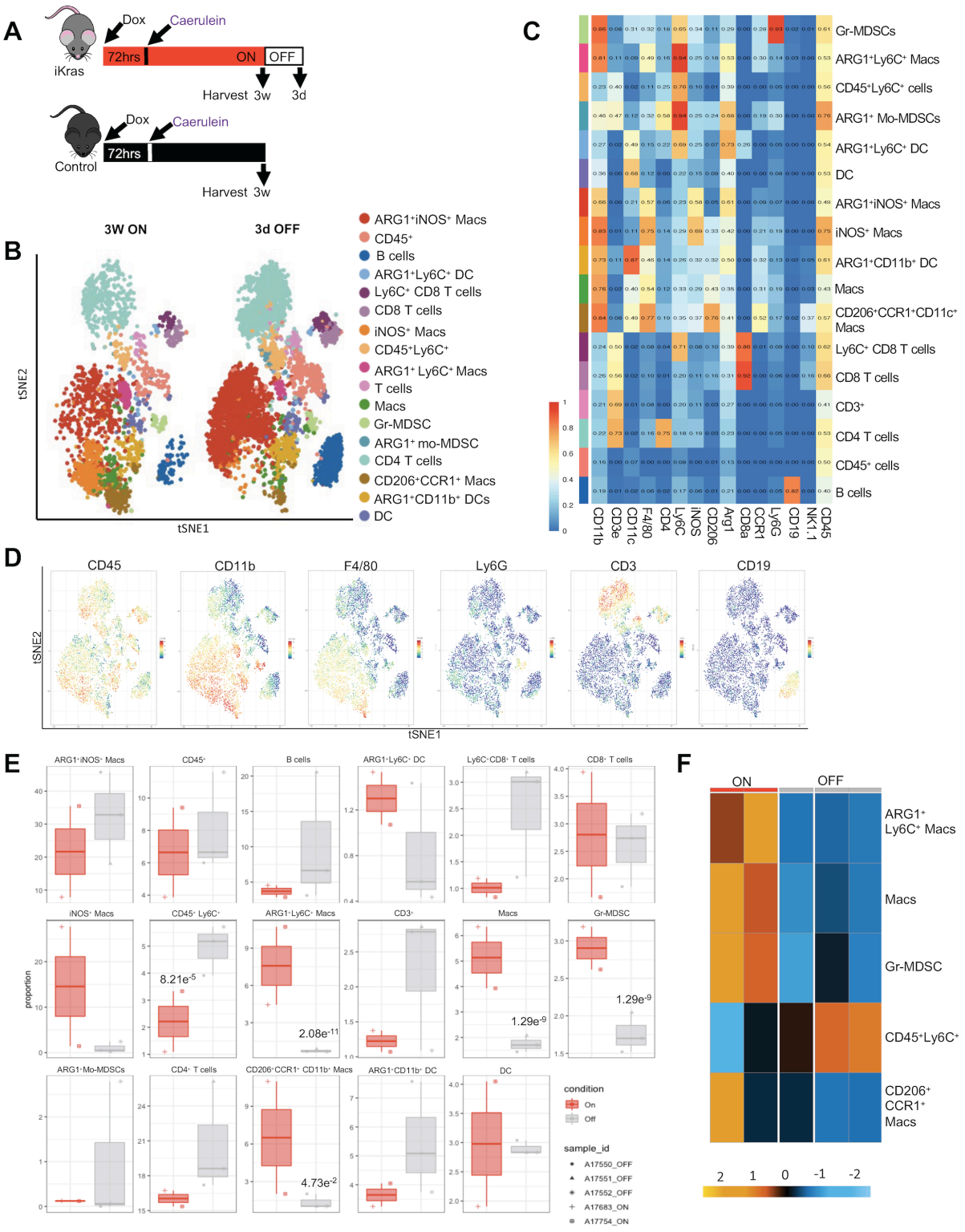
A
Dox
Caerulein
iKras
72hrs
ON
OFF
Harvest 3w
3d
Control
B
3W ON
3d OFF
tSNE2
tSNE1
ARG1+iNOS+ Macs
CD45+
B cells
ARG1+Ly6C+ DC
Ly6C+ CD8 T cells
CD8 T cells
iNOS+ Macs
CD45+Ly6C+
ARG1+ Ly6C+ Macs
T cells
Macs
Gr-MDSC
ARG1+ mo-MDSC
CD4 T cells
CD206+CCR1+ Macs
ARG1+CD11b+ DCs
DC
C
Gr-MDSCs
ARG1+Ly6C+ Macs
CD45+Ly6C+ cells
ARG1+ Mo-MDSCs
ARG1+Ly6C+ DC
DC
ARG1+iNOS+ Macs
iNOS+ Macs
ARG1+CD11b+ DC
Macs
CD206+CCR1+CD11c+ Macs
Ly6C+ CD8 T cells
CD8 T cells
CD3+
CD4 T cells
CD45+ cells
B cells
CD11b
CD3e
CD11c
F4/80
CD4
Ly6C
iNOS
CD206
Arg1
CD8a
CCR1
Ly6G
CD19
NK1.1
CD45
D
CD45
CD11b
F4/80
Ly6G
CD3
CD19
tSNE2
tSNE1
E
ARG1+iNOS+ Macs
CD45+
B cells
ARG1+Ly6C+ DC
Ly6C-CD8+ T cells
CD8+ T cells
iNOS+ Macs
CD45+ Ly6C+
ARG1+Ly6C+ Macs
CD3+
Macs
Gr-MDSC
proportion
8.21e-5
2.08e-11
1.29e-9
1.29e-9
ARG1+Mo-MDSCs
CD4+ T cells
CD206+CCR1+ CD11b+ Macs
ARG1+CD11b+ DC
DC
4.73e-2
condition
On
Off
sample_id
A17550_OFF
A17551_OFF
A17552_OFF
A17683_ON
A17754_ON
F
ON
OFF
ARG1+ Ly6C+ Macs
Macs
Gr-MDSC
CD45+Ly6C+
CD206+ CCR1+ Macs
2
1
0
-1
-2

**Figure 2-5 Oncogenic Kras regulates myeloid cell polarization status in the PME.**

**A,** Experimental Design. N=8-9 mice per group. **B,** CyTOF analysis of CD45+ cells from iKras pancreata visualized by tSNE plot for 3w ON and 3d OFF timepoints. 19 distinct cell clusters were identified by FLowSOM using 18 markers and 1061 randomly selected cells per group. N=2-3 mice per group. **C,** Heatmap of the median marker intensity generated with FlowSOM of the CyTOF samples (iKras 3w ON and 3d OFF combined). Colors on the left represent the clusters shown in the t-SNE plot. N=2-3 per group. All population were gated from $CD45^+$ cells. **D,** tSNE plots showing the expression of different immune lineage markers in the clusters from the CyTOF data. **E,** Quantification of identified clusters proportion by CyTOF analysis at the indicated time points. Statistical analysis by Wrapper function. **F,** Heatmap showing differentially abundance of clusters from CyTOF analysis of iKras pancreata for 3w ON and 3d OFF timepoints. N=2-3 mice per group.

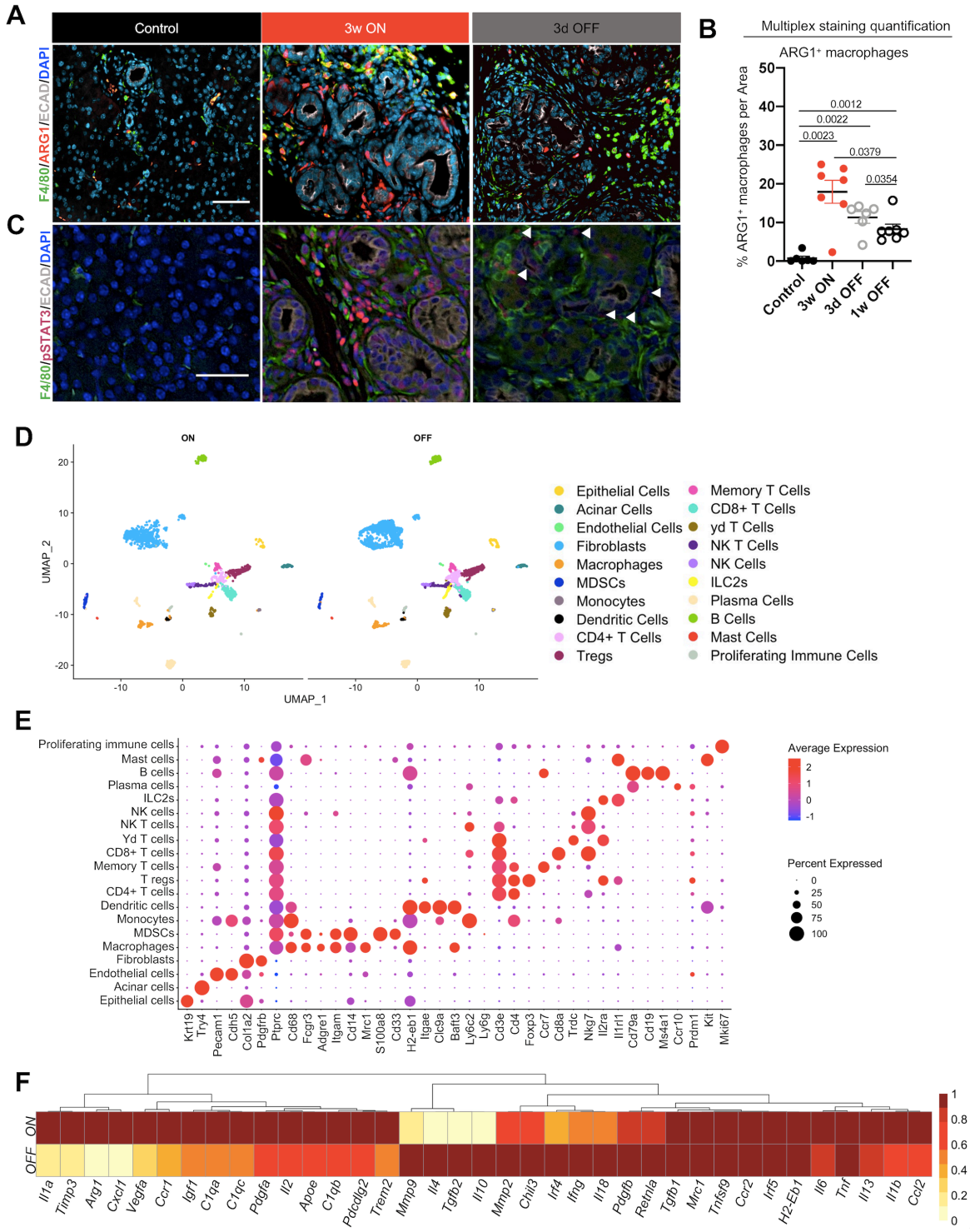
A
Control
3w ON
3d OFF
F4/80/ARG1/ECAD/DAPI
B
Multiplex staining quantification
ARG1⁺ macrophages
% ARG1⁺ macrophages per Area
0.0012
0.0022
0.0023
0.0379
0.0354
Control
3w ON
3d OFF
1w OFF
C
F4/80/pSTAT3/ECAD/DAPI
D
ON
OFF
UMAP_2
UMAP_1
Epithelial Cells
Acinar Cells
Endothelial Cells
Fibroblasts
Macrophages
MDSCs
Monocytes
Dendritic Cells
CD4+ T Cells
Tregs
Memory T Cells
CD8+ T Cells
γδ T Cells
NK T Cells
NK Cells
ILC2s
Plasma Cells
B Cells
Mast Cells
Proliferating Immune Cells
E
Proliferating immune cells
Mast cells
B cells
Plasma cells
ILC2s
NK cells
NK T cells
Yd T cells
CD8+ T cells
Memory T cells
T regs
CD4+ T cells
Dendritic cells
Monocytes
MDSCs
Macrophages
Fibroblasts
Endothelial cells
Acinar cells
Epithelial cells
Krt19 Try4 Pecam1 Cdh5 Col1a2 Pdgfrb Ptprc Cd68 Fcgr3 Adgre1 Itgam Cd14 Mrc1 S100a8 Cd33 H2-eb1 Itgae Clc9a Batf3 Ly6c2 Ly6g Cd3e Cd4 Foxp3 Ccr7 Cd8a Trdc Nkg7 Il2ra Il1rl1 Cd79a Cd19 Ms4a1 Ccr10 Prdm1 Kit Mki67
Average Expression
Percent Expressed
F
ON
OFF
Il1a Timp3 Arg1 Cxcl1 Vegfa Ccr1 Igf1 C1qa C1qc Pdgfa Il2 Apoe C1qb Pdcdlg2 Trem2 Mmp9 Il4 Tgfb2 Il10 Mmp2 Chil3 Irf4 Ifng Il18 Pdgfb Retnla Tgfb1 Mrc1 Tnfsf9 Ccr2 Irf5 H2-Eb1 Il6 Tnf Il13 Il1b Ccl2

**Figure 2-6 Oncogenic Kras inactivation results in transcriptional reprogramming of infiltrating macrophages.**

**A,** Immunostaining for F4/80 (green), ARG1 (red), and Ecad (White) in control and iKras pancreata at the indicated time points. N=3 mice per group. Scale bar 50$\mu$m. **B,** OPAL staining quantification of ARG1+ macrophages in pancreatic tissue of control or iKras mice at the indicated time points. Data shown as mean ± SEM. Statistical analysis by two-tailed unpaired t-test. **C,** Immunostaining for F4/80 (green), pSTAT3 (Magenta), and Ecad (White). N=3 mice per group. Scale bar 50$\mu$m. **D,** Uniform and manifold approximation and projection (UMAP) visualization of single-cell RNA-sequencing data showing unsupervised clustering of cells from iKras pancreatic samples (3w ON, N=2 and 3d OFF, N=3). Each color represents a distinct cellular cluster. **E,** Dot plot of the key genes used to identify different cell populations shown in the UMAP, identified by unsupervised clustering of the single cell RNA sequencing samples (3w ON and 3d OFF samples combined). Size of the dots reflects the proportion of cells expressing a determined gene and color represents average expression level. **F,** Heatmap showing the averaged single-cell RNA sequencing expression data (relative to the highest expressor) for genes in macrophages selected from a curated list of macrophage polarization and functional markers.

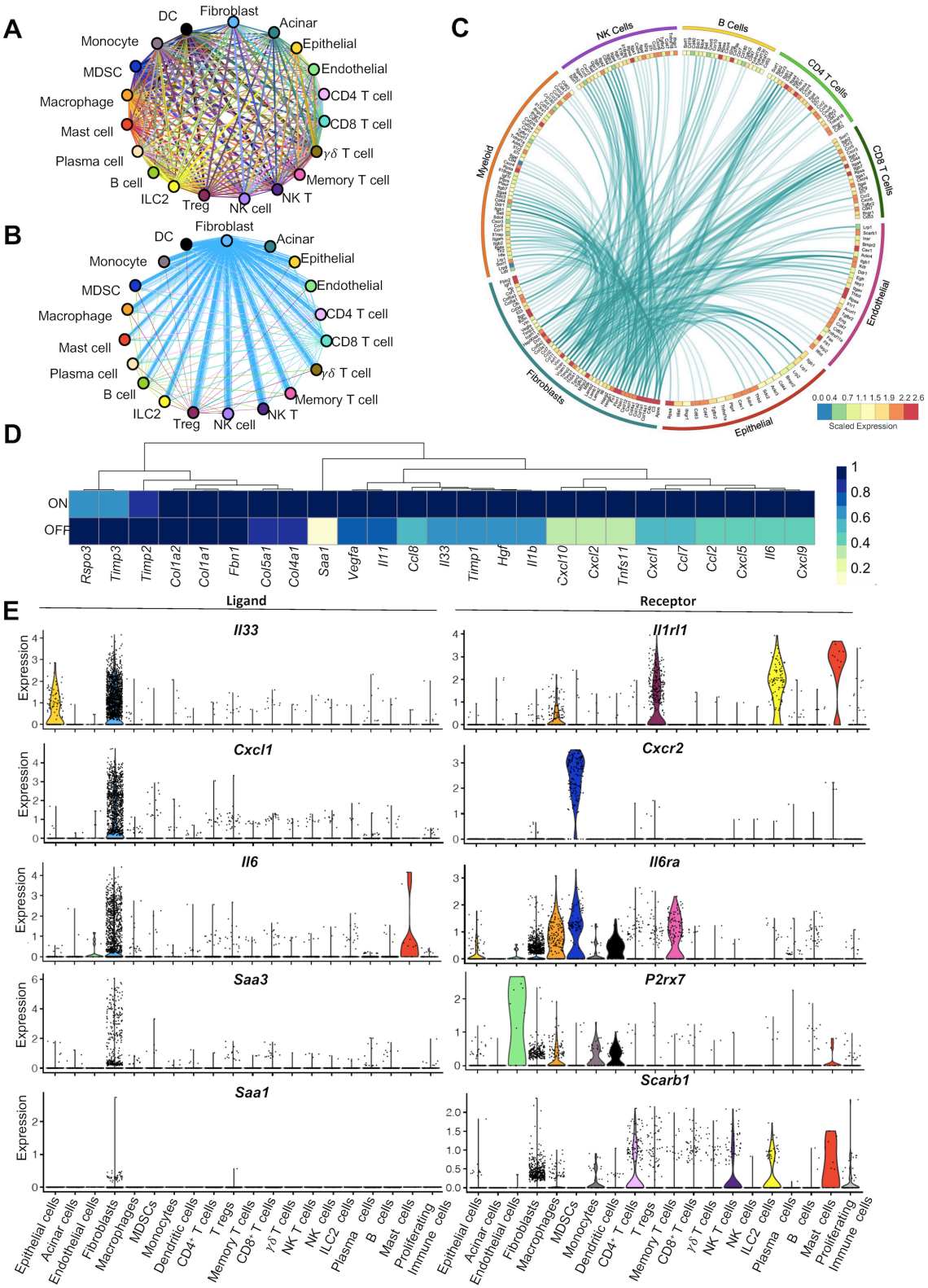
A
DC
Fibroblast
Acinar
Monocyte
Epithelial
MDSC
Endothelial
Macrophage
CD4 T cell
Mast cell
CD8 T cell
Plasma cell
γδ T cell
B cell
Memory T cell
ILC2
Treg
NK cell
NK T
B
C
NK Cells
B Cells
CD4 T Cells
CD8 T Cells
Myeloid
Endothelial
Fibroblasts
Epithelial
Scaled Expression
D
ON
OFF
Rspo3
Timp3
Timp2
Col1a2
Col1a1
Fbn1
Col5a1
Col4a1
Saa1
Vegfa
Il11
Ccl8
Il33
Timp1
Hgf
Il1b
Cxcl10
Cxcl2
Tnfs11
Cxcl1
Ccl7
Ccl2
Cxcl5
Il6
Cxcl9
E
Ligand
Receptor
Il33
Il1rl1
Cxcl1
Cxcr2
Il6
Il6ra
Saa3
P2rx7
Saa1
Scarb1
Expression
Epithelial cells
Acinar cells
Endothelial cells
Fibroblasts
Macrophages
MDSCs
Monocytes
Dendritic cells
CD4+ T cells
T regs
Memory T cells
CD8+ T cells
γδ T cells
NK T cells
NK cells
ILC2 cells
Plasma cells
B cells
Mast cells
Proliferating Immune cells

**Figure 2-7 Fibroblasts express inflammatory cytokines in response to epithelial oncogenic Kras.**

**A,** Interactome analysis showing all predicted ligand-receptor interactions between different cell populations identified in iKras pancreatic single-cell RNA sequencing analysis. Each line represents a ligand-receptor pair, color-coded by the cell-type expressing the ligand. **B,** Differential interactions from **A** positively regulated by oncogenic Kras (higher in 3w ON compared to 3d OFF) (adjusted p value <0.05). **C,** Circos plot showing average expression of fibroblast ligands connected to their predicted receptors on various cell populations as measured in the pancreatic single-cell RNA sequencing analysis. Ligands shown are from **B** (adjusted p value <0.05). **D,** Heatmap showing averaged single-cell RNA sequencing expression data (relative to the highest expressor) for genes in fibroblasts from a curated list of immunomodulatory factors. **E,** Violin plots showing expression of *Il33*, *Cxcl1, Il6*, *Saa3* and *Saa1* and their respective receptors *Il1rl1*, *Cxcr2*, *Il6ra*, *P2rx7* and *Scarb1* across all identified cell populations in both Kras* ON and OFF samples combined.

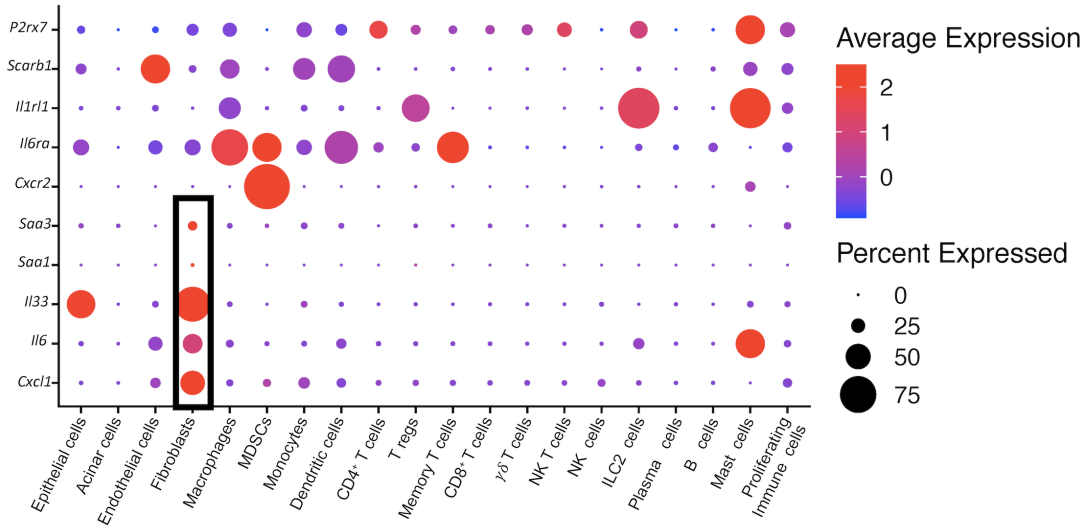


**Figure 2-8 Fibroblasts secrete immunomodulatory factors with receptors in myeloid cells.**

Dot plot showing average expression of *Il33*, *Il6*, *Cxcl1, Saa1 and Saa3* and their respective receptors *Il1rl1*, *Il6ra*, *Cxcr2 and P2rx7 and Scarb1* across cell populations. Size of the dots reflects the proportion of cells expressing a determined gene and color represents average expression level.

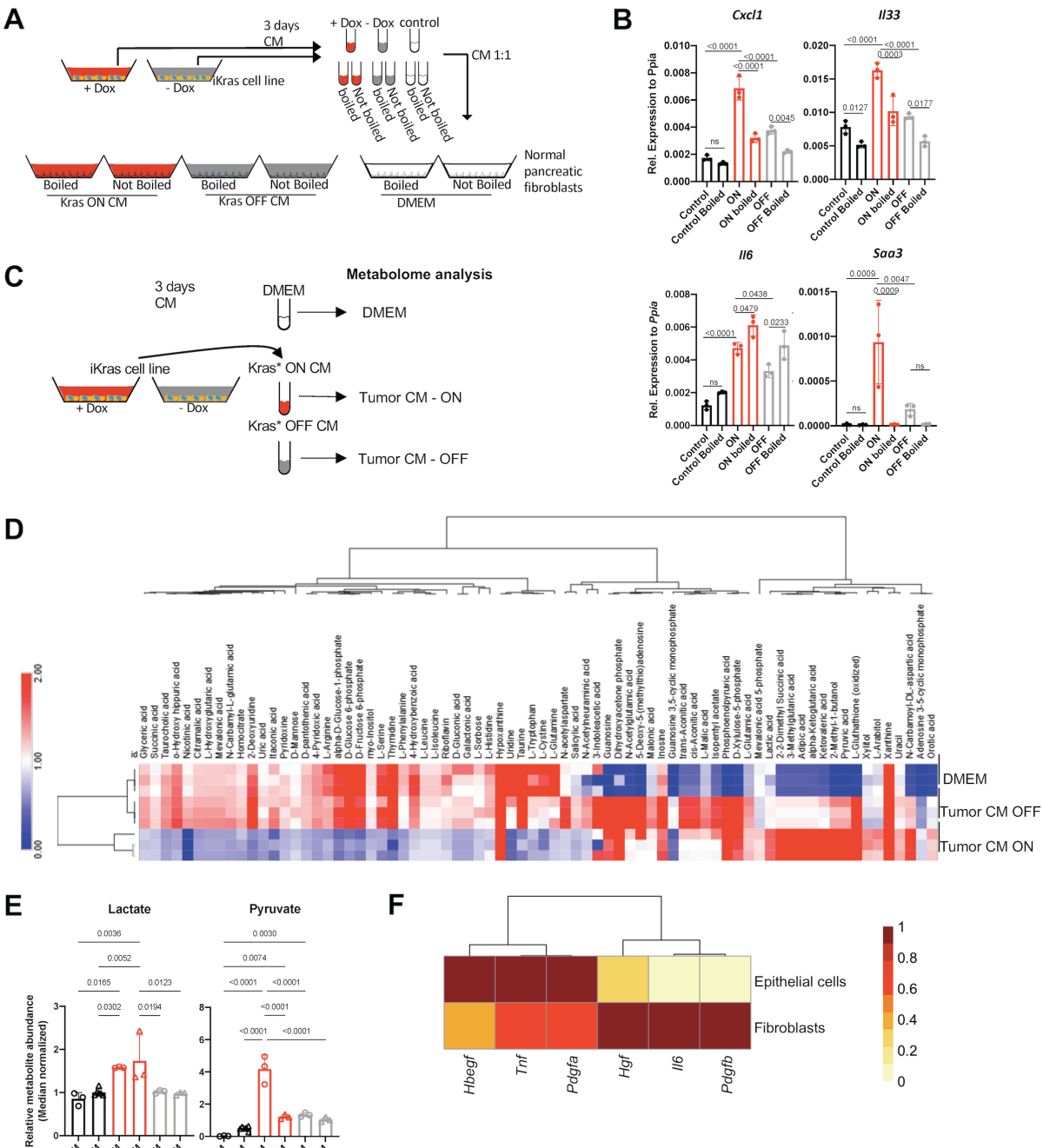
A
3 days CM
+ Dox - Dox control
CM 1:1
+ Dox
- Dox
iKras cell line
Not boiled
Boiled
Not Boiled
Kras ON CM
Kras OFF CM
DMEM
Normal pancreatic fibroblasts
B
Cxcl1
Il33
Il6
Saa3
Rel. Expression to Ppia
Control
Control Boiled
ON
ON boiled
OFF
OFF Boiled
C
Metabolome analysis
3 days CM
DMEM
iKras cell line
Kras* ON CM
Tumor CM - ON
Kras* OFF CM
Tumor CM - OFF
D
DMEM
Tumor CM OFF
Tumor CM ON
E
Lactate
Pyruvate
Relative metabolite abundance (Median normalized)
DMEM
FB CM
Tumor CM
ON
OFF
F
Epithelial cells
Fibroblasts
Hbegf
Tnf
Pdgfa
Hgf
Il6
Pdgfb

**Figure 2-9 Fibroblasts are reprogrammed through epithelial KrasG12D-induced secreted molecules.**

**A,** Experimental design. Conditioned media (CM) was collected from iKras* cancer cells cultured with Doxycycline (+DOX) to activate $Kras^{G12D}$ expression (Kras ON) or without Doxycycline (-DOX, Kras OFF). The media samples were then boiled, to denature protein factors, or left intact, and used to culture pancreatic fibroblasts. DMEM was used as control. **B,** qRT-PCR for *Cxcl1, Il33, Il6* and *Saa3* expression in fibroblasts (CD1WT) that were cultured with CM either from Kras ON, Kras OFF or DMEM, either boiled or not boiled. Gene expression was normalized to *Ppia*. Data was shown as mean ± SD. N=3 per group. The statistic differences were determined by multiple comparison ANOVA. **C**, Experimental design. CM was collected from iKras cancer cells cultured with Doxycycline (+DOX) to activate $Kras^{G12D}$ expression (Kras* ON) or without Doxycycline (-DOX, $Kras^{G12D}$ OFF), and used for metabolomic analysis. **D,** Heatmap showing levels of extracellular metabolites in iKras cancer cell CM with $Kras^{G12D}$ ON or OFF. Both conditions are compared to regular DMEM media. **E,** Fibroblasts were exposed to + DOX CM and -DOX CM for 48hrs. The resulting CM was analyzed for metabolites, in parallel with iKras cell conditioned medium and DMEM. Relative metabolite abundance of Lactate and Pyruvate from all conditions are shown. **F,** Heatmap showing averaged single-cell RNA sequencing expression data (relative to the highest expressor) for genes encoding for ligands that are secreted by fibroblasts and epithelial cells.

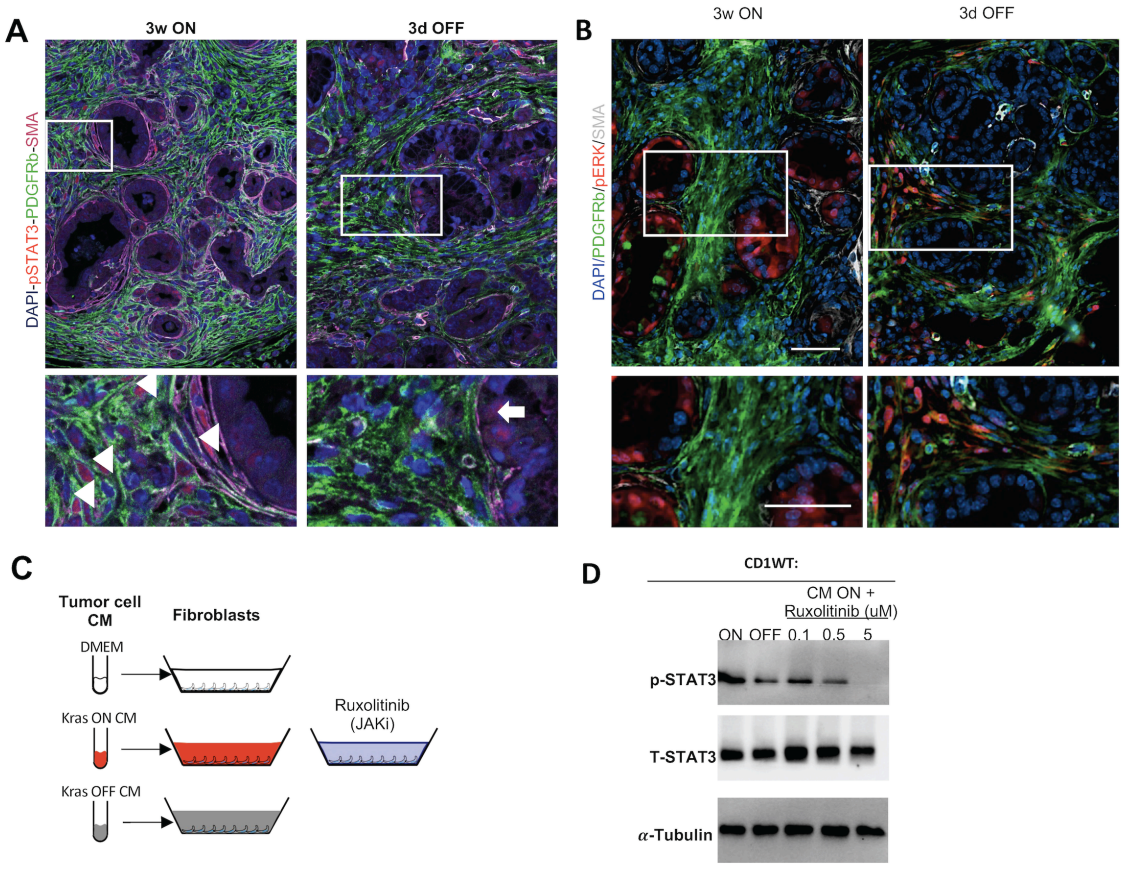
A
3w ON
3d OFF
DAPI-pSTAT3-PDGFRb-SMA
B
3w ON
3d OFF
DAPI/PDGFRb/pERK/SMA
C
Tumor cell CM
Fibroblasts
DMEM
Kras ON CM
Kras OFF CM
Ruxolitinib (JAKi)
D
CD1WT:
CM ON + Ruxolitinib (uM)
ON OFF 0.1 0.5 5
p-STAT3
T-STAT3
α-Tubulin
E
CD1WT
mRNA level normalized to Ppia
Cxcl1
Il33
Il6
Saa3
DMEM
Veh.
0.1μM
0.5μM
5 μM
OFF CM
ON CM
JAKi
F
B6318:
mRNA level normalized to Ppia
Cxcl1
Il33
Il6
Saa3
DMEM
ON CM
0.1μM
0.5μM
OFF CM
CM ON + JAKi
ns

**Figure 2-10 Fibroblast reprogramming requires JAK/STAT signaling.**

**A,** Immunofluorescent staining of pSTAT3 (red), PDGFRb (green) and SMA (Collisson et al.). N=2-3 mice per group. Arrowheads pointing at pSTAT3 positive fibroblasts and arrow pointing positive epithelial cells. **B,** Immunofluorescent staining for PDGFR beta (Green), SMA (White) and p-ERK (red). Scale bar 50$\mu$m. N=2-3 mice per group. **C,** Experimental design. Fibroblasts were exposed to iKras\tumor cell CM either from $Kras^{G12D}$ ON, $Kras^{G12D}$ OFF or DMEM. Fibroblasts cultured with $Kras^{G12D}$ ON CM media were treated with a JAK/STAT 2/3 inhibitor (Ruxolitinib) or vehicle. **D,** Western blot showing protein levels of total STAT3 or phospho-STAT3 from CD1WT fibroblasts treated as indicated. Alpha-tubulin was used as loading control. **E,** qRT-PCR results for *Cxcl1, Il33*, *Il6* and *Saa3* expression in fibroblasts (CD1WT) treated with CM as described in panel C. Data shown as mean ± SD. N=3 per group. The statistical differences were determined by multiple comparison ANOVA. **F**, qRT-PCR for *Cxcl1, Il33*, *Il6*, and *Saa3* expression in fibroblasts (B6318) treated with iKras cell CM either from $Kras^{G12D}$ ON, $Kras^{G12D}$ OFF or DMEM. Fibroblasts cultured with $Kras^{G12D}$ ON CM medium were treated with a JAK/STAT 2/3 inhibitor (Ruxolitinib) or vehicle. Data shown as mean ± SD. The statistical differences were determined by multiple comparison ANOVA.

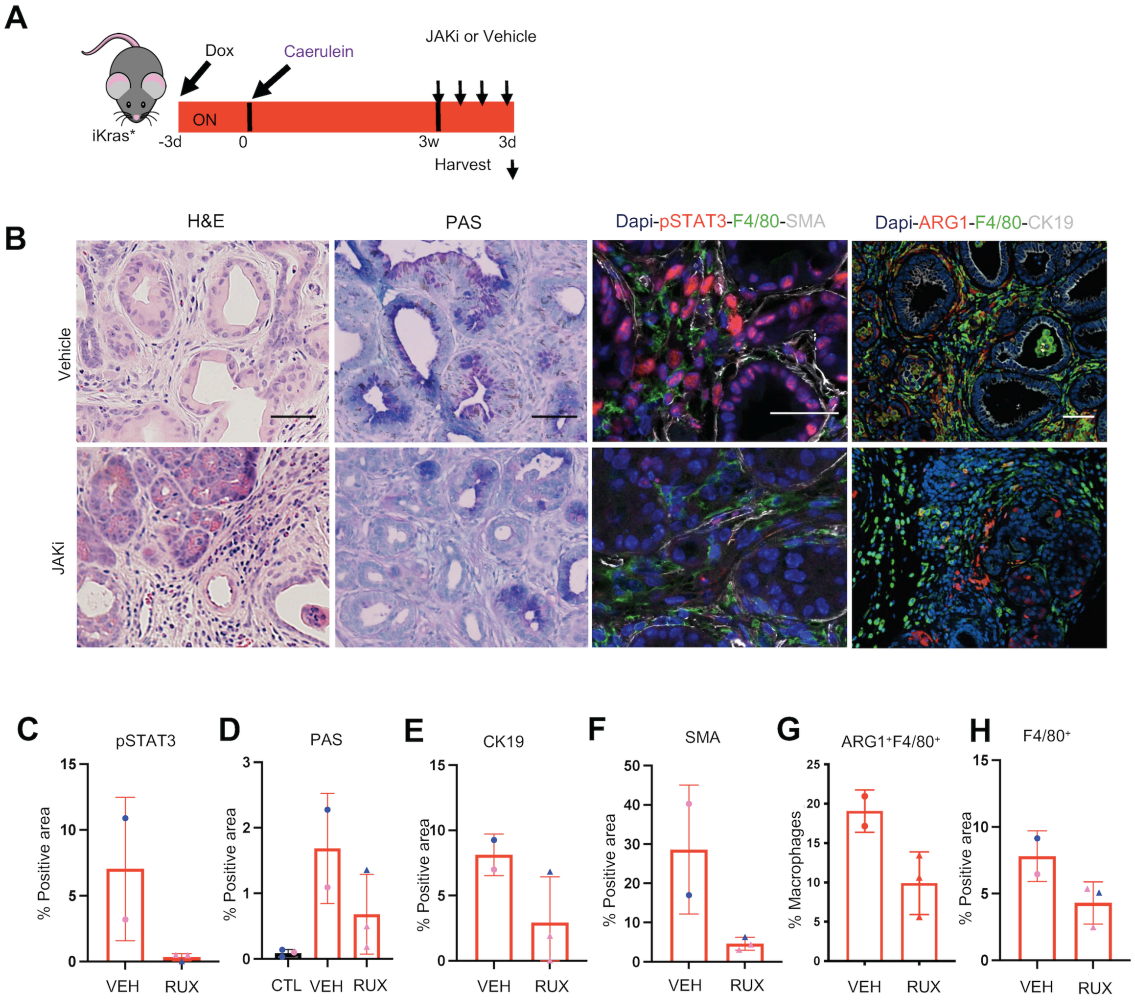


**Figure 2-11 Inhibition of the JAK/STAT pathway mimics KrasG12D inactivation induced tissue repair.**

**A**, Experimental design. iKras mice were given DOX and after 3 days acute pancreatitis was induced. Following pancreatitis, $Kras^{G12D}$ was left ON for 3 weeks and at 3 weeks mice either received Ruxolitinib (180mg/kg) daily for 3 days or were treated with Vehicle. N=2=3 mice per group. **B,** H&E, PAS and immunofluorescent staining for pSTAT3 (red), F4/80 (Green) and SMA (white) or ARG1 (red), F4/80 (green) and CK19 (white) (scale bar 50uM). N=2=3 mice per group. **C**, Quantification for the pSTAT3 staining. Blue = Male and Pink= females. **D,** Quantification for the PAS staining. Blue = Male and Pink= females. **E,** Quantification of CK19 positive area. Blue = Male and Pink= females. **F,** Quantification of SMA positive area. Blue = Male and Pink= females. **G,** Quantification of ARG1+ positive area within the F4/80+ macrophages. **H**, Quantification of F4/80+ positive area. Blue = Male and Pink= females. All data were analyzed using t-test.

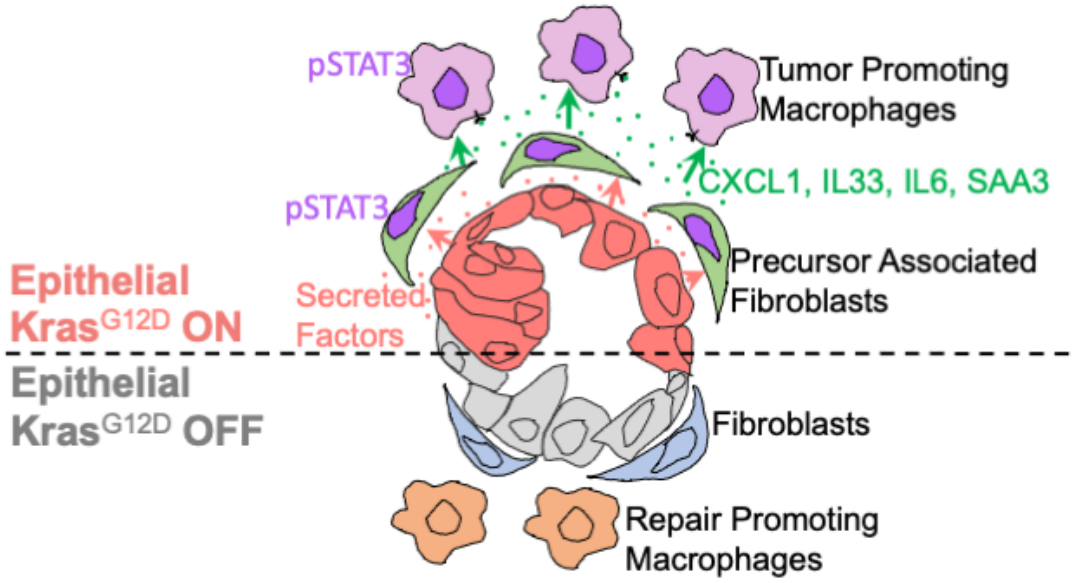


**Figure 2-12 Working model. Upon KrasG12D expression, macrophages infiltrate the pancreas.**

Molecules coming from the epithelial cells activate the JAK/STAT signaling in fibroblasts at the PanIN stage, and induce expression of *Cxcl1, Il33, Il6,* and *Saa3.* These inflammatory molecules have receptors on immune cells, many of which are myeloid cells. In turn, the JAK/STAT3 pathway becomes activated in macrophages resulting in a tumor-promoting phenotype. Upon Kras$^{G12D}$ inactivation in the epithelial cells, inflammatory molecule expression is downregulated in fibroblasts, and macrophages are reprogrammed to a tissue repair phenotype that promotes the re-differentiation of acinar cells.

**Table 2-1 IHC, IF and Western Blot antibodies**

| Antibody | Supplier | Catalog # | IHC dilution | IF dilution | WB dilution |
|---|---|---|---|---|---|
| CD45 | BD Pharmingen | 553076 | 1:200 | | |
| F4/80 | Cell Signaling | 70076S | 1:250 | 1:250 | |
| CD4 | Cell Signaling | 25229S | 1:00 | | |
| CD8 | Cell Signaling | 98941S | 1:400 | 1:100 | |
| Foxp3 | Cell Signaling | 12653S | 1:100 | | |
| Arginase 1 | Cell Signaling | 93668S | | 1:250 | |
| aSMA | Sigma Aldrich | A2547 | | 1:1000 | |
| CK19 (Troma III) | Iowa Development Hybridoma Bark | - | | 1:50 | |
| Perk1/2 | Cell Signaling | 4370L | | 1:100 | |
| Ki67 | Abcam | ab15580 | | 1:100 | |
| CC3 | Cell Signaling | 9661L | | | |
| E-cadherin | Cell Signaling | 14472S | | 1:100 | |
| CD3 | ABCAM | ab5690 | | 1:100 | |
| pStat3 Y705 | Cell Signaling | 9145S | | | 1:500 |
| Total STAT3 | Cell Signaling | 9139S | | | 1:1000 |
| p-ERK(T202/Y204) | Cell Signaling | 470L | | | 1:1000 |
| Total ERK | Cell Signaling | 4695S | | | 1:1000 |
| Vinculin | Cell Signaling | 13901 | | | 1:2000 |
| $\alpha$-tubulin | Cell Signaling | 3873S | | | 1:2000 |

| | | | | | |
|---|---|---|---|---|---|
| PDGFR beta | Abcam | ab32570 | | 1:100 | |

**Table 2-2 Flow Cytometry antibodies**

| Antibodies | Supplier | Catalog # | Clone | Dilution |
|---|---|---|---|---|
| CD45 | Invitrogen | MCD4530 | 30-F11 | 1:100 |
| CD45 | BD Horizon | 563891 | 30-F11 | 1:100 |
| CD11b | BD Pharmingen | 557657 | M1/70 | 1:100 |
| F4/80 | Invitrogen | 15-4801-82 | BM8 | 1:100 |
| Ly6G | BD Pharmingen | 551460 | 1A8 | 1:100 |
| Ly6C | BD Pharmingen | 560592 | AL-21 | 1:100 |
| Arg1 | R&D | IC5868F | Polyclonal | 1:50 |
| iNOS | Invitrogen | 12-5920-82 | CXNFT | 1:100 |
| CD206 | BD Pharmingen | 565250 | MR5D3 | 1:100 |

**Table 2-3 CyTOF antibodies**

| Antibodies | | Clone | Isotope | Dilution |
|---|---|---|---|---|
| CD45 | Fluidigm | 30-F11 | Y89 | 1:200 |
| Ly6G | Fluidigm | 1AB | Pr141 | 1:400 |
| CD11b | Fluidigm | M1/70 | Nd143 | 1:300 |
| CD4 | Fluidigm | RM4/5 | Nd145 | 1:200 |
| F480 | Fluidigm | BM8 | Nd146 | 1:100 |
| CD140a | Fluidigm | APA5 | Nd148 | 1:100 |
| CD19 | Fluidigm | 6D5 | Nd149 | 1:200 |
| Ly6C | Fluidigm | HK1.4 | Nd150 | 1:400 |
| CD3e | Fluidigm | 145-2C11 | Sm152 | 1:100 |

| | | | | |
|---|---|---|---|---|
| CD105 | Custom | MJ7/18 | Dy164 | 1:100 |
| TCR gd | Fluidigm | GL3 | Tb159 | 1:100 |
| CD191 CCR1 | Custom | S15040E | Gd160 | 1:100 |
| iNOS | Fluidigm | CXNFT | Dy161 | 1:100 |
| Arginase1 | Custom | Polyclonal | Er166 | 1:400 |
| CD8a | Fluidigm | 53-6.7 | Er168 | 1:200 |
| CD206 | Fluidigm | C068C2 | Tm169 | 1:200 |
| CD161 NK1.1 | Fluidigm | PK136 | Er170 | 1:100 |
| CD11c | Fluidigm | N418 | Bi209 | 1:100 |

**Table 2-4 Primers for quantitative RT-PCR**

| Genes | Forward Primer | Reverse Primer |
|---|---|---|
| Cxcl1 | 5’ CTGGGATTCACCTCAAGAACATC 3’ | 5’ CAGGGTCAAGGCAAGCCTC 3’ |
| Il6 | 5’ TTCCATCCAGTTGCCTTCTTGG 3’ | 5’ TTCTCATTTCCACGATTTCCCAG 3’ |
| Il33 | 5’ TGAGACTCCGTTCTGGCCTC 3’ | 5’ CTCTTCATGCTTGGTACCCGA T 3’ |
| Saa3 | 5’ TGCCATCATTCTTTGCATCTTGA 3’ | 5’ CCGTGAACTTCTGAACACCCT 3’ |

**Table 2-5 Multiplex IHC antibodies and cell phenotyping**

| **Complex Phenotype** | **Opal** | **Primary Phenotype** | **Antibody Scoring** | **Cell segment** | **Mean signal intensity** |
|---|---|---|---|---|---|
| Macrophage | F4/80-Opal 540 | Macrophage | None | n/a | n/a |
| $Arg1^+$ macrophage | Arg1-Opal 650 | Macrophage | Arg1 | Nucleus | 13 and above |

| | | | | | |
|---|---|---|---|---|---|
| Arg1$^{-}$ macrophage | - | Macrophage | Arg1 | Nucleus | <13 |
| Epithelial cell | CK19-Opal 690 | Epithelial | None | n/a | n/a |
| Acinar cell | - | Acinar cell | None | n/a | n/a |

# Chapter 3 The JAK/STAT3 Pathway Drives Immunosuppression in Pancreatic Myeloid Cells

## 3.1 Abstract

Pancreatic ductal adenocarcinoma (PDAC) is a lethal disease characterized by having an immunosuppressive microenvironment (TME). As a consequence of this immune suppressive TME the $CD8^+$ T cells are scarce in the tumor. Immunotherapies in PDAC have failed, potentially due to the low number of cytotoxic lymphocytes. Exploring new therapeutic approaches to target and reverse immunosuppression is critical. The JAK/STAT3 pathway have been identified as an immunosuppressive pathway in myeloid cells *In vitro* and *In vivo* in other cancers. Using a mouse model that deletes STAT3 specifically in the myeloid cells, we established orthotopically transplanted syngeneic PDAC model to study the effect of specific myeloid-STAT3 deletion on pancreatic tumor growth. We found that myeloid-STAT3 deletion resulted in reduced tumor growth, which could be rescued by CD8 T cell depletion. In conclusion, STAT3 is an important molecule for myeloid cell driven immunosuppression and consequently the exclusion of T cells from the tumor. Myeloid specific STAT3 is a potential therapeutic target for PDAC.

## Introduction

Pancreatic ductal adenocarcinoma (PDAC) is a lethal disease, and it is predicted to be the second leading cause of cancer related deaths in the U.S. by 2030 (Society, 2022). The current 5-year survival rate is only 11% (Society, 2022). The ongoing treatments have a moderate improvement in survival, and unfortunately many patients become resistant to these

chemotherapeutics (3rd et al., 1997) (Conroy et al., 2018) (Principe et al., 2021). Hence, a better understanding of this disease is imperative to discover new treatments.

One of the hallmarks of pancreatic cancer is the immunosuppressive microenvironment (Clark et al., 2007). This is defined by the inability of the immune system to fight a disease. In cancer, this is when cytotoxic T lymphocytes (CTLs) are absent from tumors and unable to have an anti-tumor immune response. Different mechanisms exist for immune evasion including downregulation of the MHC I molecules by tumor cells, resulting in a lack of antigen presentation to T cells (Hicklin, Marincola, & Ferrone, 1999) (Yamamoto et al., 2020). Another mechanism of immunosuppression is by the expression of immune checkpoint pathways such as PD-1 and CTLA-4 which inactivate $CD8^+$ T cells (Krummel & Allison, 1995) (Fife & Bluestone, 2008). Moreover, other immune cell types such as macrophages, myeloid derived suppressor cells (MDSCs), and regulatory T cells can express different factors such as Interleukin 10 (IL10), Arginase 1 (ARG1), Nitric oxide (NO), Tumor growth factor beta (TGF$\beta$), among other molecules that are responsible for causing the dysfunctional activity of CTLs (Smith et al., 2018) (Rodriguez et al., 2003) (Sinha et al., 2005) (Polanczyk et al., 2019). Tumor associated macrophages (TAMs) have been extensively studied due to being (1) the largest population of myeloid cells in PDAC and (2) for its immunosuppressive capacity. TAMs are known to express immunosuppressive molecules such as ARG1, tumor necrosis factor (TNF) and IL10 (DeNardo & Ruffell, 2019) (Smith et al., 2018) (Rodriguez et al., 2004). The activation of the JAK/STAT pathway has been associated with the induction of the expression of different immunosuppressive molecules in TAMs and MDSCs (Rébé & Ghiringhelli, 2019). In particular, the JAK/STAT3 pathway induces the expression of IL6, which is known to be important for PDAC progression, and IL10 which is an immunosuppressive molecule (Y. Zhang et al., 2013) (Saraiva & O'Garra, 2010). Furthermore,

the activation of the JAK/STAT3 pathway was found to be important in the development of MDSCs (immunosuppressive cells) from peripheral blood mononuclear cells (PBMCs) *in vitro* (Mace et al., 2013). Clinical trials using JAK1/2 inhibitors, that were successful in preclinical models, had been tried in PDAC patients but showed minimal effects (H. Hurwitz et al., 2018). Hence, more studies focused on the understanding of the JAK/STAT pathway in PDAC are needed. In particular, deeper understanding of the effect of each specific STAT pathway (STAT1, STAT3, STAT5, etc) in the cells and/or the distinct roles of the JAK/STAT pathway in different compartments could be beneficial.

In this study we were interested in targeting specifically the JAK/STAT3 pathway in the myeloid compartment in pancreatic cancer. To accomplish this, I generated a mouse model that lacks *Stat3* expression in the myeloid cells by crossing a mouse that has the exons 18, 19, 20 of the *Stat3* gene flanked by two LoxP sites. The LoxP sites are recognized by the Cre recombinase which is under the Lysozyme 1 (LysM) promoter (myeloid lineage specific). Cre excises the DNA in the LoxP sites, resulting in exons removal. These exons encode for the SH2 domain of the STAT3 protein which is required for the phosphorylation and subsequent activation of the protein (Takeda et al., 1999). Using this mouse model, we study the immunosuppressive role of the JAK/STAT3 pathway particularly in the myeloid compartment in pancreatic cancer by using syngeneic transplantation of tumor cells.

## 3.2 Results

### *3.2.1 Lack of pSTAT3 in myeloid cells impairs pancreatic tumor growth.*

First, we verified the expression of phospho-STAT3 (pSTAT3) in the pre-cancerous lesions of a spontaneous model of pancreatic cancer (FSF-Kras$^{G12D}$; Ptf1a-FLPO). We observed, positive

pSTAT3 areas in the stroma surrounding the ADM and low grade PanIN. The expression of pSTAT3 was particularly high in $SMA^+$ fibroblasts and $F4/80^+$ macrophages (**Fig. 3.1A**). To study the role of STAT3 in myeloid cells we generated a mouse model that lacks *Stat3* expression in the myeloid cells by crossing a mouse that has exons 18, 19, 20 (encoding for the SH2 domain) flanked by two LoxP sites. The LoxP sites are recognized by the CRE recombinase under the LysM promoter (myeloid specific), which excises the DNA, resulting in exons removal (**Fig. 3.1B**). Phenotypically, these mice were smaller in size compared to littermate control mice. They also have higher tendency to have rectal prolapse due to enterocolitis (Takeda et al., 1999). Using this mouse model, we studied pancreatic cancer by transplanting syngeneic KPC tumor cells (7940b) into the pancreas (**Fig. 3.1C**). The tumors were grown for 20 days and then harvested. The tumors that formed in the LysM-Cre;$Stat3^{f/f}$ mice were 2/3 times smaller than the tumor in the control mice (**Fig. 3.1D**). We also verified this by tumor to body weight ratio and we still found that tumors were significantly smaller in the LysM-Cre;$Stat3^{f/f}$. Histological analysis by HE did not revealed major changes in the histopathology between groups (**Fig. 3.1E**). Both control and LysM-Cre;$Stat3^{f/f}$ tumors had infiltration of macrophages, but the macrophages in the LysM-Cre;$Stat3^{f/f}$ mice did not express pSTAT3 (**Figure 3.1F**). Since the tumors were smaller, we decided to verify if the proliferation or apoptosis in the tumor was different between the conditions. Immunohistochemistry analysis of the tumor tissues showed no differences in the number of cells proliferating (Ki67) (**Fig 3.2A**) or dying by using cleave caspase 3 (CC3) as a marker (**Fig. 3.2B**). Hence, the effect of myeloid specific STAT3 knockout (KO) in tumor growth is not directly on the tumor cells at the time of being harvested.

### *3.2.2 Decrease in immunosuppressive macrophages in the myeloid-STAT3 knockout mice.*

The JAK/STAT3 pathway has been associated with immunosuppression in other malignancies. Thus, we investigated the immune infiltration in these tumor samples by using CyTOF. We used a total of 19 antibodies (table 3.3) and analysis of the data by unsupervised clustering detected a total of 20 populations in which 19 were immune cells ($CD45^+$) (**Fig. 3.3A** and **Fig. 3.3B**). Among these populations, several of them were TAMs. Manual gating analysis revealed that despite the total number of immune cells were the same in both samples, there was a decrease in the total number of macrophages defined by $CD45^+CD11b^+F4/80^+$ and increases in T cells, particularly $CD4^+$ T cells (**Fig. 3.3C**). From the unsupervised clustering, we evaluated the significantly differentially expressed populations and found a decrease in the TAM populations that expressed immunosuppressive markers such as PD-L1, CD206 and TIM3. Interestingly, the myeloid derived suppressor cells (MDSCs), which is considered as an immunosuppressive population, were increased even though they are considered an immunosuppressive population. The decrease in immunosuppressive macrophages correlated with an increase in T cells, particularly, $CD4^+$ T cells and central memory $CD8^+$ T cells (defined by Ly6C expression) (**Fig 3.3D**). These data suggest that STAT3 is an important regulator of immunosuppression driven by myeloid cells in pancreatic cancer.

### *3.2.3 Lack of STAT3 in the myeloid cells impairs tumor growth by T cell anti-tumor immunity.*

To elucidate if the mechanism leading to a diminishment in tumor growth in the LysM-Cre;$Stat3^{f/f}$ mice were due to $CD8^+$ T cell anti-tumor activity, we performed a $CD8^+$ T cell depletion. For this, we used an anti-CD8 depleting antibody in tumor bearing control or LysM-Cre;$Stat3^{f/f}$ mice (**Fig. 3.4A**). First, we confirmed the $CD8^+$ T cell depletion by CyTOF FlowSOM analysis. We saw that the depletion worked fantastically with a reduction of $CD8^+$ T cells in the tumor samples treated

with anti-CD8 compared to the IgG treated group (**Fig. 3.4B**). Comparison of tumor growth between groups showed that the LysM-Cre;Stat3$^{f/f}$ mice that received the anti-CD8 depletion antibody had an increment in tumors size compared to the IgG treated group (**Fig. 3.4C**). In this experiment the CD8 depletion did not affect tumor growth in the control group because T cells in the pancreatic tumors are suppressed. This result confirms that lack of STAT3 in myeloid cells reverse immunosuppression allowing for anti-tumor immune response by T cells, resulting in diminishment of tumor growth.

### 3.3 Discussion

In summary our results show that STAT3 activation in myeloid cells lead to the acquisition of an immunosuppressive phenotype in myeloid cells, particularly macrophages. Deletion of STAT3 in the myeloid compartment resulted in smaller pancreatic tumors. Interestingly, tumor growth was rescued by CD8$^+$ T cell depletion. Hence, we can conclude that myeloid STAT3 drives immunosuppression during pancreatic carcinogenesis (**Fig. 3.5**).

PDAC is defined as a "cold" tumor since it lacks CD8$^+$ T cell responses. Many studies are focusing on understanding the mechanisms underlying immunosuppression and how to reverse it. Unfortunately, immunotherapies by immune checkpoint blockade such as the anti-PD-L1 and anti-CTLA-4 have failed in pancreatic cancer and thus identifying different mechanism to reverse T cell suppression is imperative (Royal et al., 2010) (Brahmer et al., 2012). We have previously shown that epithelial KRAS$^{G12D}$ initiate the recruitment of suppressive cells early at the onset of carcinogenesis and that fibroblasts play a key role in this process through the activation of the JAK/STAT3 pathway (see chapter 1). STAT3 is activated in immunosuppressive macrophages and in inflammatory fibroblasts as this early stage contributing to immunosuppression. The

JAK/STAT3 pathway is known to be a regulator of IL6, IL10, and ARG1 which are immunosuppressive molecules (Rébé & Ghiringhelli, 2019). STAT3 has even been found to bind directly to the *Arg1* promoter to induce its expression (Vasquez-Dunddel et al., 2013). In our model we observe decrease of multiple macrophages populations expressing immunosuppressive molecules such as IL6, PD-L1 and CD206. Previous *in vitro* studies have also shown the role of JAK/STAT3 in promoting MDSCs (immunosuppressive cells) development *in vitro* (Mace et al., 2013). However, in our model we did not see decrease in MDSCs in the pancreatic tumors. In pancreatic cancer, the role of STAT3 has been studied by deleting it from epithelial cells, which prevented formation of PanINs (Fukuda et al., 2011) (Corcoran et al., 2011). The role of the JAK/STAT pathway was also studied in pre-clinical models by using the JAK1/2 inhibitor, Ruxolitinib, which showed promising results in murine models (Lu et al., 2017). Unfortunately, despite the successful results in pre-clinical models, PDAC clinical trials target the JAK/STAT pathway using different inhibitors, including Ruxolitinib, have failed (Herbert Hurwitz et al., 2018) (Peisl et al., 2021). Different aspects could explain this discrepancy, and two of my hypotheses are that (1) we need to target different compartments independently or (2) that we need to target the STAT3 and not all STATs proteins at once (as with the JAK1/2 inhibitors).

In my project we targeted specifically the JAK/STAT3 pathway in the myeloid compartment and to our knowledge that has never been studied in pancreatic cancer before. Although our results are promising, we still have some gaps in our methodology to confirm our findings. First, we need to repeat these experiments in different cell lines to prove the results are consistent. Second, our mouse model lacks STAT3 before tumor cells were implanted which is not clinically relevant. Thus, tumor implantation and subsequent pharmacological targeting of

STAT3 needs to be explored. Third, to better comprehend the effect of myloid-STAT3 during carcinogenesis we need to study a spontaneous mouse model of pancreatic cancer. While our current model is not perfect, the study of other cancers using a similar model have shown comparable results. For example, in a model of murine colorectal cancer (CRC), myeloid specific knockout (KO) of STAT3 decreased the number of tumors (Pathria et al., 2015). Further characterization found that analogous our model, this model had a decrease in immunosuppressive cells in the myeloid STAT3 KO mice and, similarly to my results, depletion of T cells rescued the phenotype. Moreover, in a murine lung cancer model similar results were found by using the same model of LysM-Cre;Stat3$^{f/f}$. In this lung model (induced with urethane) they observed decrease in immunosuppressive cells (MDSCs and macrophages) and the tumor growth was rescued by a CD8 KO mouse model or by IFN$\gamma$ inhibition (J. Zhou et al., 2017). These studies suggest that targeting myeloid specific STAT3 is a potential treatment avenue in different tumors. However, achieving this type of specific treatment is difficult. One way to achieve it is by developing nanoparticles that can deliver drugs to myeloid cells specifically or by targeting STAT3 specifically. More extensive studies need to be completed to understand at a deeper level this pathway and to explore better approaches to target the pathway and create better combinatorial therapies.

### 3.4 Methods

#### Mice

Mice were housed in the pathogen-free animal facilities in the Rogel Cancer Center at the University of Michigan and maintained by the unit for laboratory animal medicine (ULAM). The LysM-Cre allele mouse was kindly provided by Dr. Howard Crawford. The *Stat3* flox (B6.129S1-*Stat3*$^{tm1Xyfu}$/J) was purchased from the Jackson laboratories.

**Mouse experiments**

Orthotopic injections were done by implanting 50,000 cells of the KPC (Pdx-Cre; LSL-Kras$^{G12D}$; LSL-Trp53$^{R172H}$) cell line 7940b C57BL/6J strain (Long et al., 2016) or the 65671 (Ptf1a-Cre;LSL-Kras$^{G12D}$; Trp53$^{flox/+}$, FVB-N) cell line (Yaqing Zhang et al., 2013) (Hingorani et al., 2005). CD8+ T cell depletion was accomplished by treating mice with anti-CD8 (In vivoMAb anti-mouse CD8a, BioXCell, BE0061) every 3 days (200ug/mouse). STAT3 degrader (SD-36) was administered intravenously (I.V.) twice a week at a dose of 50mg/kg. Nanoparticles loaded with *siStat3* were administered by I.V. injections 3 times a week (1400ug/mL). Nanoparticles were prepared by Ava Mauser in Dr. Joerg Lahann laboratory.

**Cell culture**

All cell lines were cultured in DMEM with 10% Fetal Bovine Serum and 1% Penicillin Streptomycin. The tumor cell lines (7940b (C57BL/6J) and 65671(FVBN)) were derived from a KPC (Ptf1a-Cre;LSL-KrasG12D; Trp53flox/+) pancreatic cancer (Yaqing Zhang et al., 2013) (Hingorani et al., 2005) (Long et al., 2016). To generate conditioned media (CM), fresh medium was replaced and harvested after 2-3 days based on cell confluency. The media was then centrifuged (1300rpm, 10 minutes at 4ºC) to remove contaminating cancer cells. The CM was used to culture BMDM with a 1:1 ratio of CM to normal RPMI for 7 days.

**Histology and immunohistochemistry**

Pancreatic orthotopic tumors from littermates control or LysM-Cre;Stat3$^{f/f}$ mice were fixed in 10% neutral-buffered formalin (FisherBrand) overnight and then embedded in paraffin and sectioned into slides. Embedding and sections were performed by Daniel Lang from Howard Crawford

laboratory and Michael Mattea from the Yatrik Shah Lab at the University of Michigan. Hematoxylin and eosin (H&E), Gomori's Trichome, Periodic Acid Shift (PAS) and Immunofluorescence (IF) staining were performed as previously described (Collins, Bednar, et al., 2012). For immunohistochemistry, paraffin slides were freshly cut and then re-hydrated using 2 series of xylene, 2 series of 100% ethanol and then 2 series of 95% ethanol. We used water to wash all residues from the previous steps. Antigen Retrieval CITRA Plus (BioGenex) was used for antigen retrieval and slides were microwaved for total 8 minutes in the solution. Upon cool down, 1% BSA in PBS was used to block the tissue for 30 minutes and then primary antibodies in the Table 3.1 were used at their corresponding dilutions. Biotinylated secondary antibodies anti-rat, anti-rabbit, and anti-mouse were used in 1:300 dilution. Following the secondary antibody incubation, the tissue was incubated for 30 minutes with the ABC reagent from Vectastain Elite ABC kit, peroxidase. Then it was developed using DAB (Vector) followed by staining of hematoxylin (Sigma Aldrich) and dehydration of slides prior to mounting. For IF, Alexa fluor secondary antibodies (Invitrogen) were used. Prolong Diamond Antifade Mountant with DAPI (Invitrogen) was used for nuclei staining. TSA Plus Fluorescein system (PerkinElmer) was used in IF when primary antibodies raised in the same species were used. Microscope: Olympus BX53F microscope, Olympus DP80 digital camera, and CellSens Standard software. Quantification of cell number or positive area was done using 3-5 images/slide (400x magnification) taken from 2-4 samples per group by K. Brown using ImageJ. We also use the Leica STELLARIS 8 FALCON Confocal Microscopy System and the LAS X software to acquire and visualize images.

**Flow cytometry**

Pancreata or pancreatic tumors were harvested and disrupted to single cells by finely mincing the tissue using scissors and digested it using Collagenase IV (sigma) for 30 minutes at 37°C while shaking. To separate into single cells, we used a 40um mesh strainer. RBC lysis buffer was used to lyse all the red blood cells. Cells were stained for surface markers using antibodies listed in Table 3.2. Cells were also fixed and permeabilized before intracellular staining using antibodies Table 3.2. Flow-cytometric analysis were performed on the Cyan ADP analyzer (Beckman coulter) and the ZE5 analyzer (Bio-Rad). Data was analyzed using the FlowJo v10 software.

**CyTOF**

Pancreata or pancreatic tumors were harvested and disrupted to single cells as described above. To separate cells into single cells three mesh strainers were used: 500um, 100um and 40um. Cells were washed twice in PBS and labeled for viability using Cell-ID cisplatin (1.67 umol/L) for 5 min at room temperature (RT). Surface and intracellular staining (Table 3.3) was performed as detailed in manufacturer instructions (Fluidigm). Cells were shipped in intercalator buffer on ice overnight to Flow Cytometry core at the University of Rochester Medical Center or to Andrea M. Gunawan in Indiana University where the samples preparation was finalized, and CyTOF2 Mass Cytometer analysis were performed. Data analysis was performed using the Premium CytoBank Software (cytobank.org) and R studio using the CyTOF workflow from Nowicka M. Et. al. (Nowicka et al., 2017).

**Bone marrow extraction**

The femur and the tibia bones were extracted from the mice and placed in cold RPMI media. Using a 21G and a 28G syringe, we flushed the bone marrow (BM) from the bones using media. The

media containing the BM was placed in a tube and centrifuged for 10 min at 1000rmp. Then, we added RBC lysis buffer for 5 min at RT. The cells were washed and centrifuged for 5 min at 1300rpm twice. Cells were then resuspended in a plate with 50% conditioned media from KPC cell line 7940b and 50% RPMI 10% FBS. After 3 days, more media was added and after 5 days the media was changed. By day 7 the macrophages were fully polarized to tumor educated macrophages (TEMs).

**Author contribution**

Ashley Velez-Delgado[1], Kristee L. Brown[2], Rosa E. Menjivar[3], Wenting Du[2], Filip Bednar[2,4], Timothy L. Frankel[2,4], Yaqing Zhang[2,4*] and Marina Pasca di Magliano[1,2,3,4*]

[1]Department of Cell and Developmental Biology; [2]Department of Surgery, [3]Cellular and Molecular Biology Program; [4]Rogel Cancer Center

University of Michigan, Ann Arbor, MI 48109 USA

*Corresponding authors

**Grant support**

We thank Dr. Gregory Beatty at University of Pennsylvania for generously sharing the primary mouse pancreatic cancer cell line 7940b and Dr. David Tuveson at Cold Spring Harbor Laboratory for the generous gift of the primary mouse pancreatic cancer cell line mT3-2D. This project was supported by NIH/NCI grants R01CA151588, R01CA198074, the University of Michigan Cancer Center Support Grant (NCI P30CA046592), the American Cancer Society to

MPM and U01CA-224145 to MPM and HCC. YZ was funded by NCI-R50CA232985. AVD was supported by Rackham Merit Fellowship, Cellular Biotechnology Training Program (T32GM008353) and the NCI F31-CA247037. REM was supported by the NIH Cellular and Molecular Biology Training Grant T32-GM007315 and the Center for Organogenesis Training Program (NIH T32 HD007505). University of Michigan Training Program in Organogenesis non-traditional postdoctoral fellowship to WD. FB was funded by the Association of Academic Surgery Joel Roslyn Award. TF was supported by (K08CA201581). This project was also supported by the Tissue and Molecular Pathology and Flow Cytometry Shared Resources at the Rogel Cancer Center and the University of Michigan DNA Sequencing Core. CyTOF was performed at the University of Rochester University of Rochester Medical Center Flow Cytometry Shared Resource and at the Indiana University Simon Cancer Center Flow Cytometry Service. This work used a Leica STELLARIS 8 FALCON Confocal Microscopy System that was purchased with funds from a National Institutes of Health SIG grant *NIH* S10OD28612-01-A1.

## 3.5 Figures

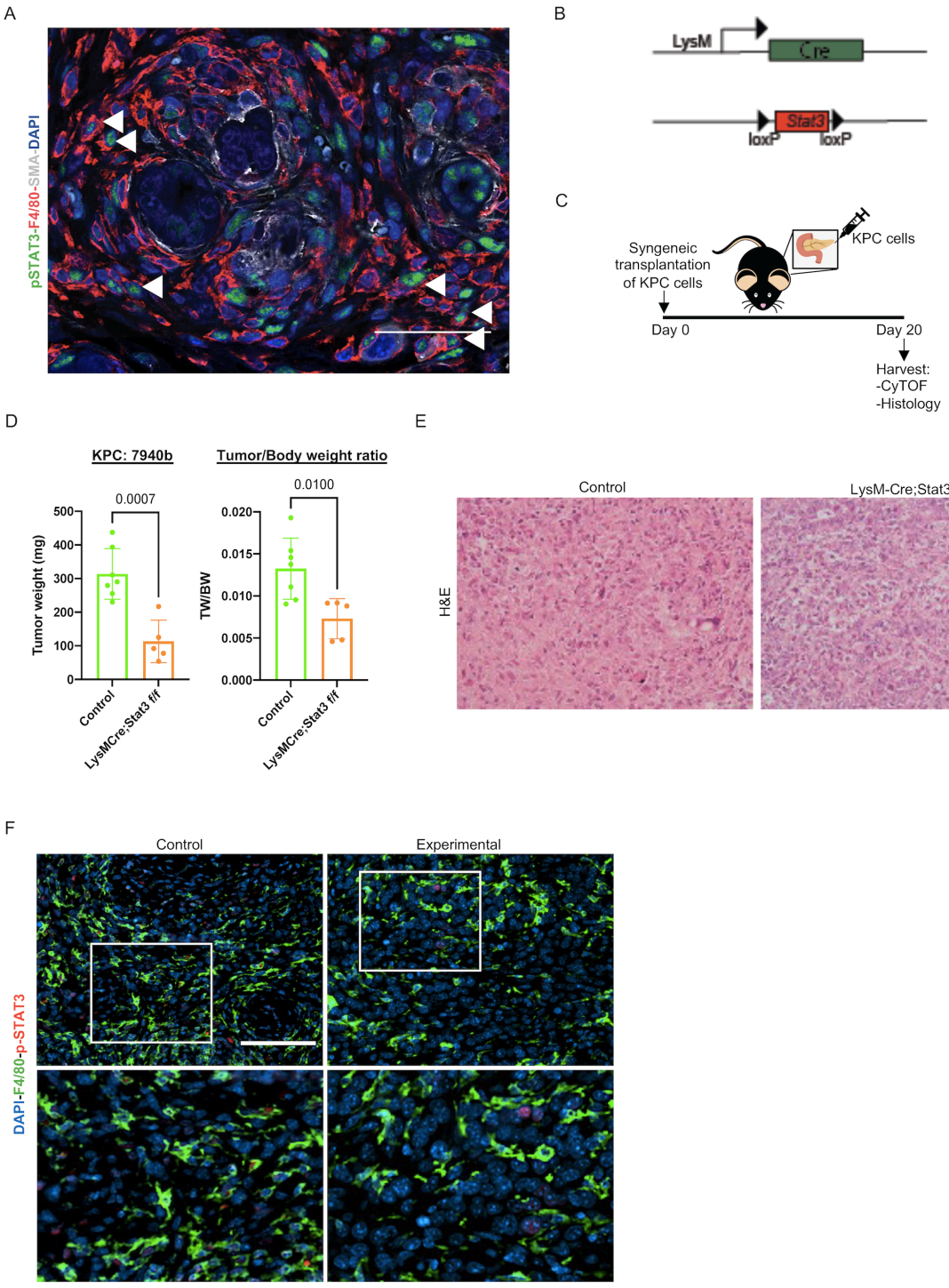
A
pSTAT3-F4/80-SMA-DAPI
B
LysM
Cre
Stat3
loxP
loxP
C
Syngeneic transplantation of KPC cells
KPC cells
Day 0
Day 20
Harvest:
-CyTOF
-Histology
D
KPC: 7940b
Tumor/Body weight ratio
0.0007
0.0100
Tumor weight (mg)
TW/BW
Control
LysMCre;Stat3 f/f
E
Control
LysM-Cre;Stat3 f/f
H&E
F
Control
Experimental
DAPI-F4/80-p-STAT3

**Figure 3-1: Lack of myeloid-STAT3 impairs pancreatic tumor growth.**

(A) Representative immunofluorescence image of pSTAT3 (Green), F4/80 (Red) and SMA (White) in an early PanIN stage. Arrowheads points to positive pSTAT3 in macrophages (F4/80+). Scale bar 50um. (B) Genetic make-up of the LysM-Cre;Stat3$^{f/f}$ mice. (C) Experimental plan. KPC cell line (7940b) was injected orthotopically in syngeneic control or LysM-Cre;Stat3$^{f/f}$ mice. Tumor were harvested 20 days later. (D) Plot showing tumor weight in milligrams (mg) and tumor to body weight ratio from control or LysM-Cre;Stat3$^{f/f}$ mice. Data shown as mean ± SD. Statistical analysis by unpaired t-test. (E) Representative Hematoxylin and Eosin (H&E) staining of the tumors from control or LysM-Cre;Stat3$^{f/f}$ mice. (F) Representative immunofluorescence images of pSTAT3 (Magenta), and F4/80 (Green) of tumors from control or LysM-Cre;Stat3$^{f/f}$ mice, scale bar 100um.

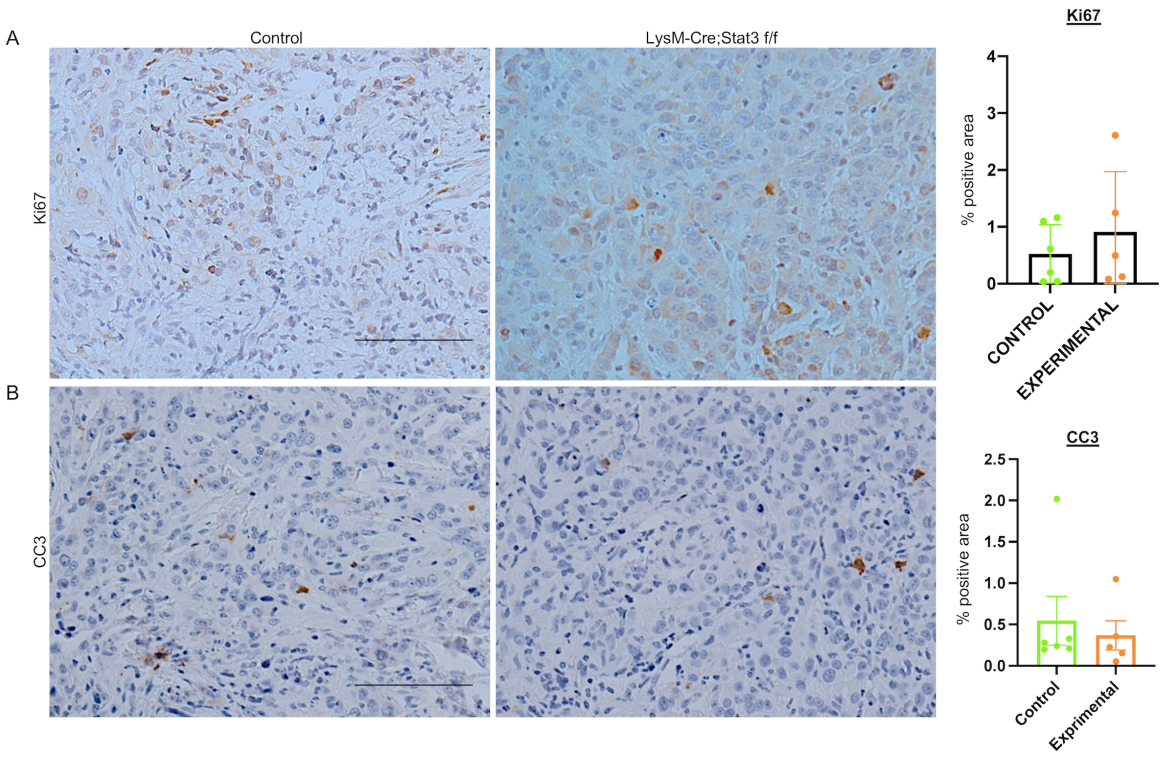


**Figure 3-2: Myeloid-STAT3 knockout affects tumor growth indirectly.**

(A) Representative immunohistochemistry images of Ki67 and its quantification on the right from control or LysM-Cre;Stat3$^{f/f}$ tumors. N=5-7 per group. Data shown as mean ± SD. Statistical analysis by unpaired t-test. (B) Representative immunohistochemistry images of cleaved caspase 3 (CC3) and its quantification on the right from control or LysM-Cre;Stat3$^{f/f}$ tumors. N=5-7 per group. Data shown as mean ± SEM. Statistical analysis by unpaired t-test. Scale bars 100um.

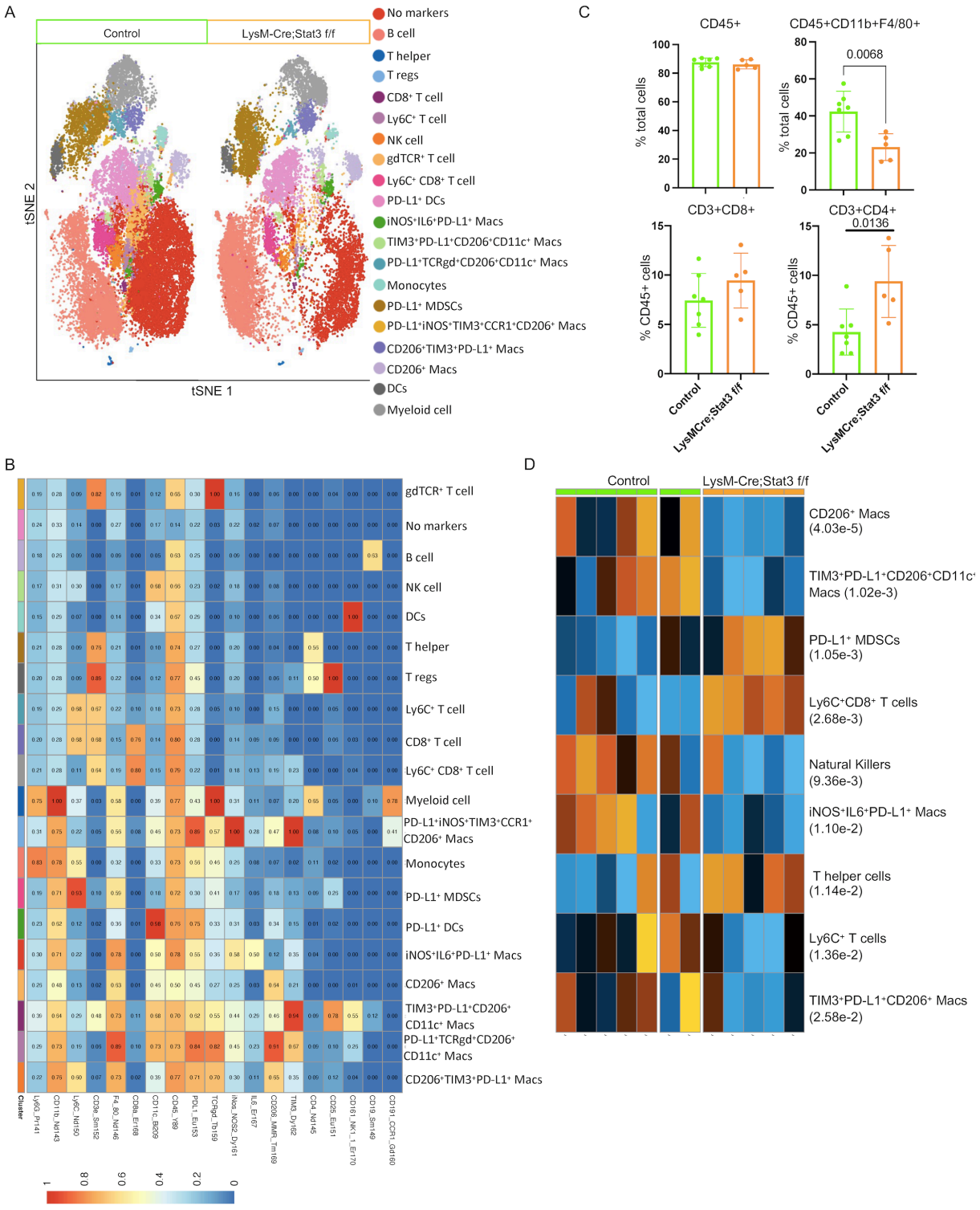
A
Control
LysM-Cre;Stat3 f/f
tSNE 2
tSNE 1
No markers
B cell
T helper
T regs
CD8⁺ T cell
Ly6C⁺ T cell
NK cell
gdTCR⁺ T cell
Ly6C⁺ CD8⁺ T cell
PD-L1⁺ DCs
iNOS⁺IL6⁺PD-L1⁺ Macs
TIM3⁺PD-L1⁺CD206⁺CD11c⁺ Macs
PD-L1⁺TCRgd⁺CD206⁺CD11c⁺ Macs
Monocytes
PD-L1⁺ MDSCs
PD-L1⁺iNOS⁺TIM3⁺CCR1⁺CD206⁺ Macs
CD206⁺TIM3⁺PD-L1⁺ Macs
CD206⁺ Macs
DCs
Myeloid cell
C
CD45+
CD45+CD11b+F4/80+
% total cells
0.0068
CD3+CD8+
CD3+CD4+
0.0136
% CD45+ cells
Control
LysMCre;Stat3 f/f
B
gdTCR⁺ T cell
No markers
B cell
NK cell
DCs
T helper
T regs
Ly6C⁺ T cell
CD8⁺ T cell
Ly6C⁺ CD8⁺ T cell
Myeloid cell
PD-L1⁺iNOS⁺TIM3⁺CCR1⁺ CD206⁺ Macs
Monocytes
PD-L1⁺ MDSCs
PD-L1⁺ DCs
iNOS⁺IL6⁺PD-L1⁺ Macs
CD206⁺ Macs
TIM3⁺PD-L1⁺CD206⁺ CD11c⁺ Macs
PD-L1⁺TCRgd⁺CD206⁺ CD11c⁺ Macs
CD206⁺TIM3⁺PD-L1⁺ Macs
Cluster
Ly6G_Pr141
CD11b_Nd143
Ly6C_Nd150
CD3e_Sm152
F4_80_Nd146
CD8a_Er168
CD11c_Bi209
CD45_Y89
PDL1_Eu153
TCRgd_Tb159
iNos_NOS2_Dy161
IL6_Er167
CD206_MMR_Tm169
TIM3_Dy162
CD4_Nd145
CD25_Eu151
CD161_NK1.1_Er170
CD19_Sm149
CD191_CCR1_Gd160
1
0.8
0.6
0.4
0.2
0
D
Control
LysM-Cre;Stat3 f/f
CD206⁺ Macs (4.03e-5)
TIM3⁺PD-L1⁺CD206⁺CD11c⁺ Macs (1.02e-3)
PD-L1⁺ MDSCs (1.05e-3)
Ly6C⁺CD8⁺ T cells (2.68e-3)
Natural Killers (9.36e-3)
iNOS⁺IL6⁺PD-L1⁺ Macs (1.10e-2)
T helper cells (1.14e-2)
Ly6C⁺ T cells (1.36e-2)
TIM3⁺PD-L1⁺CD206⁺ Macs (2.58e-2)

**Figure 3-3 STAT3 is a driver of immunosuppressive phenotype in macrophages.**

(A) CyTOF analysis of cells from Control or LysM-Cre;Stat3$^{f/f}$ tumor samples visualized by tSNE plots. 20 clusters were identified by FlowSOM using 19 markers and 4000 randomly selected cells per group. (B) Heatmap of the median marker intensity generated with FlowSOM of the CyTOF samples (Control or LysM-Cre;Stat3$^{f/f}$ combined). Colors on the left represent the clusters shown in the t-SNE plots. N=5-7per group. (C) Plots representing the numbers of cell populations obtained by manual gating from the CyTOF data. Data shown as mean ± SD. Statistical analysis by unpaired t-test. N=5-7 per group. (D) Heatmap showing differentially abundance of clusters from CyTOF analysis. Statistical analysis by Wrapper function.

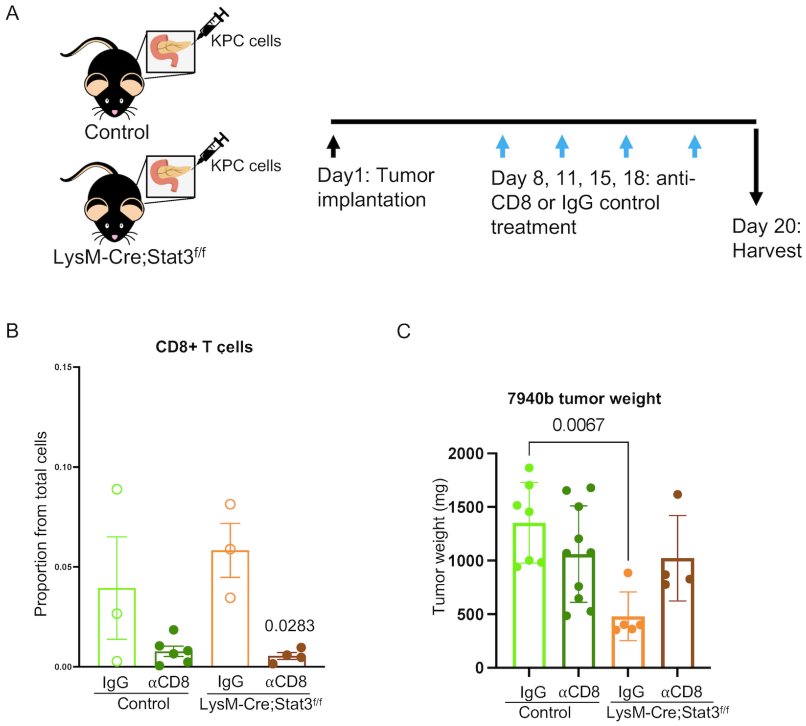


**Figure 3-4 Lack of myeloid-STAT3 impairs tumor growth by T cell anti-tumor immunity.**

(A) Experimental plan. Control or LysM-Cre;Stat3$^{f/f}$ mice were injected with the KPC cell line 7940b orthotopically in the pancreas. Mice were treated with IgG or anti-CD8 to deplete CD8$^{+}$ T cells every 3 days. Tumor were harvested at 20 days post injection of tumor cells. (B) Amount of CD8$^{+}$ T cell as a proportion of total cells from the CyTOF data. Data shown as mean ± SEM. Statistical analysis by unpaired t-test. N=3-6 per group. (C) Plot showing tumor weight of control or LysM-Cre;Stat3$^{f/f}$ mice at different conditions. Data shown as mean ± SD. Statistical analysis by Kruskal-Wallis. N=4-10 per group.

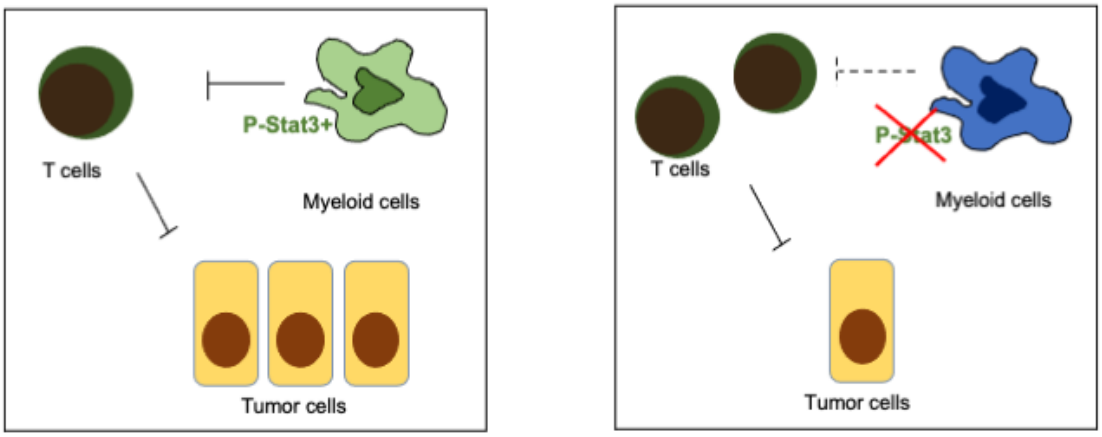


**Figure 3-5 Myeloid specific STAT3 is a driver of immunosuppression in pancreatic cancer.**

**Activation of the JAK/STAT3 pathway in myeloid cells drive an immunosuppressive phenotype that inhibit T cell activity allowing for tumor growth. Deletion of STAT3 from myeloid cells decrease the immunosuppressive phenotype of macrophages. Consequently, T cells are more active and able to control tumor growth.**

**Table 3-1 IHC and IF antibodies**

| Antibody | Supplier | Catalog # | IHC dilution | IF dilution |
|---|---|---|---|---|
| F4/80 | Cell Signaling | 70076S | | 1:250 |
| aSMA | Sigma Aldrich | A2547 | | 1:1000 |
| Ki67 | Abcam | ab15580 | 1:100 | |
| CC3 | Cell Signaling | 9661L | 1:100 | |
| pStat3 Y705 | Cell Signaling | 9145S | 1:100 | 1:100 |

**Table 3-2 Flow cytometry antibodies**

| **Antibodies** | **Supplier** | **Catalog #** | **Clone** | **Dilution** |
|---|---|---|---|---|
| CD45 | Invitrogen | MCD4530 | 30-F11 | 1:100 |
| CD45 | BD Horizon | 563891 | 30-F11 | 1:100 |
| CD11b | BD Pharmingen | 557657 | M1/70 | 1:100 |
| F4/80 | Invitrogen, eBioscience | 15-4801-82 | BM8 | 1:100 |
| CD3 | BD Pharmingen | 17A2 | 555275 | 1:100 |
| CD4 | BD Pharmingen | RM4-5 | 558107 | 1:100 |

| | | | | |
|---|---|---|---|---|
| CD8 | BD Pharmingen | 53-6.7 | 557654 | 1:100 |
| Foxp3 | eBioscience | FJK-16s | 53-5773-82 | 1:100 |

**Table 3-3 CyTOF antibodies**

| Antibodies | | Clone | Isotope | Dilution |
|---|---|---|---|---|
| CD45 | Fluidigm | 30-F11 | Y89 | 1:200 |
| Ly6G | Fluidigm | 1AB | Pr141 | 1:400 |
| CD11b | Fluidigm | M1/70 | Nd143 | 1:300 |
| CD4 | Fluidigm | RM4/5 | Nd145 | 1:200 |
| F480 | Fluidigm | BM8 | Nd146 | 1:100 |
| CD140a | Fluidigm | APA5 | Nd148 | 1:100 |
| CD19 | Fluidigm | 6D5 | Nd149 | 1:200 |
| Ly6C | Fluidigm | HK1.4 | Nd150 | 1:400 |
| CD3e | Fluidigm | 145-2C11 | Sm152 | 1:100 |
| TCR gd | Fluidigm | GL3 | Tb159 | 1:100 |
| CD191 CCR1 | Custom | S15040E | Gd160 | 1:100 |
| iNOS | Fluidigm | CXNFT | Dy161 | 1:100 |
| Arginase1 | Custom | Polyclonal | Er166 | 1:400 |
| CD8a | Fluidigm | 53-6.7 | Er168 | 1:200 |
| CD206 | Fluidigm | C068C2 | Tm169 | 1:200 |
| CD161 NK1.1 | Fluidigm | PK136 | Er170 | 1:100 |
| CD11c | Fluidigm | N418 | Bi209 | 1:100 |
| CD274 PD-L1 | Fluidigm | 10F.9G2 | Eu153 | 1:100 |

| | | | | |
|---|---|---|---|---|
| IL6 | Fluidigm | | Er167 | 1:100 |
| CD25 | Fluidgm | 3C7 | Eu151 | 1:100 |
| TIM3 | Fluidgm | | Dy162 | 1:100 |

# Chapter 4 Discussion and Future Directions

Pancreatic cancer has a dismal prognosis due to its late detection, high metastatic capability, and scarcity of effective treatments. New therapeutic approaches or combinations are to be explored. Effectiveness of immune checkpoint inhibitors in solid tumors such as melanoma have driven the attention to the immunotherapies. However, immunotherapies have been unsuccessful in pancreatic cancer mainly because there are scarce number of cytotoxic T lymphocytes (CTLs) in the tumor. Augmenting the number of CTLs and then using immune checkpoint inhibitors in murine models have been effective. Therefore, investigating ways to increase CTLs in pancreatic tumors by reversing immunosuppression is important to develop combinatorial therapies. In this section, I summarized the projects presented in the pasts chapters and discuss potential future directions for both projects.

## 4.1 Extrinsic KRAS signaling shapes the pancreatic microenvironment through fibroblast reprogramming.

Previously, our lab showed that $KRAS^{G12D}$ is required for the initiation and maintenance of low grade PanIN (Collins, Bednar, et al., 2012). *Kras*$^{G12D}$ inactivation in ADM/early PanINs (3w ON post-pancreatitis) led to regression of the lesions through dedifferentiation of the PanINs to acinar cells (Collins, Bednar, et al., 2012). Interestingly, we found that at this stage of ADM/early PanINs myeloid cells were required for the tissue recovery after *Kras*$^{G12D}$ inactivation (Y. Zhang, W. Yan, et al., 2017). Due to these findings, during my thesis we explored the role of

KRAS$^{G12D}$ in modulating the precursor lesion microenvironment (PME). In chapter 2, I described the role of epithelial KRAS$^{G12D}$ in reprogramming fibroblasts (extrinsic signaling) to create and maintain an immunosuppressive PME. Upon *Kras*$^{G12D}$ expression in epithelial cells, different factors are secreted and in turn fibroblasts become reprogrammed to an inflammatory phenotype expressing *Cxcl1*, *Il1*, *Il33* and *Saa3*. Myeloid cells (TAMs and MDSCs) possess receptors for these genes and in turn activate STAT3 expression upon *Kras*$^{G12D}$ activation and express immunosuppressive molecules. Interestingly, upon *Kras*$^{G12D}$ inactivation, fibroblasts downregulated expression of inflammatory cytokines and macrophages decreased STAT3 expression as well as upregulating genes related to a tissue repair phenotype. The data presented in chapter 2 provided further insight in the establishment of the immunosuppressive PME and deepened our understanding of the dual role of the macrophages upon extrinsic signaling from KRAS$^{G12D}$.

In this project, we focused primarily on the role of epithelial oncogenic KRAS in the myeloid cells. However, T cells play a role in pancreatic cancer progression, and it was previously shown that CD4$^{+}$ T cells were tumor promoting during PanIN stage (Zhang et al., 2014). Hence, we also interrogated whether epithelial KRAS$^{G12D}$ also modulated T cell infiltration and function. To understand this, we investigated the infiltration of T cells comparing 3w ON to 3d OFF or 1w OFF tissues (**Fig. 4.1A**). Surprisingly, T cells did not decrease upon *Kras*$^{G12D}$ inactivation (**Fig 4.1B**). Interestingly, analysis of OPAL staining determined that even though the numbers of T cells did not decrease upon *Kras*$^{G12D}$ inactivation, they appear to be in close proximity to epithelial cells (**Fig 4.1C-E**). This data suggests that T cells might also have a role in tissue repair as the myeloid cells. Previously, we discovered that depletion of CD8$^{+}$ T cells either during PanIN progression or during tissue recovery did not have an effect, suggesting that T cells do not possess

anti-tumor immunity at this early stage and that they do not mediate tissue recovery (Y. Zhang, W. Yan, et al., 2017). Given this finding, we decided to investigate the role of T regs in tissue repair upon *Kras*$^{G12D}$ inactivation. We utilized a mouse model (iKras*Foxp3$^{DTR}$) that was generated by crossing the iKras* with a mouse that expresses the diphtheria toxin receptor (DTR) in the FoxP3 promoter (T regs specific) (Zhang et al., 2020). Using the iKras*Foxp3$^{DTR}$ and the iKras* we turned ON *Kras*$^{G12D}$ for 3 weeks and then we turn OFF *Kras*$^{G12D}$ and at the same time we treated with diphtheria toxin (DT) to deplete T regs (**Fig 4.2A**). Surprisingly, depletion of T regs impaired tissue recovery as shown by histology (**Fig. 4.2B-C**). These results are interesting, however further studies are needed to comprehend the mechanisms underlying T regs mediated tissue repair. In conclusion, expression of oncogenic KRAS by epithelial cells drives the establishment of a suppressive microenvironment in the onset of carcinogenesis. Furthermore, the microenvironment remains plastic at this early stage and the macrophages and T regs can promote tissue repair upon KRAS$^{G12D}$ signaling extinction.

Another interesting aspect presented in Collins et al. paper when describing the iKras* mouse model, was that inactivation of *Kras*$^{G12D}$ in established PanINs (5w ON post-pancreatitis) resulted in impaired recovery. At this timepoint (5w ON), inactivation of *Kras*$^{G12D}$ also led to the redifferentiation of PanIN to acinar cells but it was not as extensive as in the earlier time points (3w ON). What remains to be understood is whether immune cells respond in a similar manner to *Kras*$^{G12D}$ inactivation at these later stages of carcinogenesis. Giving that myeloid cells and T regs have a role in tissue repair during early PanIN, we wondered if they can retain this tissue repair phenotype in later stages. We observed that inactivating *Kras*$^{G12D}$ for 1 week (1w OFF) after 5 weeks ON post pancreatitis led to an impairment in tissue recovery as shown before (**Fig. 4.3A**

**and 4.3B**). Further, we showed that similar to the 3w ON time points, *Kras*$^{G12D}$ inactivation led to a decrease in pERK, and SMA (**Fig. 4.3C and 4.3D**). Interestingly, we observed that contrary to the 3w ON time point, inactivation of *Kras*$^{G12D}$ led to a decrease in macrophages, including ARG1$^{+}$ macrophages, and decrease in CD4$^{+}$ T cells by 1w OFF (**Fig. 4.3C-F**). The decrease in macrophages and CD4$^{+}$ T cells, was accompanied by increase in CD8$^{+}$ T cells (**Fig. 4.3D and 4.3F**). However, CD8$^{+}$ T cell depletion did not re-establish tissue repair, hence CD8$^{+}$ T cells are not mediating the impairment in tissue repair (data not shown). These data suggest that keeping *Kras*$^{G12D}$ activated for a longer period affects the PME differently. The decrease in macrophages could explain the impairment in tissue repair since myeloid cells are required for tissue repair (Zhang, 2020, 31911451). Further studies to understand the role of *Kras*$^{G12D}$ at this stage are needed to elucidate the mechanism leading to a differential response to *Kras*$^{G12D}$ inactivation at different stages of carcinogenesis.

All the aforementioned studies have been done early during carcinogenesis and the question remains of how KRAS$^{G12D}$ modulates the TME at later stages of carcinogenesis. To study the effect of KRAS$^{G12D}$ at advance stages of carcinogenesis our lab developed the iKras*P53* mouse model (Collins, Brisset, et al., 2012). This model express *Kras*$^{G12D}$ in the pancreas (inducible and reversible) and it also expresses a mutated P53$^{R172H}$ allele. The iKras*P53* mice developed tumors with high metastatic capability to the liver. In this model, inactivation of *Kras*$^{G12D}$ led to decrease in tumor burden and metastasis (Collins, Brisset, et al., 2012). The iKras*P53* cell lines were derived from this model and then were implanted subcutaneously in NOD/SCID mice. As in the spontaneous model, inactivation of *Kras*$^{G12D}$ let to tumor regression. However, how the TME changes upon inactivation of *Kras*$^{G12D}$ it is still poorly understood. Recently, the role of epithelial-KRAS$^{G12D}$ in the immune cells during later stages of carcinogenesis

was studied in a syngeneic orthotopic mouse model using iKras*P53* cell line or KRAS knockout (KO) cell lines (I. Ischenko et al., 2021). They found that inactivation of *Kras*$^{G12D}$ or the use of *Kras* KO cell lines led to a decrease in immunosuppressive myeloid cells and an increase in T cells (I. Ischenko et al., 2021).

We performed similar experiments but comparing *Kras*$^{G12D}$ inactivation to MEK inhibition using trametinib (TRAM). To study this, we did implantation of pancreatic tumor cells lines derived from iKras* P53* mice in syngeneic mouse model similar to the iKras* P53* cell line published previously from our lab (Collins, Brisset, et al., 2012). In our transplanted model we either turn *Kras*$^{G12D}$ ON and harvested after 2 weeks or we turn *Kras*$^{G12D}$ OFF for 3 days or inhibited the MAPK pathway using TRAM for 3 days before completion of the 2 weeks (**Fig. 4.4A**). Upon harvesting, we observed smaller tumors after turning *Kras*$^{G12D}$ OFF (**Fig. 4.4B**). This was accompanied by decrease in pERK expression as a readout of MAPK activation (**Fig. 4.4C**). We verified the immune infiltration using CyTOF and we observed no decrease in the overall immune infiltration after *Kras*$^{G12D}$ inactivation (**Fig. 4.4D**). Further analysis of immunosuppressive markers on myeloid cells, revealed a trend towards decrease in PD-L1 and CD206 expression in macrophages as well as increase in iNOS in the *Kras*$^{G12D}$ OFF or TRAM treated groups (**Fig. 4.4E**). The role of the MAPK pathway in regulating the expression of PD-L1 in tumor cells was shown before (Y. Zhang, A. Velez-Delgado, et al., 2017). These data suggest that trametinib treatment have similar effect in the immunosuppressive cells as turning OFF *Kras*$^{G12D}$. However, clinical trials using trametinib has been unsuccessful, hence more studies are required to find new combinatorial treatments (Infante et al., 2014).

## 4.2 The JAK/STAT3 pathway drives immunosuppression in pancreatic cancer myeloid cells

In chapter 3, we used a mouse model that lacks STAT3 in the myeloid cells and we transplanted syngeneic pancreatic tumor cells lines into the pancreas to understand pancreatic cancer progression. Lack of STAT3 in myeloid cells impaired tumor growth by decreasing immunosuppressive cells in the tumor and hence augmenting the number of T cells. $CD8^+$ T cells depletion increases tumor growth. Although, the results are promising, further experiments need to be completed to validate these results. First, these experiments were done utilizing only one cell line, hence multiple cell lines need to be tested to validate the findings. Second, our mouse model lacks the expression of STAT3 prior to tumor implantation which is not clinically relevant. Clinical trials for multiple JAKs inhibitors, including Ruxolitinib, have been tried in PDAC but unfortunately, they have not improved survival (Peisl et al., 2021) (Herbert Hurwitz et al., 2018). Therefore, we need to test STAT3 inhibitors or alternative treatments in tumor bearing mice. However, since our main goal is to target myeloid specific STAT3 we need to develop ways to therapeutically achieve this. One way to achieve it is by developing nanoparticles that can deliver drugs to myeloid cells specifically.

In our lab we started exploring the use of nanoparticles to deliver drugs. For this, we established collaborations with two different laboratories at the University of Michigan. First, we tried the nanoparticles developed by Dr. Cheng Xu from Dr. James Moon lab. These nanoparticles were loaded with Ruxolitinib but results need further characterization (data not shown). We also tried the previously published nanoparticles containing siRNA against *Stat3* by Dr. Joerg Lahann laboratory (Gregory et al., 2020). We treated tumor bearing mice with PBS, empty nanoparticles or nanoparticles containing si*Stat3*. As a preliminary experiment, we did treatments for a week

(**Fig 4.5A**) and after harvesting we observed a trend of smaller tumors (not significant) in the pancreatic tumor treated with the nanoparticles containing siRNA (**Fig 4.5B**). We also confirmed that the delivery was efficient to the pancreas by assessing the expression of pSTAT3 in the tumor tissues (**Fig 4.5C**). More extensive work remains to be done in this area to develop nanoparticles that specifically target myeloid cells.

Another potential avenue is that instead of using JAK1/2 inhibitors, we target STAT3 directly, keeping other STATs proteins intact. In collaboration with Dr. Shaomeng Shang we started to explore the role of a highly potent STAT3 degrader (SD-36) in pancreatic tumors (Bai et al., 2019). After treatments for two weeks, we did not observe decrease in tumor growth (**Fig 4.6A and 4.6B**). However, we confirmed that the inhibitor degraded STAT3 in the pancreatic tumors (**Fig 4.6C**). Although tumors did not regress, we observed decrease in all different immune populations, indicating that immune cell were affected by the treatments (**Fig 4.6D**). A potential explanation to why we did not observe tumor regression is because the turnover of STAT3 activation is fast in pancreatic tumors. Pharmacokinetic experiments indicated that after 12hr, activity of STAT3 starts to return (**Fig. 4.6E**). Recently, a clinical trial using a STAT3 specific inhibitor (Napabucasin) in metastatic pancreatic cancer was terminated due to futility (Bekaii-Saab T, 2021). This inhibitor was also previously tested in CRC patients, although it did not improve overall survival the results suggested that it might be effective in patients with high expression of pSTAT3 (Peisl et al., 2021) (Jonker et al., 2018). These results indicates that we need to understand better the mechanism underlying STAT3 inhibition in humans to develop combinatorial therapies.

## 4.3 Summary

PDAC remains a lethal disease and combinatorial therapies are needed. The data provided in this thesis dissects the establishment of an immunosuppressive microenvironment early during carcinogenesis by the oncogenic KRAS-expressing epithelial cells. Also, my thesis shows the potential of using compartment specific therapies to target individual pathways, such as the JAK/STAT3 signaling pathway. Taken together my data supports the notion that the immunosuppressive microenvironment is created early during carcinogenesis supporting the findings about T cell exclusion at the earlies stages of PDAC (Clark et al., 2007).

## 4.4 Figures

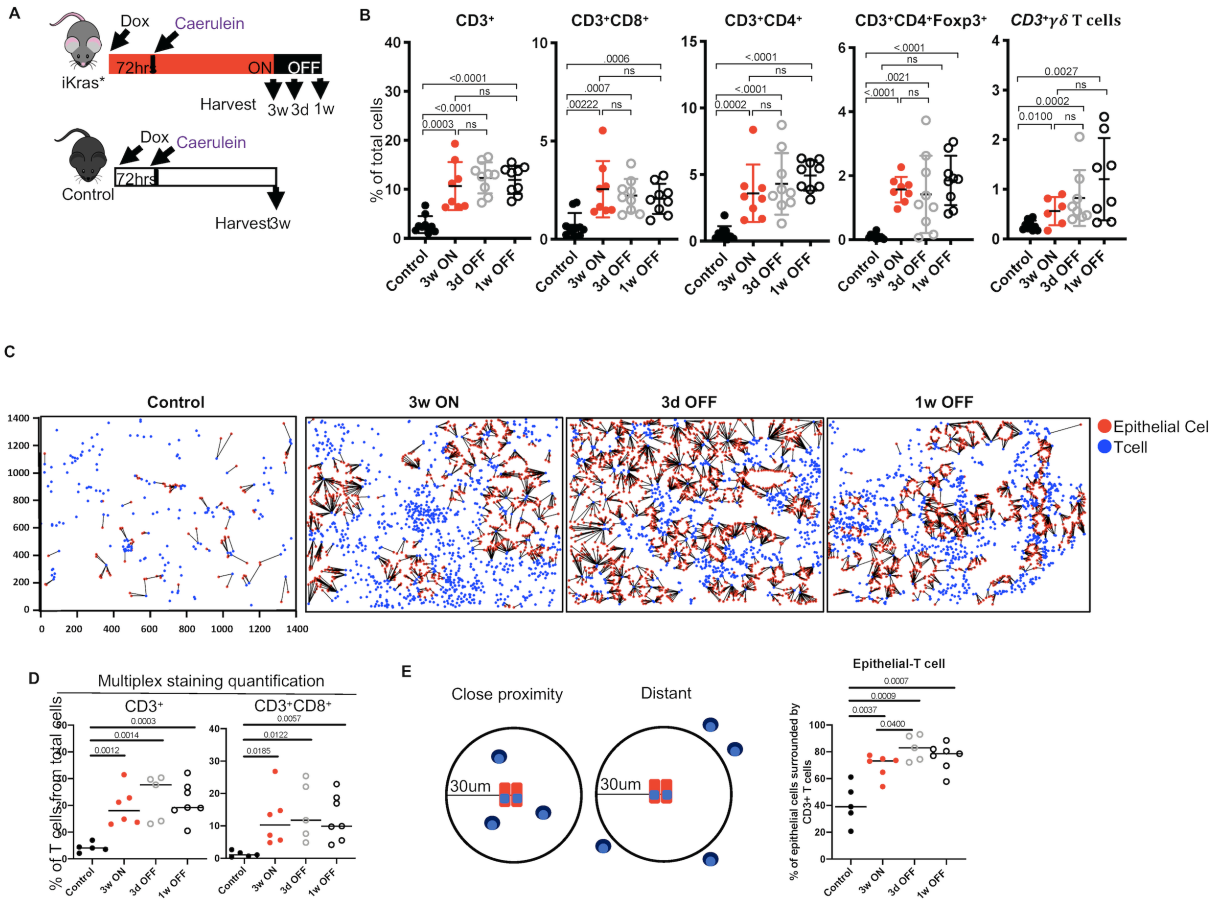


**Figure 4-1 *Kras*$^{G12D}$ activation modulates T cell recruitment in early PanINs.**

A) Experimental design. Wild type control and iKras* mice were given DOX chow to activate Kras$^{G12D}$ followed by induction of acute pancreatitis. Mice either remained on DOX chow for three weeks, and pancreata were harvested (3w ON) or DOX chow was removed and the pancreata were harvested after 3 days or 1 week (labeled 3d OFF or 1w OFF respectively). N=8 mice per group. (B) Quantification of flow cytometry results. T cell populations are expressed as percentage of total cells in control or iKras pancreata at the indicated time points, shown as mean ± SD. N=9-11 mice per group. Statistical analysis by multiple comparison ANOVA and multiple comparison Kruskal Wallis. (C) Identification of cell types using inForm Cell Analysis software and representative measurements of distance between T cells and epithelial cells. (D) OPAL staining quantification of the percentage of CD3 and CD8 positive cells from total cells in the pancreatic tissue of control or iKras* mice at the indicated time points. Data is shown as mean ± SEM. N= 5-7 mice per group. Statistical analysis by two-tailed unpaired t-test. (E) Measurement of the proximity of T cells to epithelial cells. Close proximity was determined by T cells that were within a 30um radius. Distant were defined as T cells outside of the 30um radius.

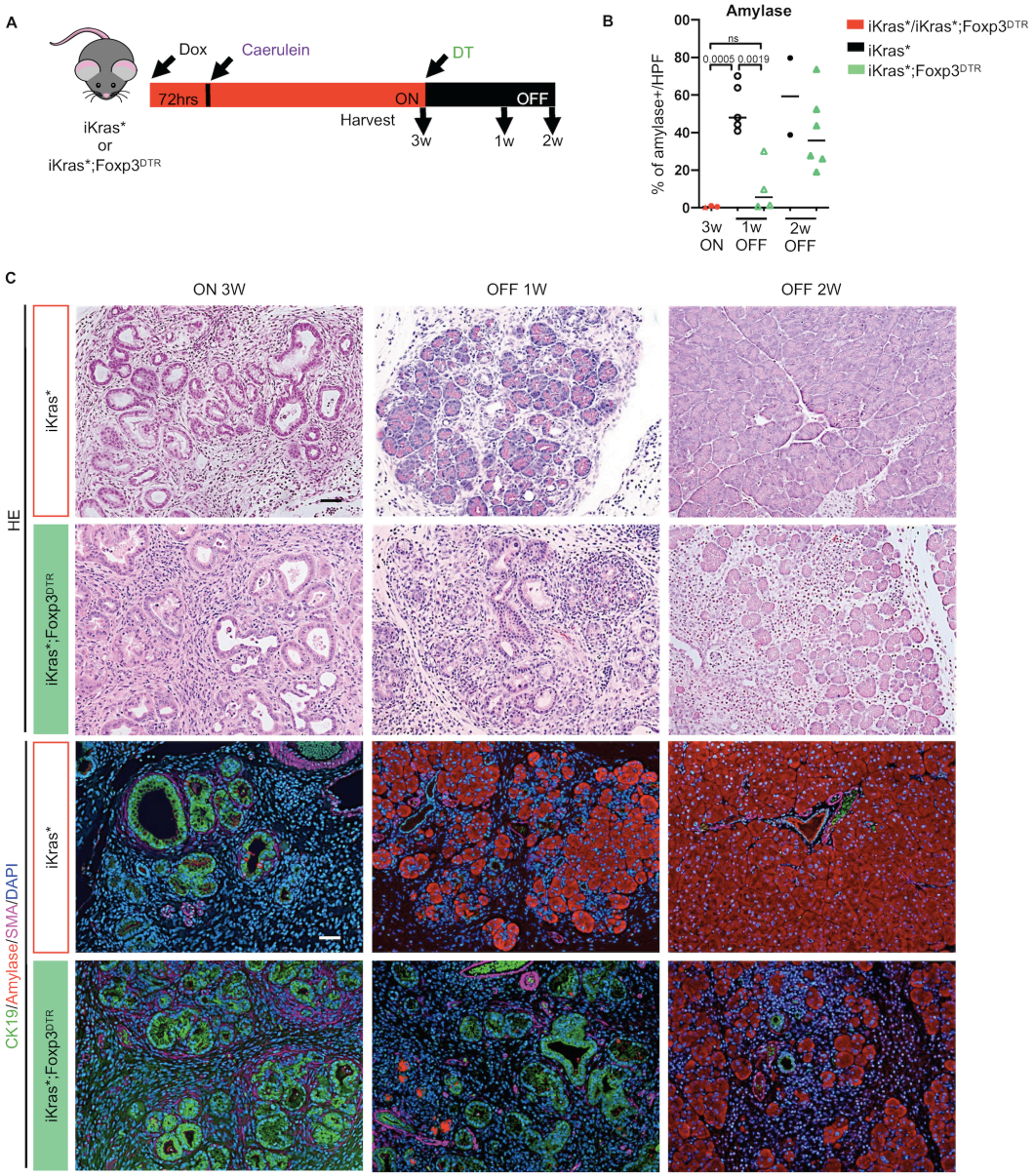


**Figure 4-2 Treg depletion delays PanIN regression and tissue repair upon *Kras*$^{G12D}$ inactivation.**

A) Experimental design, n=5-8 mice/cohort. (B) Quantification of Amylase positive area from the co-immunofluorescent staining shown in panel C. Shown as ± mean SEM. Analyzed by unpaired t-test. **(C)** H&E staining, co-immunofluorescent staining for CK19 (green), Amylase (red), SMA (magenta) and DAPI (Fife & Bluestone), in iKras* and iKras*;Foxp3$^{DTR}$ pancreata 3 weeks post caerulein with Kras ON and 1 week, 2 weeks upon Kras$^{G12D}$ inactivation. Scale bar 50 µm.

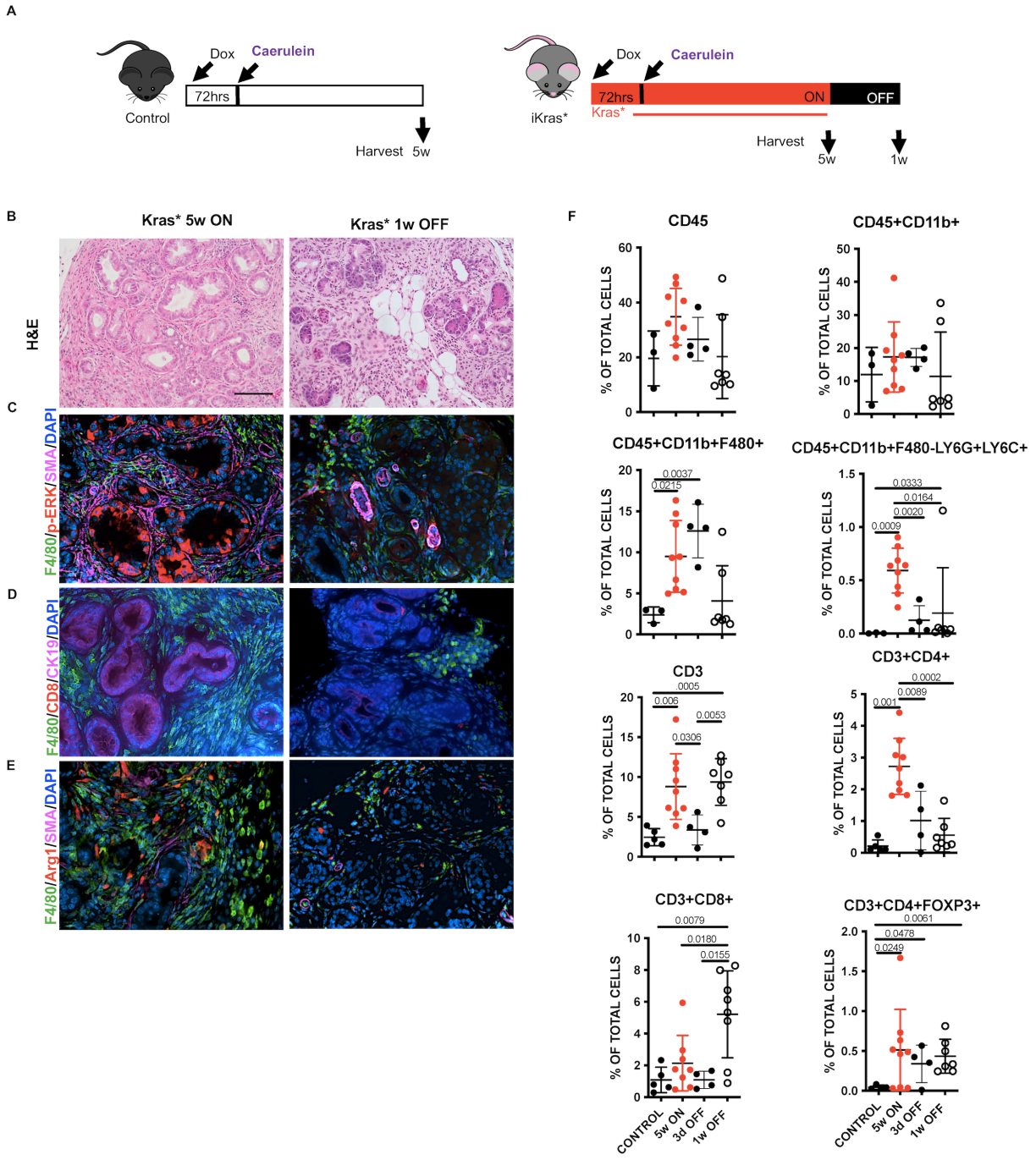


**Figure 4-3 Inactivation of *Kras*$^{G12D}$ in late PanINs led to decrease in macrophages and increase in T lymphocytes.**

(A) Experimental plan, n=3-8 mice/cohort. (B) H&E staining of iKras* pancreata at the indicated time points. (C) Co-immunofluorescent staining for F4/80 (green), pERK (red), SMA (magenta) and DAPI (blue) of iKras* pancreata at the indicated time points. (D) Co-immunofluorescent staining for F4/80 (green), CD8 (red), CK19 (magenta) and DAPI (blue) of iKras* pancreata at the indicated time points. (E) Co-immunofluorescent staining for CD8 (green), CC3 (red), CK19 (magenta) and DAPI (blue) of iKras* pancreata at the indicated time points. (F) Co-immunofluorescent staining for F4/80 (green), ARG1 (red), SMA (magenta) and DAPI (blue) of iKras* pancreata at the indicated time points. (G) Quantification of flow cytometry results. Immune cell populations are expressed as percentage of total cells in control or iKras* pancreata at the indicated time points, shown as mean ± SD. N=3-8 mice per group. Statistical analysis by multiple comparison ANOVA and multiple comparison Kruskal Wallis.

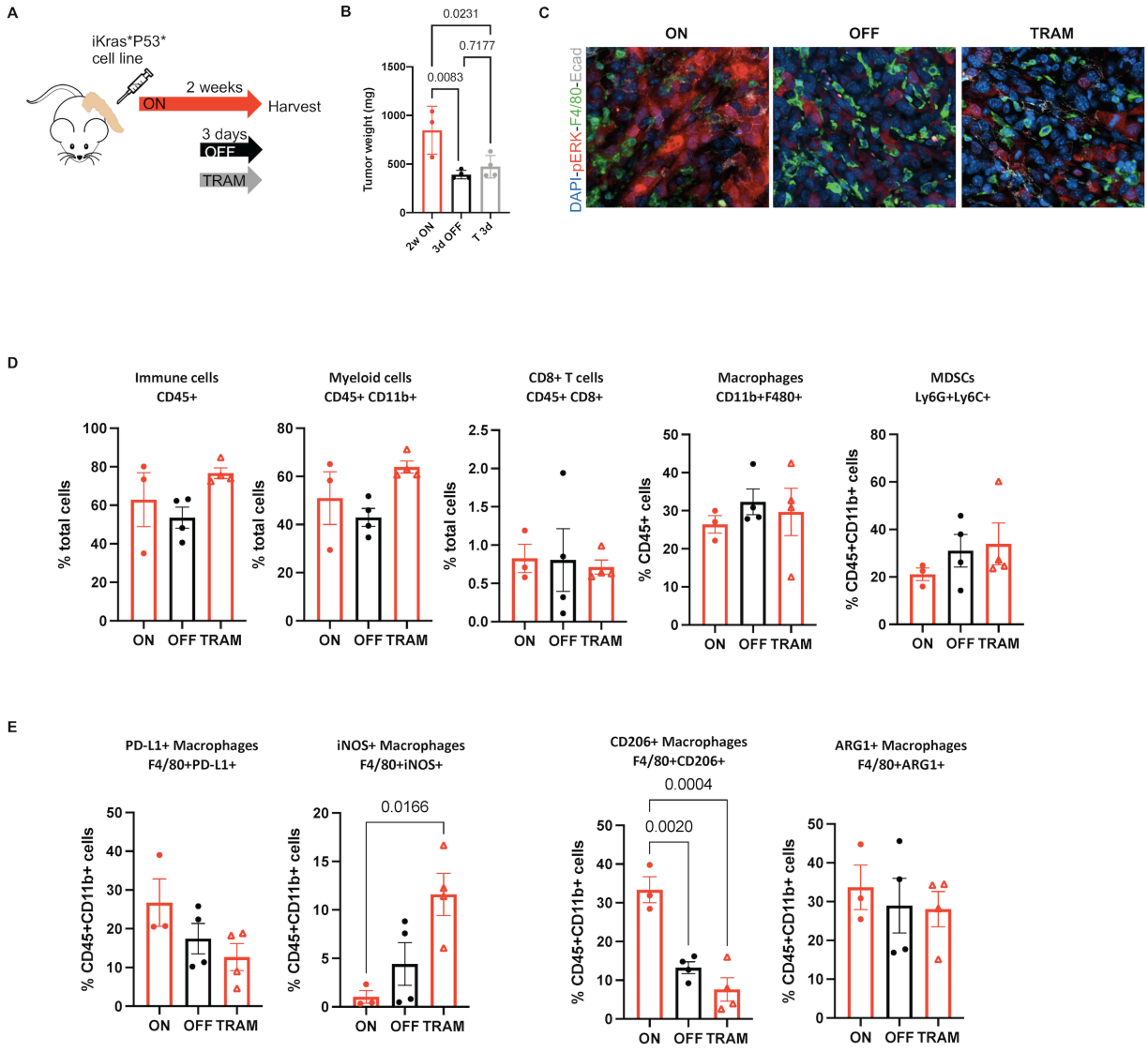


**Figure 4-4 *Kras*$^{G12D}$ inactivation in established tumors led to a decrease in tumor burden and immunosuppressive cells.**

(A) Experimental plan. N=3-4 per group. (B) Bar plot showing the tumor weight (mg). Data shown as mean ± SD. Statistical analysis by one way ANOVA with multiple comparisons. (C) Representative immunofluorescence staining of pERK (red), F4/80 (green) and Ecad (white) at the specified time points. (D) CyTOF manual gating quantification of immune cells, Myeloid cells, CD8$^{+}$ T cells, macrophages and MDSCs. Data shown as mean ± SEM. Statistical analysis by one way ANOVA with multiple comparisons. (E) CyTOF manual gating quantification of immunosuppressive markers in macrophages. Data shown as mean ± SEM. Statistical analysis by one way ANOVA with multiple comparisons.

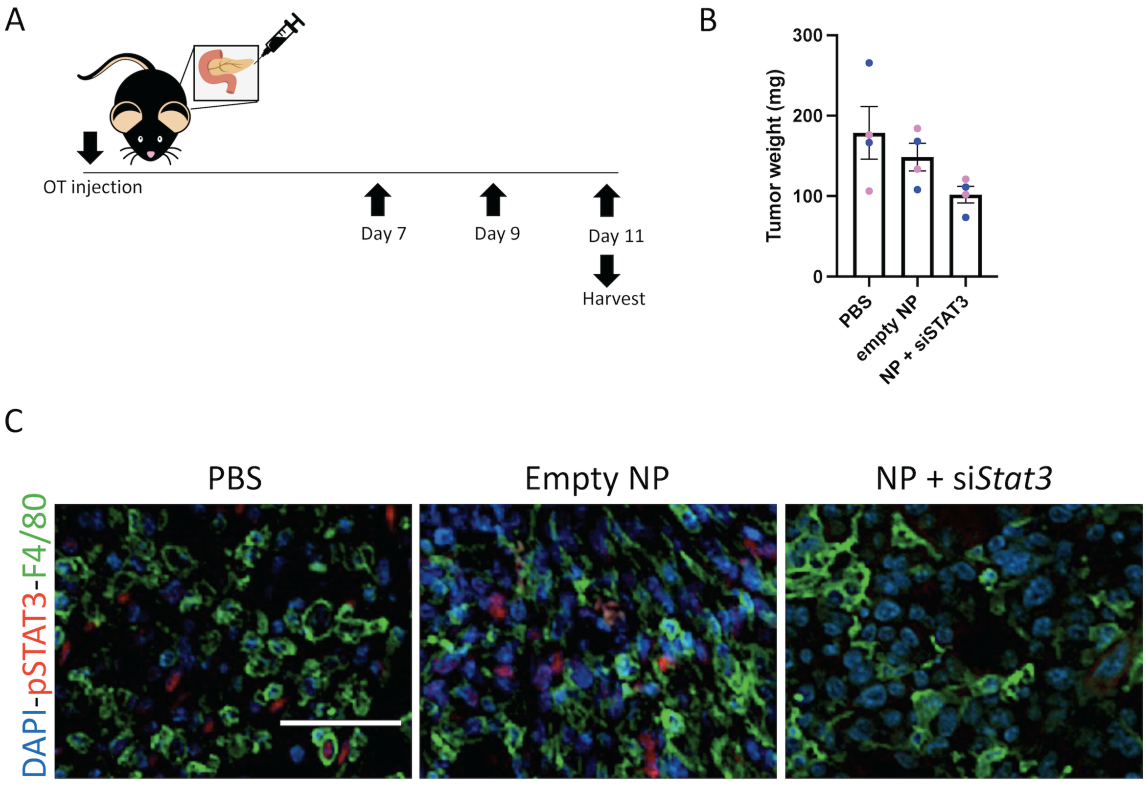


**Figure 4-5 siStat3 containing nanoparticles effectively downregulated STAT3 expression in pancreatic tumors.**

(A) Experimental plan. Syngeneic KPC (65671) cell line was transplanted orthotopically into the pancreas. The mice were treated 3 times in a week with PBS, empty nanoparticles or nanoparticles carrying siRNA for *Stat3*. (B) Plot showing tumor weight in milligrams (mg). Data shown as mean ± SEM. Statistical analysis by one way ANOVA with multiple comparisons. (C) Representative immunofluorescent images of pSTAT3 (red) and F4/80 (green). Scale bar 50um.

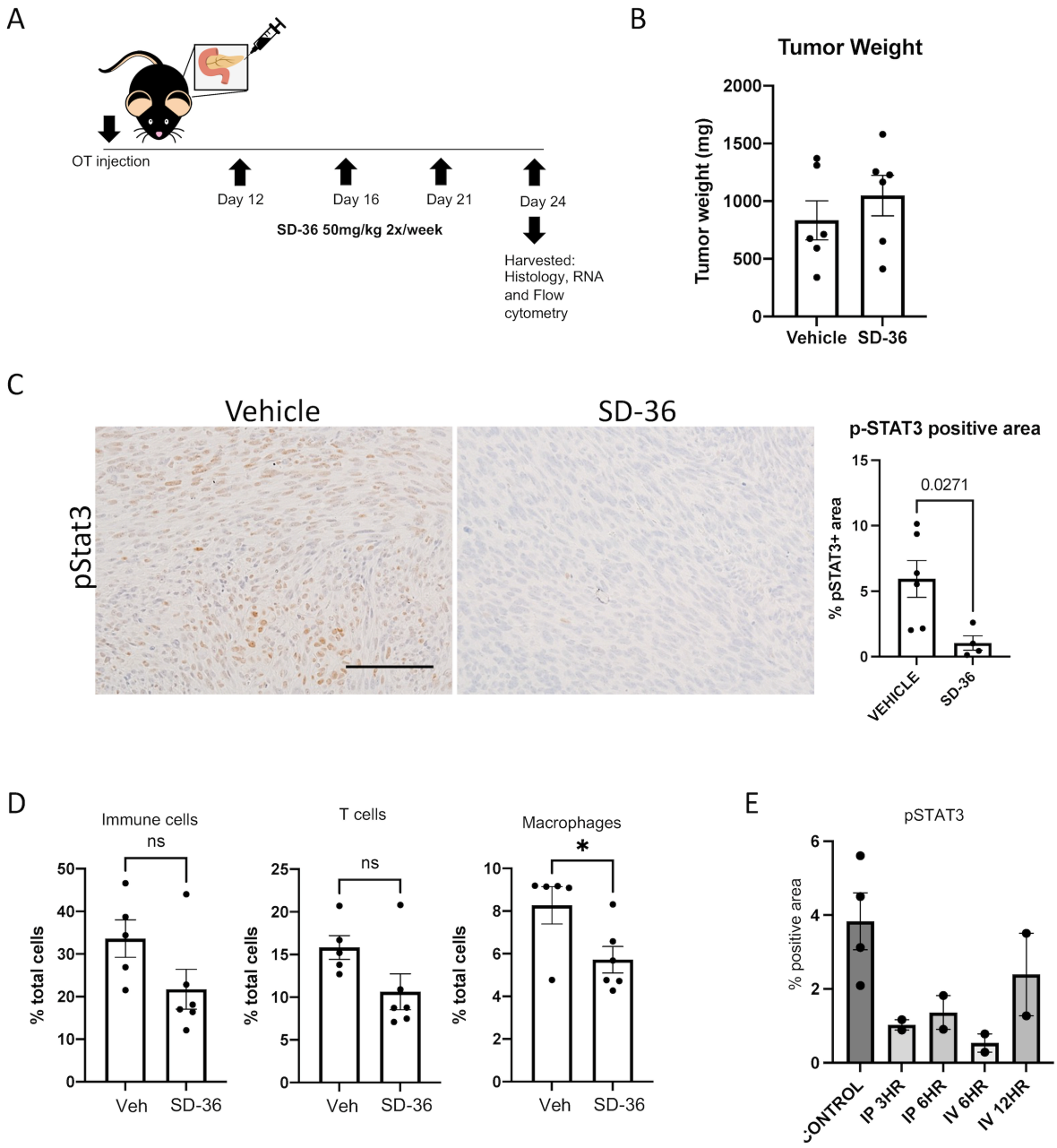


**Figure 4-6 Figure 4.6: SD-36 effectively degraded STAT3 in pancreatic tumor and decreased immune infiltration.**

(A) Experimental plan. Syngeneic KPC (65671) cell line was transplanted orthotopically into the pancreas. SD-36 was administered twice a week for 2 weeks. (B) Plot showing tumor weight of vehicle or SD-36 treated mice. Data shown as mean ± SEM. Statistical analysis by unpaired t-test. (C) Representative immunohistochemistry images showing expression of pSTAT3 in vehicle or SD-36 treated mice. Quantification shown on the right. Data shown as mean ± SEM. Statistical analysis by unpaired t-test. Scale bar 100um. (D) Quantification of flow cytometry data of immune cells, including T cells and Macrophages. Data shown as mean ± SEM. Statistical analysis by unpaired t-test. (E) Quantification of pSTAT3 positive area from immunohistochemistry of tumor tissues from tumor bearing mice treated with vehicle or SD-36 and harvested at the indicated time points. Data shown as mean ± SEM. Statistical analysis by one-way ANOVA.

## Bibliography


3rd, H. A. B., Moore, M. J., Andersen, J., Green, M. R., Rothenberg, M. L., Modiano, M. R., . . . Hoff, D. D. V. (1997). Improvements in survival and clinical benefit with gemcitabine as first-line therapy for patients with advanced pancreas cancer: a randomized trial. *Journal of Clinical Oncology, 15*(6), 2403-2413. doi:10.1200/jco.1997.15.6.2403

Aguirre, A. J., Bardeesy, N., Sinha, M., Lopez, L., Tuveson, D. A., Horner, J., . . . DePinho, R. A. (2003). Activated Kras and Ink4a/Arf deficiency cooperate to produce metastatic pancreatic ductal adenocarcinoma. *Genes Dev, 17*(24), 3112-3126. doi:10.1101/gad.1158703

Almand, B., Clark, J. I., Nikitina, E., van Beynen, J., English, N. R., Knight, S. C., . . . Gabrilovich, D. I. (2001). Increased production of immature myeloid cells in cancer patients: a mechanism of immunosuppression in cancer. *The Journal of Immunology, 166*(1), 678-689.

Almoguera, C., Shibata, D., Forrester, K., Martin, J., Arnheim, N., & Perucho, M. (1988). Most human carcinomas of the exocrine pancreas contain mutant c-K-ras genes. *Cell, 53*(4), 549-554. doi:10.1016/0092-8674(88)90571-5

Alonso-Curbelo, D., Ho, Y. J., Burdziak, C., Maag, J. L. V., Morris, J. P. t., Chandwani, R., . . . Lowe, S. W. (2021). A gene-environment-induced epigenetic program initiates tumorigenesis. *Nature, 590*(7847), 642-648. doi:10.1038/s41586-020-03147-x

Andersson, P., Yang, Y., Hosaka, K., Zhang, Y., Fischer, C., Braun, H., . . . Cao, Y. (2018). Molecular mechanisms of IL-33-mediated stromal interactions in cancer metastasis. *JCI Insight, 3*(20). doi:10.1172/jci.insight.122375

Ardito, Christine M., Grüner, Barbara M., Takeuchi, Kenneth K., Lubeseder-Martellato, C., Teichmann, N., Mazur, Pawel K., . . . Siveke, Jens T. (2012). EGF Receptor Is Required for KRAS-Induced Pancreatic Tumorigenesis. *Cancer Cell, 22*(3), 304-317. doi:https://doi.org/10.1016/j.ccr.2012.07.024

Ardito, C. M., Gruner, B. M., Takeuchi, K. K., Lubeseder-Martellato, C., Teichmann, N., Mazur, P. K., . . . Siveke, J. T. (2012). EGF receptor is required for KRAS-induced pancreatic tumorigenesis. *Cancer Cell, 22*(3), 304-317. doi:10.1016/j.ccr.2012.07.024
S1535-6108(12)00337-6 [pii]

Bai, L., Zhou, H., Xu, R., Zhao, Y., Chinnaswamy, K., McEachern, D., . . . Wang, S. (2019). A Potent and Selective Small-Molecule Degrader of STAT3 Achieves Complete Tumor Regression In Vivo. *Cancer Cell, 36*(5), 498-511.e417. doi:10.1016/j.ccell.2019.10.002

Bailey, J. M., Swanson, B. J., Hamada, T., Eggers, J. P., Singh, P. K., Caffery, T., . . . Hollingsworth, M. A. (2008). Sonic hedgehog promotes desmoplasia in pancreatic cancer. *Clin Cancer Res, 14*(19), 5995-6004. doi:10.1158/1078-0432.CCR-08-0291

Bauer, T. M., Patel, M. R., Forero-Torres, A., George, T. J., Jr., Assad, A., Du, Y., & Hurwitz, H. (2018). A Phase Ib study of ruxolitinib + gemcitabine ± nab-paclitaxel in patients with advanced solid tumors. *Onco Targets Ther, 11*, 2399-2407. doi:10.2147/ott.S157331

Bayne, L. J., Beatty, G. L., Jhala, N., Clark, C. E., Rhim, A. D., Stanger, B. Z., & Vonderheide, R. H. (2012). Tumor-derived granulocyte-macrophage colony-stimulating factor

regulates myeloid inflammation and T cell immunity in pancreatic cancer. *Cancer Cell, 21*(6), 822-835. doi:10.1016/j.ccr.2012.04.025

Beatty, G. L., Chiorean, E. G., Fishman, M. P., Saboury, B., Teitelbaum, U. R., Sun, W., . . . Vonderheide, R. H. (2011). CD40 agonists alter tumor stroma and show efficacy against pancreatic carcinoma in mice and humans. *Science, 331*(6024), 1612-1616. doi:10.1126/science.1198443

Becker, L. M., O'Connell, J. T., Vo, A. P., Cain, M. P., Tampe, D., Bizarro, L., . . . Kalluri, R. (2020). Epigenetic Reprogramming of Cancer-Associated Fibroblasts Deregulates Glucose Metabolism and Facilitates Progression of Breast Cancer. *Cell Rep, 31*(9), 107701. doi:10.1016/j.celrep.2020.107701

Bekaii-Saab T, O. T., Goldstein D, et al. (2021). *Napabucasin + nab-paclitaxel with gemcitabine in patients (pts) with metastatic pancreatic adenocarcinoma (mPDAC): Results from the phase III CanStem111P study.* Paper presented at the European Society for Medical Oncology (ESMO) Congress. https://oncologypro.esmo.org/meeting-resources/esmo-congress/napabucasin-nab-paclitaxel-with-gemcitabine-in-patients-pts-with-metastatic-pancreatic-adenocarcinoma-mpdac-results-from-the-phase-iii-canst

Biankin, A. V., Waddell, N., Kassahn, K. S., Gingras, M. C., Muthuswamy, L. B., Johns, A. L., . . . Grimmond, S. M. (2012). Pancreatic cancer genomes reveal aberrations in axon guidance pathway genes. *Nature, 491*(7424), 399-405. doi:10.1038/nature11547

Biffi, G., Oni, T. E., Spielman, B., Hao, Y., Elyada, E., Park, Y., . . . Tuveson, D. A. (2019). IL1-Induced JAK/STAT Signaling Is Antagonized by TGFbeta to Shape CAF Heterogeneity in Pancreatic Ductal Adenocarcinoma. *Cancer Discov, 9*(2), 282-301. doi:10.1158/2159-8290.CD-18-0710

Biffi, G., & Tuveson, D. A. (2021). Diversity and Biology of Cancer-Associated Fibroblasts. *Physiol Rev, 101*(1), 147-176. doi:10.1152/physrev.00048.2019

Bilimoria, K. Y., Bentrem, D. J., Ko, C. Y., Stewart, A. K., Winchester, D. P., & Talamonti, M. S. (2007). National failure to operate on early stage pancreatic cancer. *Ann Surg, 246*(2), 173-180. doi:10.1097/SLA.0b013e3180691579

Brahmer, J. R., Drake, C. G., Wollner, I., Powderly, J. D., Picus, J., Sharfman, W. H., . . . Topalian, S. L. (2010). Phase I study of single-agent anti-programmed death-1 (MDX-1106) in refractory solid tumors: safety, clinical activity, pharmacodynamics, and immunologic correlates. *J Clin Oncol, 28*(19), 3167-3175. doi:10.1200/JCO.2009.26.7609

Brahmer, J. R., Tykodi, S. S., Chow, L. Q., Hwu, W. J., Topalian, S. L., Hwu, P., . . . Wigginton, J. M. (2012). Safety and activity of anti-PD-L1 antibody in patients with advanced cancer. *N Engl J Med, 366*(26), 2455-2465. doi:10.1056/NEJMoa1200694

Bronte, V., Serafini, P., De Santo, C., Marigo, I., Tosello, V., Mazzoni, A., . . . Zanovello, P. (2003). IL-4-induced arginase 1 suppresses alloreactive T cells in tumor-bearing mice. *J Immunol, 170*(1), 270-278. doi:10.4049/jimmunol.170.1.270

Butler, A., Hoffman, P., Smibert, P., Papalexi, E., & Satija, R. (2018). Integrating single-cell transcriptomic data across different conditions, technologies, and species. *Nat Biotechnol, 36*(5), 411-420. doi:10.1038/nbt.4096

Byrne, K. T., & Vonderheide, R. H. (2016). CD40 Stimulation Obviates Innate Sensors and Drives T Cell Immunity in Cancer. *Cell Rep, 15*(12), 2719-2732. doi:10.1016/j.celrep.2016.05.058

Cancer Genome Atlas Research Network. Electronic address, a. a. d. h. e., & Cancer Genome Atlas Research, N. (2017). Integrated Genomic Characterization of Pancreatic Ductal Adenocarcinoma. *Cancer Cell, 32*(2), 185-203 e113. doi:10.1016/j.ccell.2017.07.007

Canon, J., Rex, K., Saiki, A. Y., Mohr, C., Cooke, K., Bagal, D., . . . Lipford, J. R. (2019). The clinical KRAS(G12C) inhibitor AMG 510 drives anti-tumour immunity. *Nature, 575*(7781), 217-223. doi:10.1038/s41586-019-1694-1

Capasso, M., Franceschi, M., Rodriguez-Castro, K. I., Crafa, P., Cambiè, G., Miraglia, C., . . . Di Mario, F. (2018). Epidemiology and risk factors of pancreatic cancer. *Acta Biomed, 89*(9-s), 141-146. doi:10.23750/abm.v89i9-S.7923

Carriere, C., Young, A. L., Gunn, J. R., Longnecker, D. S., & Korc, M. (2009). Acute pancreatitis markedly accelerates pancreatic cancer progression in mice expressing oncogenic Kras. *Biochem Biophys Res Commun, 382*(3), 561-565. doi:10.1016/j.bbrc.2009.03.068

Carrière, C., Young, A. L., Gunn, J. R., Longnecker, D. S., & Korc, M. (2009). Acute pancreatitis markedly accelerates pancreatic cancer progression in mice expressing oncogenic Kras. *Biochemical and Biophysical Research Communications, 382*(3), 561-565. doi:https://doi.org/10.1016/j.bbrc.2009.03.068

Chen, H., Bian, A., Yang, L.-f., Yin, X., Wang, J., Ti, C., . . . Yi, Z. (2021). Targeting STAT3 by a small molecule suppresses pancreatic cancer progression. *Oncogene, 40*(8), 1440-1457. doi:10.1038/s41388-020-01626-z

Chen, Y., Kim, J., Yang, S., Wang, H., Wu, C. J., Sugimoto, H., . . . Kalluri, R. (2021). Type I collagen deletion in αSMA(+) myofibroblasts augments immune suppression and accelerates progression of pancreatic cancer. *Cancer Cell, 39*(4), 548-565.e546. doi:10.1016/j.ccell.2021.02.007

Chraa, D., Naim, A., Olive, D., & Badou, A. (2019). T lymphocyte subsets in cancer immunity: Friends or foes. *J Leukoc Biol, 105*(2), 243-255. doi:10.1002/JLB.MR0318-097R

Clark, C. E., Hingorani, S. R., Mick, R., Combs, C., Tuveson, D. A., & Vonderheide, R. H. (2007). Dynamics of the immune reaction to pancreatic cancer from inception to invasion. *Cancer Res, 67*(19), 9518-9527. doi:10.1158/0008-5472.CAN-07-0175

clinic, C. (2020). Pancreatitis. Retrieved from https://my.clevelandclinic.org/health/diseases/8103-pancreatitis#:~:text=There%20are%20two%20forms%20of,Chronic%20pancreatitis%20is%20ongoing%20inflammation.

Cobo, I., Martinelli, P., Flandez, M., Bakiri, L., Zhang, M., Carrillo-de-Santa-Pau, E., . . . Real, F. X. (2018). Transcriptional regulation by NR5A2 links differentiation and inflammation in the pancreas. *Nature, 554*(7693), 533-537. doi:10.1038/nature25751

Colegio, O. R., Chu, N. Q., Szabo, A. L., Chu, T., Rhebergen, A. M., Jairam, V., . . . Medzhitov, R. (2014). Functional polarization of tumour-associated macrophages by tumour-derived lactic acid. *Nature, 513*(7519), 559-563. doi:10.1038/nature13490

Collins, M. A., Bednar, F., Zhang, Y., Brisset, J. C., Galban, S., Galban, C. J., . . . Pasca di Magliano, M. (2012). Oncogenic Kras is required for both the initiation and maintenance of pancreatic cancer in mice. *J Clin Invest, 122*(2), 639-653. doi:10.1172/JCI59227

Collins, M. A., Brisset, J. C., Zhang, Y., Bednar, F., Pierre, J., Heist, K. A., . . . di Magliano, M. P. (2012). Metastatic pancreatic cancer is dependent on oncogenic Kras in mice. *PLoS One, 7*(12), e49707. doi:10.1371/journal.pone.0049707

Collins, M. A., Yan, W., Sebolt-Leopold, J. S., & Pasca di Magliano, M. (2014). MAPK signaling is required for dedifferentiation of acinar cells and development of pancreatic intraepithelial neoplasia in mice. *Gastroenterology, 146*(3), 822-834 e827. doi:10.1053/j.gastro.2013.11.052
S0016-5085(13)01734-4 [pii]
Collisson, E. A., Trejo, C. L., Silva, J. M., Gu, S., Korkola, J. E., Heiser, L. M., . . . McMahon, M. (2012). A central role for RAF-->MEK-->ERK signaling in the genesis of pancreatic ductal adenocarcinoma. *Cancer Discov, 2*(8), 685-693. doi:10.1158/2159-8290.CD-11-0347
Conroy, T., Desseigne, F., Ychou, M., Bouché, O., Guimbaud, R., Bécouarn, Y., . . . Ducreux, M. (2011). FOLFIRINOX versus gemcitabine for metastatic pancreatic cancer. *N Engl J Med, 364*(19), 1817-1825. doi:10.1056/NEJMoa1011923
Conroy, T., Hammel, P., Hebbar, M., Ben Abdelghani, M., Wei, A. C., Raoul, J. L., . . . the Unicancer, G. I. P. G. (2018). FOLFIRINOX or Gemcitabine as Adjuvant Therapy for Pancreatic Cancer. *N Engl J Med, 379*(25), 2395-2406. doi:10.1056/NEJMoa1809775
Corcoran, R. B., Contino, G., Deshpande, V., Tzatsos, A., Conrad, C., Benes, C. H., . . . Bardeesy, N. (2011). STAT3 plays a critical role in KRAS-induced pancreatic tumorigenesis. *Cancer Res, 71*(14), 5020-5029. doi:10.1158/0008-5472.Can-11-0908
Criscimanna, A., Coudriet, G. M., Gittes, G. K., Piganelli, J. D., & Esni, F. (2014). Activated macrophages create lineage-specific microenvironments for pancreatic acinar- and beta-cell regeneration in mice. *Gastroenterology, 147*(5), 1106-1118 e1111. doi:10.1053/j.gastro.2014.08.008
Dalin, S., Sullivan, M. R., Lau, A. N., Grauman-Boss, B., Mueller, H. S., Kreidl, E., . . . Hemann, M. T. (2019). Deoxycytidine Release from Pancreatic Stellate Cells Promotes Gemcitabine Resistance. *Cancer Res, 79*(22), 5723-5733. doi:10.1158/0008-5472.CAN-19-0960
De La, O. J., Emerson, L. L., Goodman, J. L., Froebe, S. C., Illum, B. E., Curtis, A. B., & Murtaugh, L. C. (2008). Notch and Kras reprogram pancreatic acinar cells to ductal intraepithelial neoplasia. *Proc Natl Acad Sci U S A, 105*(48), 18907-18912. doi:10.1073/pnas.0810111105
Del Poggetto, E., Ho, I. L., Balestrieri, C., Yen, E. Y., Zhang, S., Citron, F., . . . Viale, A. (2021). Epithelial memory of inflammation limits tissue damage while promoting pancreatic tumorigenesis. *Science, 373*(6561), eabj0486. doi:10.1126/science.abj0486
DeNardo, D. G., & Ruffell, B. (2019). Macrophages as regulators of tumour immunity and immunotherapy. *Nature Reviews Immunology, 19*(6), 369-382. doi:10.1038/s41577-019-0127-6
di Magliano, M. P., & Logsdon, C. D. (2013). Roles for KRAS in pancreatic tumor development and progression. *Gastroenterology, 144*(6), 1220-1229. doi:10.1053/j.gastro.2013.01.071
Dighe, A. S., Richards, E., Old, L. J., & Schreiber, R. D. (1994). Enhanced in vivo growth and resistance to rejection of tumor cells expressing dominant negative IFN gamma receptors. *Immunity, 1*(6), 447-456. doi:10.1016/1074-7613(94)90087-6
Disibio, G., & French, S. W. (2008). Metastatic patterns of cancers: results from a large autopsy study. *Arch Pathol Lab Med, 132*(6), 931-939. doi:10.5858/2008-132-931-mpocrf
Djurec, M., Grana, O., Lee, A., Troule, K., Espinet, E., Cabras, L., . . . Barbacid, M. (2018). Saa3 is a key mediator of the protumorigenic properties of cancer-associated fibroblasts in

pancreatic tumors. *Proc Natl Acad Sci U S A, 115*(6), E1147-E1156. doi:10.1073/pnas.1717802115

Downey, S. G., Klapper, J. A., Smith, F. O., Yang, J. C., Sherry, R. M., Royal, R. E., . . . Rosenberg, S. A. (2007). Prognostic factors related to clinical response in patients with metastatic melanoma treated by CTL-associated antigen-4 blockade. *Clin Cancer Res, 13*(22 Pt 1), 6681-6688. doi:10.1158/1078-0432.Ccr-07-0187

Elyada, E., Bolisetty, M., Laise, P., Flynn, W. F., Courtois, E. T., Burkhart, R. A., . . . Tuveson, D. A. (2019). Cross-Species Single-Cell Analysis of Pancreatic Ductal Adenocarcinoma Reveals Antigen-Presenting Cancer-Associated Fibroblasts. *Cancer Discov, 9*(8), 1102-1123. doi:10.1158/2159-8290.CD-19-0094

Feig, C., Jones, J. O., Kraman, M., Wells, R. J., Deonarine, A., Chan, D. S., . . . Fearon, D. T. (2013). Targeting CXCL12 from FAP-expressing carcinoma-associated fibroblasts synergizes with anti-PD-L1 immunotherapy in pancreatic cancer. *Proc Natl Acad Sci U S A, 110*(50), 20212-20217. doi:10.1073/pnas.1320318110

Fife, B. T., & Bluestone, J. A. (2008). Control of peripheral T-cell tolerance and autoimmunity via the CTLA-4 and PD-1 pathways. *Immunol Rev, 224*, 166-182. doi:10.1111/j.1600-065X.2008.00662.x

Fukuda, A., Wang, S. C., Morris, J. P. t., Folias, A. E., Liou, A., Kim, G. E., . . . Hebrok, M. (2011). Stat3 and MMP7 contribute to pancreatic ductal adenocarcinoma initiation and progression. *Cancer Cell, 19*(4), 441-455. doi:10.1016/j.ccr.2011.03.002

Gabrilovich, D. I., Velders, M. P., Sotomayor, E. M., & Kast, W. M. (2001). Mechanism of immune dysfunction in cancer mediated by immature Gr-1+ myeloid cells. *The Journal of Immunology, 166*(9), 5398-5406.

Garcia, P. E., Adoumie, M., Kim, E. C., Zhang, Y., Scales, M. K., El-Tawil, Y. S., . . . Pasca di Magliano, M. (2020). Differential Contribution of Pancreatic Fibroblast Subsets to the Pancreatic Cancer Stroma. *Cell Mol Gastroenterol Hepatol, 10*(3), 581-599. doi:10.1016/j.jcmgh.2020.05.004

Geiger, R., Rieckmann, J. C., Wolf, T., Basso, C., Feng, Y., Fuhrer, T., . . . Lanzavecchia, A. (2016). L-Arginine Modulates T Cell Metabolism and Enhances Survival and Anti-tumor Activity. *Cell, 167*(3), 829-842.e813. doi:10.1016/j.cell.2016.09.031

Grady, T., Mah'Moud, M., Otani, T., Rhee, S., Lerch, M. M., & Gorelick, F. S. (1998). Zymogen proteolysis within the pancreatic acinar cell is associated with cellular injury. *Am J Physiol, 275*(5), G1010-1017. doi:10.1152/ajpgi.1998.275.5.G1010

Gregory, J. V., Kadiyala, P., Doherty, R., Cadena, M., Habeel, S., Ruoslahti, E., . . . Lahann, J. (2020). Systemic brain tumor delivery of synthetic protein nanoparticles for glioblastoma therapy. *Nat Commun, 11*(1), 5687. doi:10.1038/s41467-020-19225-7

Guerra, C., Collado, M., Navas, C., Schuhmacher, A. J., Hernandez-Porras, I., Canamero, M., . . . Barbacid, M. (2011). Pancreatitis-induced inflammation contributes to pancreatic cancer by inhibiting oncogene-induced senescence. *Cancer Cell, 19*(6), 728-739. doi:10.1016/j.ccr.2011.05.011

Guerra, C., Schuhmacher, A. J., Cañamero, M., Grippo, P. J., Verdaguer, L., Pérez-Gallego, L., . . . Barbacid, M. (2007). Chronic pancreatitis is essential for induction of pancreatic ductal adenocarcinoma by K-Ras oncogenes in adult mice. *Cancer Cell, 11*(3), 291-302. doi:10.1016/j.ccr.2007.01.012

Habbe, N., Shi, G., Meguid, R. A., Fendrich, V., Esni, F., Chen, H., . . . Maitra, A. (2008). Spontaneous induction of murine pancreatic intraepithelial neoplasia (mPanIN) by acinar

cell targeting of oncogenic Kras in adult mice. *Proc Natl Acad Sci U S A, 105*(48), 18913-18918. doi:10.1073/pnas.0810097105

Hackert, T., Sachsenmaier, M., Hinz, U., Schneider, L., Michalski, C. W., Springfeld, C., . . . Buchler, M. W. (2016). Locally Advanced Pancreatic Cancer: Neoadjuvant Therapy With Folfirinox Results in Resectability in 60% of the Patients. *Ann Surg, 264*(3), 457-463. doi:10.1097/SLA.0000000000001850

Hallin, J., Engstrom, L. D., Hargis, L., Calinisan, A., Aranda, R., Briere, D. M., . . . Christensen, J. G. (2020). The KRAS(G12C) Inhibitor MRTX849 Provides Insight toward Therapeutic Susceptibility of KRAS-Mutant Cancers in Mouse Models and Patients. *Cancer Discov, 10*(1), 54-71. doi:10.1158/2159-8290.CD-19-1167

Hamid, O., Robert, C., Daud, A., Hodi, F. S., Hwu, W. J., Kefford, R., . . . Ribas, A. (2013). Safety and tumor responses with lambrolizumab (anti-PD-1) in melanoma. *N Engl J Med, 369*(2), 134-144. doi:10.1056/NEJMoa1305133

Hartmann, N., Giese, N. A., Giese, T., Poschke, I., Offringa, R., Werner, J., & Ryschich, E. (2014). Prevailing role of contact guidance in intrastromal T-cell trapping in human pancreatic cancer. *Clin Cancer Res, 20*(13), 3422-3433. doi:10.1158/1078-0432.CCR-13-2972

Helms, E., Onate, M. K., & Sherman, M. H. (2020). Fibroblast Heterogeneity in the Pancreatic Tumor Microenvironment. *Cancer Discov, 10*(5), 648-656. doi:10.1158/2159-8290.CD-19-1353

Helms, E. J., Berry, M. W., Chaw, R. C., DuFort, C. C., Sun, D., Onate, M. K., . . . Sherman, M. H. (2021). Mesenchymal Lineage Heterogeneity Underlies Non-Redundant Functions of Pancreatic Cancer-Associated Fibroblasts. *bioRxiv*, 2021.2005.2001.442252. doi:10.1101/2021.05.01.442252

Helms, E. J., Berry, M. W., Chaw, R. C., DuFort, C. C., Sun, D., Onate, M. K., . . . Sherman, M. H. (2021). Mesenchymal Lineage Heterogeneity Underlies Nonredundant Functions of Pancreatic Cancer-Associated Fibroblasts. *Cancer Discov*. doi:10.1158/2159-8290.Cd-21-0601

Hicklin, D. J., Marincola, F. M., & Ferrone, S. (1999). HLA class I antigen downregulation in human cancers: T-cell immunotherapy revives an old story. *Mol Med Today, 5*(4), 178-186. doi:10.1016/s1357-4310(99)01451-3

Hingorani, S. R., Petricoin, E. F., Maitra, A., Rajapakse, V., King, C., Jacobetz, M. A., . . . Tuveson, D. A. (2003). Preinvasive and invasive ductal pancreatic cancer and its early detection in the mouse. *Cancer Cell, 4*(6), 437-450. Retrieved from https://www.ncbi.nlm.nih.gov/pubmed/14706336

Hingorani, S. R., Wang, L., Multani, A. S., Combs, C., Deramaudt, T. B., Hruban, R. H., . . . Tuveson, D. A. (2005). Trp53R172H and KrasG12D cooperate to promote chromosomal instability and widely metastatic pancreatic ductal adenocarcinoma in mice. *Cancer Cell, 7*(5), 469-483. doi:10.1016/j.ccr.2005.04.023

Hiraoka, N., Onozato, K., Kosuge, T., & Hirohashi, S. (2006). Prevalence of FOXP3+ regulatory T cells increases during the progression of pancreatic ductal adenocarcinoma and its premalignant lesions. *Clin Cancer Res, 12*(18), 5423-5434. doi:10.1158/1078-0432.CCR-06-0369

Hooftman, A., & O'Neill, L. A. J. (2019). The Immunomodulatory Potential of the Metabolite Itaconate. *Trends Immunol, 40*(8), 687-698. doi:10.1016/j.it.2019.05.007

Hosein, A. N., Huang, H., Wang, Z., Parmar, K., Du, W., Huang, J., . . . Brekken, R. A. (2019). Cellular heterogeneity during mouse pancreatic ductal adenocarcinoma progression at single-cell resolution. *JCI Insight, 5*. doi:10.1172/jci.insight.129212

Hou, P., Kapoor, A., Zhang, Q., Li, J., Wu, C. J., Li, J., . . . DePinho, R. A. (2020). Tumor Microenvironment Remodeling Enables Bypass of Oncogenic KRAS Dependency in Pancreatic Cancer. *Cancer Discov, 10*(7), 1058-1077. doi:10.1158/2159-8290.CD-19-0597

Hurwitz, H., Van Cutsem, E., Bendell, J., Hidalgo, M., Li, C.-P., Salvo, M. G., . . . O'Reilly, E. M. (2018). Ruxolitinib + capecitabine in advanced/metastatic pancreatic cancer after disease progression/intolerance to first-line therapy: JANUS 1 and 2 randomized phase III studies. *Investigational New Drugs, 36*(4), 683-695. doi:10.1007/s10637-018-0580-2

Hurwitz, H., Van Cutsem, E., Bendell, J., Hidalgo, M., Li, C. P., Salvo, M. G., . . . O'Reilly, E. M. (2018). Ruxolitinib + capecitabine in advanced/metastatic pancreatic cancer after disease progression/intolerance to first-line therapy: JANUS 1 and 2 randomized phase III studies. *Invest New Drugs, 36*(4), 683-695. doi:10.1007/s10637-018-0580-2

Ijichi, H., Chytil, A., Gorska, A. E., Aakre, M. E., Bierie, B., Tada, M., . . . Moses, H. L. (2011). Inhibiting Cxcr2 disrupts tumor-stromal interactions and improves survival in a mouse model of pancreatic ductal adenocarcinoma. *J Clin Invest, 121*(10), 4106-4117. doi:10.1172/JCI42754

Infante, J. R., Somer, B. G., Park, J. O., Li, C.-P., Scheulen, M. E., Kasubhai, S. M., . . . Le, N. (2014). A randomised, double-blind, placebo-controlled trial of trametinib, an oral MEK inhibitor, in combination with gemcitabine for patients with untreated metastatic adenocarcinoma of the pancreas. *European Journal of Cancer, 50*(12), 2072-2081. doi:https://doi.org/10.1016/j.ejca.2014.04.024

Ischenko, I., D'Amico, S., Rao, M., Li, J., Hayman, M. J., Powers, S., . . . Reich, N. C. (2021). KRAS drives immune evasion in a genetic model of pancreatic cancer. *Nat Commun, 12*(1), 1482. doi:10.1038/s41467-021-21736-w

Ischenko, I., D'Amico, S., Rao, M., Li, J., Hayman, M. J., Powers, S., . . . Reich, N. C. (2021). KRAS drives immune evasion in a genetic model of pancreatic cancer. *Nature Communications, 12*(1), 1482. doi:10.1038/s41467-021-21736-w

Janes, M. R., Zhang, J., Li, L. S., Hansen, R., Peters, U., Guo, X., . . . Liu, Y. (2018). Targeting KRAS Mutant Cancers with a Covalent G12C-Specific Inhibitor. *Cell, 172*(3), 578-589 e517. doi:10.1016/j.cell.2018.01.006

Jang, J. E., Hajdu, C. H., Liot, C., Miller, G., Dustin, M. L., & Bar-Sagi, D. (2017). Crosstalk between Regulatory T Cells and Tumor-Associated Dendritic Cells Negates Anti-tumor Immunity in Pancreatic Cancer. *Cell Rep, 20*(3), 558-571. doi:10.1016/j.celrep.2017.06.062

Jhappan, C., Stahle, C., Harkins, R. N., Fausto, N., Smith, G. H., & Merlino, G. T. (1990). TGF alpha overexpression in transgenic mice induces liver neoplasia and abnormal development of the mammary gland and pancreas. *Cell, 61*(6), 1137-1146. doi:10.1016/0092-8674(90)90076-q

Jiang, H., Hegde, S., Knolhoff, B. L., Zhu, Y., Herndon, J. M., Meyer, M. A., . . . DeNardo, D. G. (2016). Targeting focal adhesion kinase renders pancreatic cancers responsive to checkpoint immunotherapy. *Nat Med, 22*(8), 851-860. doi:10.1038/nm.4123

Jones, R. P., Psarelli, E.-E., Jackson, R., Ghaneh, P., Halloran, C. M., Palmer, D. H., . . . Cancer, f. t. E. S. G. f. P. (2019). Patterns of Recurrence After Resection of Pancreatic Ductal

Adenocarcinoma: A Secondary Analysis of the ESPAC-4 Randomized Adjuvant Chemotherapy Trial. *JAMA Surgery, 154*(11), 1038-1048. doi:10.1001/jamasurg.2019.3337

Jonker, D. J., Nott, L., Yoshino, T., Gill, S., Shapiro, J., Ohtsu, A., . . . O'Callaghan, C. J. (2018). Napabucasin versus placebo in refractory advanced colorectal cancer: a randomised phase 3 trial. *The Lancet Gastroenterology & Hepatology, 3*(4), 263-270. doi:https://doi.org/10.1016/S2468-1253(18)30009-8

Kalbasi, A., Komar, C., Tooker, G. M., Liu, M., Lee, J. W., Gladney, W. L., . . . Beatty, G. L. (2017). Tumor-Derived CCL2 Mediates Resistance to Radiotherapy in Pancreatic Ductal Adenocarcinoma. *Clin Cancer Res, 23*(1), 137-148. doi:10.1158/1078-0432.CCR-16-0870

Kamisawa, T., Isawa, T., Koike, M., Tsuruta, K., & Okamoto, A. (1995). Hematogenous metastases of pancreatic ductal carcinoma. *Pancreas, 11*(4), 345-349. doi:10.1097/00006676-199511000-00005

Kanda, M., Matthaei, H., Wu, J., Hong, S. M., Yu, J., Borges, M., . . . Goggins, M. (2012). Presence of somatic mutations in most early-stage pancreatic intraepithelial neoplasia. *Gastroenterology, 142*(4), 730-733 e739. doi:10.1053/j.gastro.2011.12.042

Kaplan, D. H., Shankaran, V., Dighe, A. S., Stockert, E., Aguet, M., Old, L. J., & Schreiber, R. D. (1998). Demonstration of an interferon gamma-dependent tumor surveillance system in immunocompetent mice. *Proc Natl Acad Sci U S A, 95*(13), 7556-7561. doi:10.1073/pnas.95.13.7556

Katzenelenbogen, Y., Sheban, F., Yalin, A., Yofe, I., Svetlichnyy, D., Jaitin, D. A., . . . Amit, I. (2020). Coupled scRNA-Seq and Intracellular Protein Activity Reveal an Immunosuppressive Role of TREM2 in Cancer. *Cell, 182*(4), 872-885 e819. doi:10.1016/j.cell.2020.06.032

Kawaguchi, Y., Cooper, B., Gannon, M., Ray, M., MacDonald, R. J., & Wright, C. V. E. (2002). The role of the transcriptional regulator Ptf1a in converting intestinal to pancreatic progenitors. *Nature Genetics, 32*(1), 128-134. doi:10.1038/ng959

Kemp, S. B., Carpenter, E. S., Steele, N. G., Donahue, K. L., Nwosu, Z. C., Pacheco, A., . . . Crawford, H. C. (2021). Apolipoprotein E promotes immune suppression in pancreatic cancer through NF-kB-mediated production of CXCL1. *Cancer Res*. doi:10.1158/0008-5472.CAN-20-3929

Kemp, S. B., Steele, N. G., Carpenter, E. S., Donahue, K. L., Bushnell, G. G., Morris, A. H., . . . Pasca di Magliano, M. (2021). Pancreatic cancer is marked by complement-high blood monocytes and tumor-associated macrophages. *Life Sci Alliance, 4*(6). doi:10.26508/lsa.202000935

Kim, E. J., Sahai, V., Abel, E. V., Griffith, K. A., Greenson, J. K., Takebe, N., . . . Balis, U. G. (2014). Pilot clinical trial of hedgehog pathway inhibitor GDC-0449 (vismodegib) in combination with gemcitabine in patients with metastatic pancreatic adenocarcinoma. *Clinical cancer research, 20*(23), 5937-5945.

Ko, A. H., LoConte, N., Tempero, M. A., Walker, E. J., Kelley, R. K., Lewis, S., . . . Catenacci, D. V. (2016). A phase I study of FOLFIRINOX plus IPI-926, a hedgehog pathway inhibitor, for advanced pancreatic adenocarcinoma. *Pancreas, 45*(3), 370.

Kopp, J. L., von Figura, G., Mayes, E., Liu, F. F., Dubois, C. L., Morris, J. P. t., . . . Sander, M. (2012). Identification of Sox9-dependent acinar-to-ductal reprogramming as the principal

mechanism for initiation of pancreatic ductal adenocarcinoma. *Cancer Cell, 22*(6), 737-750. doi:10.1016/j.ccr.2012.10.025
Kortlever, R. M., Sodir, N. M., Wilson, C. H., Burkhart, D. L., Pellegrinet, L., Brown Swigart, L., . . . Evan, G. I. (2017). Myc Cooperates with Ras by Programming Inflammation and Immune Suppression. *Cell, 171*(6), 1301-1315 e1314. doi:10.1016/j.cell.2017.11.013
Krah, N. M., De La, O. J., Swift, G. H., Hoang, C. Q., Willet, S. G., Chen Pan, F., . . . Murtaugh, L. C. (2015). The acinar differentiation determinant PTF1A inhibits initiation of pancreatic ductal adenocarcinoma. *Elife, 4*. doi:10.7554/eLife.07125
Krah, N. M., & Murtaugh, L. C. (2016). Differentiation and Inflammation: 'Best Enemies' in Gastrointestinal Carcinogenesis. *Trends Cancer, 2*(12), 723-735. doi:10.1016/j.trecan.2016.11.005
Krah, N. M., Narayanan, S. M., Yugawa, D. E., Straley, J. A., Wright, C. V. E., MacDonald, R. J., & Murtaugh, L. C. (2019). Prevention and Reversion of Pancreatic Tumorigenesis through a Differentiation-Based Mechanism. *Dev Cell, 50*(6), 744-754 e744. doi:10.1016/j.devcel.2019.07.012
Krummel, M. F., & Allison, J. P. (1995). CD28 and CTLA-4 have opposing effects on the response of T cells to stimulation. *J Exp Med, 182*(2), 459-465. doi:10.1084/jem.182.2.459
Kusmartsev, S., Nefedova, Y., Yoder, D., & Gabrilovich, D. I. (2004). Antigen-specific inhibition of CD8+ T cell response by immature myeloid cells in cancer is mediated by reactive oxygen species. *J Immunol, 172*(2), 989-999. doi:10.4049/jimmunol.172.2.989
Kusmartsev, S. A., Li, Y., & Chen, S. H. (2000). Gr-1+ myeloid cells derived from tumor-bearing mice inhibit primary T cell activation induced through CD3/CD28 costimulation. *J Immunol, 165*(2), 779-785. doi:10.4049/jimmunol.165.2.779
Lampel, M., & Kern, H. F. (1977). Acute interstitial pancreatitis in the rat induced by excessive doses of a pancreatic secretagogue. *Virchows Archiv A, 373*(2), 97-117. doi:10.1007/BF00432156
Lesina, M., Kurkowski, M. U., Ludes, K., Rose-John, S., Treiber, M., Kloppel, G., . . . Algul, H. (2011). Stat3/Socs3 activation by IL-6 transsignaling promotes progression of pancreatic intraepithelial neoplasia and development of pancreatic cancer. *Cancer Cell, 19*(4), 456-469. doi:10.1016/j.ccr.2011.03.009
S1535-6108(11)00119-X [pii]
Li, H., Huang, C., Huang, K., Wu, W., Jiang, T., Cao, J., . . . Qiu, Z. (2011). STAT3 knockdown reduces pancreatic cancer cell invasiveness and matrix metalloproteinase-7 expression in nude mice. *PLoS One, 6*(10), e25941. doi:10.1371/journal.pone.0025941
Li, J., Byrne, K. T., Yan, F., Yamazoe, T., Chen, Z., Baslan, T., . . . Stanger, B. Z. (2018). Tumor Cell-Intrinsic Factors Underlie Heterogeneity of Immune Cell Infiltration and Response to Immunotherapy. *Immunity, 49*(1), 178-193 e177. doi:10.1016/j.immuni.2018.06.006
Liou, G. Y., Bastea, L., Fleming, A., Doppler, H., Edenfield, B. H., Dawson, D. W., . . . Storz, P. (2017). The Presence of Interleukin-13 at Pancreatic ADM/PanIN Lesions Alters Macrophage Populations and Mediates Pancreatic Tumorigenesis. *Cell Rep, 19*(7), 1322-1333. doi:10.1016/j.celrep.2017.04.052
Liou, G. Y., Doppler, H., Necela, B., Edenfield, B., Zhang, L., Dawson, D. W., & Storz, P. (2015). Mutant KRAS-induced expression of ICAM-1 in pancreatic acinar cells causes attraction of macrophages to expedite the formation of precancerous lesions. *Cancer Discov, 5*(1), 52-63. doi:10.1158/2159-8290.CD-14-0474

Liou, G. Y., Doppler, H., Necela, B., Krishna, M., Crawford, H. C., Raimondo, M., & Storz, P. (2013). Macrophage-secreted cytokines drive pancreatic acinar-to-ductal metaplasia through NF-kappaB and MMPs. *J Cell Biol, 202*(3), 563-577. doi:10.1083/jcb.201301001
jcb.201301001 [pii]
Liu, C. Y., Xu, J. Y., Shi, X. Y., Huang, W., Ruan, T. Y., Xie, P., & Ding, J. L. (2013). M2-polarized tumor-associated macrophages promoted epithelial-mesenchymal transition in pancreatic cancer cells, partially through TLR4/IL-10 signaling pathway. *Lab Invest, 93*(7), 844-854. doi:10.1038/labinvest.2013.69
Long, K. B., Gladney, W. L., Tooker, G. M., Graham, K., Fraietta, J. A., & Beatty, G. L. (2016). IFNgamma and CCL2 Cooperate to Redirect Tumor-Infiltrating Monocytes to Degrade Fibrosis and Enhance Chemotherapy Efficacy in Pancreatic Carcinoma. *Cancer Discov, 6*(4), 400-413. doi:10.1158/2159-8290.CD-15-1032
Longnecker, D. S. (2021). *The Pancreas Biology and Physiology*: Michigan Publishing.
Lu, C., Talukder, A., Savage, N. M., Singh, N., & Liu, K. (2017). JAK-STAT-mediated chronic inflammation impairs cytotoxic T lymphocyte activation to decrease anti-PD-1 immunotherapy efficacy in pancreatic cancer. *Oncoimmunology, 6*(3), e1291106. doi:10.1080/2162402x.2017.1291106
Mace, T. A., Ameen, Z., Collins, A., Wojcik, S., Mair, M., Young, G. S., . . . Lesinski, G. B. (2013). Pancreatic cancer-associated stellate cells promote differentiation of myeloid-derived suppressor cells in a STAT3-dependent manner. *Cancer Res, 73*(10), 3007-3018. doi:10.1158/0008-5472.Can-12-4601
Mace, T. A., Shakya, R., Pitarresi, J. R., Swanson, B., McQuinn, C. W., Loftus, S., . . . Lesinski, G. B. (2016). IL-6 and PD-L1 antibody blockade combination therapy reduces tumour progression in murine models of pancreatic cancer. *Gut*. doi:10.1136/gutjnl-2016-311585
Masugi, Y., Abe, T., Ueno, A., Fujii-Nishimura, Y., Ojima, H., Endo, Y., . . . Sakamoto, M. (2019). Characterization of spatial distribution of tumor-infiltrating CD8(+) T cells refines their prognostic utility for pancreatic cancer survival. *Mod Pathol, 32*(10), 1495-1507. doi:10.1038/s41379-019-0291-z
Mathew, E., Collins, M. A., Fernandez-Barrena, M. G., Holtz, A. M., Yan, W., Hogan, J. O., . . . di Magliano, M. P. (2014). The transcription factor GLI1 modulates the inflammatory response during pancreatic tissue remodeling. *J Biol Chem, 289*(40), 27727-27743. doi:10.1074/jbc.M114.556563
Mathew, E., Zhang, Y., Holtz, A. M., Kane, K. T., Song, J. Y., Allen, B. L., & Pasca di Magliano, M. (2014). Dosage-dependent regulation of pancreatic cancer growth and angiogenesis by hedgehog signaling. *Cell Rep, 9*(2), 484-494. doi:10.1016/j.celrep.2014.09.010
Matsuda, Y., Furukawa, T., Yachida, S., Nishimura, M., Seki, A., Nonaka, K., . . . Mino-Kenudson, M. (2017). The Prevalence and Clinicopathological Characteristics of High-Grade Pancreatic Intraepithelial Neoplasia: Autopsy Study Evaluating the Entire Pancreatic Parenchyma. *Pancreas, 46*(5), 658-664. doi:10.1097/MPA.0000000000000786
MedlinePlus. (2021). Common disorders of the pancreas. Retrieved from https://pancreasfoundation.org/patient-information/about-the-pancreas/common-disorders-of-the-pancreas/

Mills, C. D., Kincaid, K., Alt, J. M., Heilman, M. J., & Hill, A. M. (2000). M-1/M-2 macrophages and the Th1/Th2 paradigm. *J Immunol, 164*(12), 6166-6173. doi:10.4049/jimmunol.164.12.6166

Mitchem, J. B., Brennan, D. J., Knolhoff, B. L., Belt, B. A., Zhu, Y., Sanford, D. E., . . . DeNardo, D. G. (2013). Targeting tumor-infiltrating macrophages decreases tumor-initiating cells, relieves immunosuppression, and improves chemotherapeutic responses. *Cancer Res, 73*(3), 1128-1141. doi:10.1158/0008-5472.CAN-12-2731

0008-5472.CAN-12-2731 [pii]

Morris, J. P. t., Wang, S. C., & Hebrok, M. (2010). KRAS, Hedgehog, Wnt and the twisted developmental biology of pancreatic ductal adenocarcinoma. *Nat Rev Cancer, 10*(10), 683-695. doi:10.1038/nrc2899

Navas, C., Hernandez-Porras, I., Schuhmacher, A. J., Sibilia, M., Guerra, C., & Barbacid, M. (2012). EGF receptor signaling is essential for k-ras oncogene-driven pancreatic ductal adenocarcinoma. *Cancer Cell, 22*(3), 318-330. doi:10.1016/j.ccr.2012.08.001

S1535-6108(12)00338-8 [pii]

Nowicka, M., Krieg, C., Crowell, H. L., Weber, L. M., Hartmann, F. J., Guglietta, S., . . . Robinson, M. D. (2017). CyTOF workflow: differential discovery in high-throughput high-dimensional cytometry datasets. *F1000Res, 6*, 748. doi:10.12688/f1000research.11622.3

O'Hara, M. H., O'Reilly, E. M., Wolff, R. A., Wainberg, Z. A., Ko, A. H., Rahma, O. E., . . . Vonderheide, R. H. (2021). Gemcitabine (Gem) and nab-paclitaxel (NP) ± nivolumab (nivo) ± CD40 agonistic monoclonal antibody APX005M (sotigalimab), in patients (Pts) with untreated metastatic pancreatic adenocarcinoma (mPDAC): Phase (Ph) 2 final results. *Journal of Clinical Oncology, 39*(15_suppl), 4019-4019. doi:10.1200/JCO.2021.39.15_suppl.4019

Ohlund, D., Handly-Santana, A., Biffi, G., Elyada, E., Almeida, A. S., Ponz-Sarvise, M., . . . Tuveson, D. A. (2017). Distinct populations of inflammatory fibroblasts and myofibroblasts in pancreatic cancer. *J Exp Med*. doi:10.1084/jem.20162024

Olive, K. P., Jacobetz, M. A., Davidson, C. J., Gopinathan, A., McIntyre, D., Honess, D., . . . Allard, D. (2009). Inhibition of Hedgehog signaling enhances delivery of chemotherapy in a mouse model of pancreatic cancer. *Science, 324*(5933), 1457-1461.

Olive, K. P., Jacobetz, M. A., Davidson, C. J., Gopinathan, A., McIntyre, D., Honess, D., . . . Tuveson, D. A. (2009). Inhibition of Hedgehog signaling enhances delivery of chemotherapy in a mouse model of pancreatic cancer. *Science, 324*(5933), 1457-1461. doi:10.1126/science.1171362

Orecchioni, M., Ghosheh, Y., Pramod, A. B., & Ley, K. (2019). Macrophage Polarization: Different Gene Signatures in M1(LPS+) vs. Classically and M2(LPS-) vs. Alternatively Activated Macrophages. *Front Immunol, 10*, 1084. doi:10.3389/fimmu.2019.01084

Orth, M., Metzger, P., Gerum, S., Mayerle, J., Schneider, G., Belka, C., . . . Lauber, K. (2019). Pancreatic ductal adenocarcinoma: biological hallmarks, current status, and future perspectives of combined modality treatment approaches. *Radiation Oncology, 14*(1), 141. doi:10.1186/s13014-019-1345-6

Ozdemir, B. C., Pentcheva-Hoang, T., Carstens, J. L., Zheng, X., Wu, C. C., Simpson, T. R., . . . Kalluri, R. (2014). Depletion of carcinoma-associated fibroblasts and fibrosis induces immunosuppression and accelerates pancreas cancer with reduced survival. *Cancer Cell, 25*(6), 719-734. doi:10.1016/j.ccr.2014.04.005

Pathria, P., Gotthardt, D., Prchal-Murphy, M., Putz, E.-M., Holcmann, M., Schlederer, M., . . . Eferl, R. (2015). Myeloid STAT3 promotes formation of colitis-associated colorectal cancer in mice. *Oncoimmunology, 4*(4), e998529-e998529. doi:10.1080/2162402X.2014.998529

Peisl, S., Mellenthin, C., Vignot, L., Gonelle-Gispert, C., Buhler, L., & Egger, B. (2021). Therapeutic targeting of STAT3 pathways in pancreatic adenocarcinoma: A systematic review of clinical and preclinical literature. *PLoS One, 16*(6), e0252397. doi:10.1371/journal.pone.0252397

Polanczyk, M. J., Walker, E., Haley, D., Guerrouahen, B. S., & Akporiaye, E. T. (2019). Blockade of TGF-β signaling to enhance the antitumor response is accompanied by dysregulation of the functional activity of CD4+CD25+Foxp3+ and CD4+CD25−Foxp3+ T cells. *Journal of Translational Medicine, 17*(1), 219. doi:10.1186/s12967-019-1967-3

Pour, P. M., Sayed, S., & Sayed, G. (1982). Hyperplastic, preneoplastic and neoplastic lesions found in 83 human pancreases. *Am J Clin Pathol, 77*(2), 137-152. doi:10.1093/ajcp/77.2.137

Principe, D. R., Underwood, P. W., Korc, M., Trevino, J. G., Munshi, H. G., & Rana, A. (2021). The Current Treatment Paradigm for Pancreatic Ductal Adenocarcinoma and Barriers to Therapeutic Efficacy. *Front Oncol, 11*, 688377. doi:10.3389/fonc.2021.688377

Prokopchuk, O., Liu, Y., Henne-Bruns, D., & Kornmann, M. (2005). Interleukin-4 enhances proliferation of human pancreatic cancer cells: evidence for autocrine and paracrine actions. *British Journal of Cancer, 92*(5), 921-928. doi:10.1038/sj.bjc.6602416

Ramilowski, J. A., Goldberg, T., Harshbarger, J., Kloppmann, E., Lizio, M., Satagopam, V. P., . . . Forrest, A. R. (2015). A draft network of ligand-receptor-mediated multicellular signalling in human. *Nat Commun, 6*, 7866. doi:10.1038/ncomms8866

Rébé, C., & Ghiringhelli, F. (2019). STAT3, a Master Regulator of Anti-Tumor Immune Response. *Cancers, 11*(9), 1280. doi:10.3390/cancers11091280

Rengarajan, J., Szabo, S. J., & Glimcher, L. H. (2000). Transcriptional regulation of Th1/Th2 polarization. *Immunology Today, 21*(10), 479-483. doi:https://doi.org/10.1016/S0167-5699(00)01712-6

Rhim, A. D., Oberstein, P. E., Thomas, D. H., Mirek, E. T., Palermo, C. F., Sastra, S. A., . . . Stanger, B. Z. (2014). Stromal elements act to restrain, rather than support, pancreatic ductal adenocarcinoma. *Cancer Cell, 25*(6), 735-747. doi:10.1016/j.ccr.2014.04.021

Rodriguez, P. C., Quiceno, D. G., Zabaleta, J., Ortiz, B., Zea, A. H., Piazuelo, M. B., . . . Ochoa, A. C. (2004). Arginase I production in the tumor microenvironment by mature myeloid cells inhibits T-cell receptor expression and antigen-specific T-cell responses. *Cancer Res, 64*(16), 5839-5849. doi:10.1158/0008-5472.CAN-04-0465

Rodriguez, P. C., Zea, A. H., DeSalvo, J., Culotta, K. S., Zabaleta, J., Quiceno, D. G., . . . Ochoa, A. C. (2003). L-arginine consumption by macrophages modulates the expression of CD3 zeta chain in T lymphocytes. *J Immunol, 171*(3), 1232-1239. doi:10.4049/jimmunol.171.3.1232

Roy, N., Takeuchi, K. K., Ruggeri, J. M., Bailey, P., Chang, D., Li, J., . . . Crawford, H. C. (2016). PDX1 dynamically regulates pancreatic ductal adenocarcinoma initiation and maintenance. *Genes Dev, 30*(24), 2669-2683. doi:10.1101/gad.291021.116

Royal, R. E., Levy, C., Turner, K., Mathur, A., Hughes, M., Kammula, U. S., . . . Rosenberg, S. A. (2010). Phase 2 trial of single agent Ipilimumab (anti-CTLA-4) for locally advanced

or metastatic pancreatic adenocarcinoma. *J Immunother, 33*(8), 828-833. doi:10.1097/CJI.0b013e3181eec14c
Sandgren, E. P., Luetteke, N. C., Palmiter, R. D., Brinster, R. L., & Lee, D. C. (1990). Overexpression of TGF alpha in transgenic mice: induction of epithelial hyperplasia, pancreatic metaplasia, and carcinoma of the breast. *Cell, 61*(6), 1121-1135. doi:10.1016/0092-8674(90)90075-p
Sanford, D. E., Belt, B. A., Panni, R. Z., Mayer, A., Deshpande, A. D., Carpenter, D., . . . Linehan, D. C. (2013). Inflammatory monocyte mobilization decreases patient survival in pancreatic cancer: a role for targeting the CCL2/CCR2 axis. *Clin Cancer Res, 19*(13), 3404-3415. doi:10.1158/1078-0432.CCR-13-0525
Sarabi, M., Mais, L., Oussaid, N., Desseigne, F., Guibert, P., & De La Fouchardiere, C. (2017). Use of gemcitabine as a second-line treatment following chemotherapy with folfirinox for metastatic pancreatic adenocarcinoma. *Oncology letters, 13*(6), 4917-4924. doi:10.3892/ol.2017.6061
Saraiva, M., & O'Garra, A. (2010). The regulation of IL-10 production by immune cells. *Nature Reviews Immunology, 10*(3), 170-181. doi:10.1038/nri2711
Saxton, R. A., & Sabatini, D. M. (2017). mTOR Signaling in Growth, Metabolism, and Disease. *Cell, 169*(2), 361-371. doi:10.1016/j.cell.2017.03.035
Scheufele, F., Hartmann, D., & Friess, H. (2019). Treatment of pancreatic cancer-neoadjuvant treatment in borderline resectable/locally advanced pancreatic cancer. *Transl Gastroenterol Hepatol, 4*, 32. doi:10.21037/tgh.2019.04.09
Seif, F., Khoshmirsafa, M., Aazami, H., Mohsenzadegan, M., Sedighi, G., & Bahar, M. (2017). The role of JAK-STAT signaling pathway and its regulators in the fate of T helper cells. *Cell Communication and Signaling, 15*(1), 23. doi:10.1186/s12964-017-0177-y
Shankaran, V., Ikeda, H., Bruce, A. T., White, J. M., Swanson, P. E., Old, L. J., & Schreiber, R. D. (2001). IFNgamma and lymphocytes prevent primary tumour development and shape tumour immunogenicity. *Nature, 410*(6832), 1107-1111. doi:10.1038/35074122
Shannon, P., Markiel, A., Ozier, O., Baliga, N. S., Wang, J. T., Ramage, D., . . . Ideker, T. (2003). Cytoscape: a software environment for integrated models of biomolecular interaction networks. *Genome Res, 13*(11), 2498-2504. doi:10.1101/gr.1239303
Shi, G., DiRenzo, D., Qu, C., Barney, D., Miley, D., & Konieczny, S. F. (2013). Maintenance of acinar cell organization is critical to preventing Kras-induced acinar-ductal metaplasia. *Oncogene, 32*(15), 1950-1958. doi:10.1038/onc.2012.210
Shi, L., Chen, S., Yang, L., & Li, Y. (2013). The role of PD-1 and PD-L1 in T-cell immune suppression in patients with hematological malignancies. *Journal of Hematology & Oncology, 6*(1), 74. doi:10.1186/1756-8722-6-74
Sinha, P., Clements, V. K., & Ostrand-Rosenberg, S. (2005). Reduction of myeloid-derived suppressor cells and induction of M1 macrophages facilitate the rejection of established metastatic disease. *J Immunol, 174*(2), 636-645. doi:10.4049/jimmunol.174.2.636
Smit, V. T., Boot, A. J., Smits, A. M., Fleuren, G. J., Cornelisse, C. J., & Bos, J. L. (1988). KRAS codon 12 mutations occur very frequently in pancreatic adenocarcinomas. *Nucleic Acids Res, 16*(16), 7773-7782. doi:10.1093/nar/16.16.7773
Smith, L. K., Boukhaled, G. M., Condotta, S. A., Mazouz, S., Guthmiller, J. J., Vijay, R., . . . Richer, M. J. (2018). Interleukin-10 Directly Inhibits CD8(+) T Cell Function by Enhancing N-Glycan Branching to Decrease Antigen Sensitivity. *Immunity, 48*(2), 299-312 e295. doi:10.1016/j.immuni.2018.01.006

Society, A. C. (2020). Cancer Facts & Figures. *Atlanta: American Cancer Society;2020*. Retrieved from https://www.cancer.org/content/dam/cancer-org/research/cancer-facts-and-statistics/annual-cancer-facts-and-figures/2020/cancer-facts-and-figures-2020.pdf

Society, A. C. (2022). Cancer Facts & Figures 2022. *Atlanta American Cancer Society*.

Steele, C. W., Karim, S. A., Leach, J. D., Bailey, P., Upstill-Goddard, R., Rishi, L., . . . Morton, J. P. (2016a). CXCR2 Inhibition Profoundly Suppresses Metastases and Augments Immunotherapy in Pancreatic Ductal Adenocarcinoma. *Cancer Cell, 29*(6), 832-845. doi:10.1016/j.ccell.2016.04.014

Steele, C. W., Karim, S. A., Leach, J. D. G., Bailey, P., Upstill-Goddard, R., Rishi, L., . . . Morton, J. P. (2016b). CXCR2 Inhibition Profoundly Suppresses Metastases and Augments Immunotherapy in Pancreatic Ductal Adenocarcinoma. *Cancer Cell, 29*(6), 832-845. doi:10.1016/j.ccell.2016.04.014

Steele, N. G., Biffi, G., Kemp, S. B., Zhang, Y., Drouillard, D., Syu, L., . . . Pasca di Magliano, M. (2021). Inhibition of Hedgehog Signaling Alters Fibroblast Composition in Pancreatic Cancer. *Clin Cancer Res, 27*(7), 2023-2037. doi:10.1158/1078-0432.CCR-20-3715

Steele, N. G., Carpenter, E. S., Kemp, S. B., Sirihorachai, V. R., The, S., Delrosario, L., . . . Pasca di Magliano, M. (2020). Multimodal mapping of the tumor and peripheral blood immune landscape in human pancreatic cancer. *Nature Cancer, 1*(11), 1097-1112. doi:10.1038/s43018-020-00121-4

Storz, P. (2017). Acinar cell plasticity and development of pancreatic ductal adenocarcinoma. *Nat Rev Gastroenterol Hepatol*. doi:10.1038/nrgastro.2017.12

Stromnes, I. M., Brockenbrough, J. S., Izeradjene, K., Carlson, M. A., Cuevas, C., Simmons, R. M., . . . Hingorani, S. R. (2014). Targeted depletion of an MDSC subset unmasks pancreatic ductal adenocarcinoma to adaptive immunity. *Gut, 63*(11), 1769-1781. doi:10.1136/gutjnl-2013-306271

Stuart, T., Butler, A., Hoffman, P., Hafemeister, C., Papalexi, E., Mauck, W. M., 3rd, . . . Satija, R. (2019). Comprehensive Integration of Single-Cell Data. *Cell, 177*(7), 1888-1902 e1821. doi:10.1016/j.cell.2019.05.031

Takeda, K., Clausen, B. E., Kaisho, T., Tsujimura, T., Terada, N., Forster, I., & Akira, S. (1999). Enhanced Th1 activity and development of chronic enterocolitis in mice devoid of Stat3 in macrophages and neutrophils. *Immunity, 10*(1), 39-49. doi:10.1016/s1074-7613(00)80005-9

Thyagarajan, A., Alshehri, M. S. A., Miller, K. L. R., Sherwin, C. M., Travers, J. B., & Sahu, R. P. (2019). Myeloid-Derived Suppressor Cells and Pancreatic Cancer: Implications in Novel Therapeutic Approaches. *Cancers (Basel), 11*(11). doi:10.3390/cancers11111627

Topalian, S. L., Hodi, F. S., Brahmer, J. R., Gettinger, S. N., Smith, D. C., McDermott, D. F., . . . Sznol, M. (2012). Safety, activity, and immune correlates of anti-PD-1 antibody in cancer. *N Engl J Med, 366*(26), 2443-2454. doi:10.1056/NEJMoa1200690

Trovato, R., Fiore, A., Sartori, S., Canè, S., Giugno, R., Cascione, L., . . . Ugel, S. (2019). Immunosuppression by monocytic myeloid-derived suppressor cells in patients with pancreatic ductal carcinoma is orchestrated by STAT3. *Journal for ImmunoTherapy of Cancer, 7*(1), 255. doi:10.1186/s40425-019-0734-6

Tuveson, D. A., Shaw, A. T., Willis, N. A., Silver, D. P., Jackson, E. L., Chang, S., . . . Jacks, T. (2004). Endogenous oncogenic K-ras(G12D) stimulates proliferation and widespread neoplastic and developmental defects. *Cancer Cell, 5*(4), 375-387. doi:10.1016/s1535-6108(04)00085-6

Tuveson, D. A., Zhu, L., Gopinathan, A., Willis, N. A., Kachatrian, L., Grochow, R., . . . Konieczny, S. F. (2006). Mist1-KrasG12D knock-in mice develop mixed differentiation metastatic exocrine pancreatic carcinoma and hepatocellular carcinoma. *Cancer Res, 66*(1), 242-247. doi:10.1158/0008-5472.CAN-05-2305

van den Broek, M. E., Kägi, D., Ossendorp, F., Toes, R., Vamvakas, S., Lutz, W. K., . . . Hengartner, H. (1996). Decreased tumor surveillance in perforin-deficient mice. *The Journal of experimental medicine, 184*(5), 1781-1790.

Vasquez-Dunddel, D., Pan, F., Zeng, Q., Gorbounov, M., Albesiano, E., Fu, J., . . . Kim, Y. (2013). STAT3 regulates arginase-I in myeloid-derived suppressor cells from cancer patients. *The Journal of clinical investigation, 123*(4), 1580-1589. doi:10.1172/JCI60083

Verreck, F. A., de Boer, T., Langenberg, D. M., Hoeve, M. A., Kramer, M., Vaisberg, E., . . . Ottenhoff, T. H. (2004). Human IL-23-producing type 1 macrophages promote but IL-10-producing type 2 macrophages subvert immunity to (myco)bacteria. *Proc Natl Acad Sci U S A, 101*(13), 4560-4565. doi:10.1073/pnas.0400983101

von Figura, G., Fukuda, A., Roy, N., Liku, M. E., Morris Iv, J. P., Kim, G. E., . . . Hebrok, M. (2014). The chromatin regulator Brg1 suppresses formation of intraductal papillary mucinous neoplasm and pancreatic ductal adenocarcinoma. *Nat Cell Biol, 16*(3), 255-267. doi:10.1038/ncb2916

von Figura, G., Morris, J. P. t., Wright, C. V., & Hebrok, M. (2014). Nr5a2 maintains acinar cell differentiation and constrains oncogenic Kras-mediated pancreatic neoplastic initiation. *Gut, 63*(4), 656-664. doi:10.1136/gutjnl-2012-304287

Von Hoff, D. D., Ervin, T., Arena, F. P., Chiorean, E. G., Infante, J., Moore, M., . . . Renschler, M. F. (2013). Increased survival in pancreatic cancer with nab-paclitaxel plus gemcitabine. *N Engl J Med, 369*(18), 1691-1703. doi:10.1056/NEJMoa1304369

Wen, H. J., Gao, S., Wang, Y., Ray, M., Magnuson, M. A., Wright, C. V. E., . . . Crawford, H. C. (2019). Myeloid Cell-Derived HB-EGF Drives Tissue Recovery After Pancreatitis. *Cell Mol Gastroenterol Hepatol, 8*(2), 173-192. doi:10.1016/j.jcmgh.2019.05.006

Wilhelm, S., Carter, C., Lynch, M., Lowinger, T., Dumas, J., Smith, R. A., . . . Kelley, S. (2006). Discovery and development of sorafenib: a multikinase inhibitor for treating cancer. *Nat Rev Drug Discov, 5*(10), 835-844. doi:10.1038/nrd2130

Wu, J. Y., Huang, T. W., Hsieh, Y. T., Wang, Y. F., Yen, C. C., Lee, G. L., . . . Kuo, C. C. (2020). Cancer-Derived Succinate Promotes Macrophage Polarization and Cancer Metastasis via Succinate Receptor. *Mol Cell, 77*(2), 213-227 e215. doi:10.1016/j.molcel.2019.10.023

Yamamoto, K., Venida, A., Yano, J., Biancur, D. E., Kakiuchi, M., Gupta, S., . . . Kimmelman, A. C. (2020). Autophagy promotes immune evasion of pancreatic cancer by degrading MHC-I. *Nature, 581*(7806), 100-105. doi:10.1038/s41586-020-2229-5

Yang, J. C., Hughes, M., Kammula, U., Royal, R., Sherry, R. M., Topalian, S. L., . . . Rosenberg, S. A. (2007). Ipilimumab (anti-CTLA4 antibody) causes regression of metastatic renal cell cancer associated with enteritis and hypophysitis. *J Immunother, 30*(8), 825-830. doi:10.1097/CJI.0b013e318156e47e

Ying, H., Dey, P., Yao, W., Kimmelman, A. C., Draetta, G. F., Maitra, A., & DePinho, R. A. (2016). Genetics and biology of pancreatic ductal adenocarcinoma. *Genes Dev, 30*(4), 355-385. doi:10.1101/gad.275776.115

Ying, H., Kimmelman, A. C., Lyssiotis, C. A., Hua, S., Chu, G. C., Fletcher-Sananikone, E., . . . DePinho, R. A. (2012). Oncogenic Kras maintains pancreatic tumors through regulation of anabolic glucose metabolism. *Cell, 149*(3), 656-670. doi:10.1016/j.cell.2012.01.058

Young, A., Lyons, J., Miller, A. L., Phan, V. T., Alarcón, I. R., & McCormick, F. (2009). Chapter 1 Ras Signaling and Therapies. In *Advances in Cancer Research* (Vol. 102, pp. 1-17): Academic Press.

Yu, H., Kortylewski, M., & Pardoll, D. (2007). Crosstalk between cancer and immune cells: role of STAT3 in the tumour microenvironment. *Nat Rev Immunol, 7*(1), 41-51. doi:10.1038/nri1995

Zhang, A., Qian, Y., Ye, Z., Chen, H., Xie, H., Zhou, L., . . . Zheng, S. (2017). Cancer-associated fibroblasts promote M2 polarization of macrophages in pancreatic ductal adenocarcinoma. *Cancer Med, 6*(2), 463-470. doi:10.1002/cam4.993

Zhang, Y., Lazarus, J., Steele, N. G., Yan, W., Lee, H. J., Nwosu, Z. C., . . . Pasca di Magliano, M. (2020). Regulatory T-cell Depletion Alters the Tumor Microenvironment and Accelerates Pancreatic Carcinogenesis. *Cancer Discov, 10*(3), 422-439. doi:10.1158/2159-8290.CD-19-0958

Zhang, Y., Morris, J. P. t., Yan, W., Schofield, H. K., Gurney, A., Simeone, D. M., . . . Pasca di Magliano, M. (2013). Canonical wnt signaling is required for pancreatic carcinogenesis. *Cancer Research, 73*(15), 4909-4922. doi:10.1158/0008-5472.CAN-12-4384

Zhang, Y., Velez-Delgado, A., Mathew, E., Li, D., Mendez, F. M., Flannagan, K., . . . Pasca di Magliano, M. (2017). Myeloid cells are required for PD-1/PD-L1 checkpoint activation and the establishment of an immunosuppressive environment in pancreatic cancer. *Gut, 66*(1), 124-136. doi:10.1136/gutjnl-2016-312078

Zhang, Y., Yan, W., Collins, M. A., Bednar, F., Rakshit, S., Zetter, B. R., . . . di Magliano, M. P. (2013). Interleukin-6 is required for pancreatic cancer progression by promoting MAPK signaling activation and oxidative stress resistance. *Cancer Res, 73*(20), 6359-6374. doi:10.1158/0008-5472.CAN-13-1558-T

Zhang, Y., Yan, W., Mathew, E., Bednar, F., Wan, S., Collins, M. A., . . . di Magliano, M. P. (2014). CD4+ T lymphocyte ablation prevents pancreatic carcinogenesis in mice. *Cancer Immunol Res, 2*(5), 423-435. doi:10.1158/2326-6066.CIR-14-0016-T

Zhang, Y., Yan, W., Mathew, E., Kane, K. T., Brannon, A., Adoumie, M., . . . Pasca di Magliano, M. (2017). Epithelial-Myeloid cell crosstalk regulates acinar cell plasticity and pancreatic remodeling in mice. *Elife, 6*. doi:10.7554/eLife.27388

Zhou, J., Qu, Z., Sun, F., Han, L., Li, L., Yan, S., . . . Xiao, G. (2017). Myeloid STAT3 Promotes Lung Tumorigenesis by Transforming Tumor Immunosurveillance into Tumor-Promoting Inflammation. *Cancer Immunol Res, 5*(3), 257-268. doi:10.1158/2326-6066.CIR-16-0073

Zhou, J., Tang, Z., Gao, S., Li, C., Feng, Y., & Zhou, X. (2020). Tumor-Associated Macrophages: Recent Insights and Therapies. *Frontiers in Oncology, 10*. doi:10.3389/fonc.2020.00188

Zhu, Y., Herndon, J. M., Sojka, D. K., Kim, K. W., Knolhoff, B. L., Zuo, C., . . . DeNardo, D. G. (2017). Tissue-Resident Macrophages in Pancreatic Ductal Adenocarcinoma Originate from Embryonic Hematopoiesis and Promote Tumor Progression. *Immunity, 47*(3), 597. doi:10.1016/j.immuni.2017.08.018

Zhu, Y., Knolhoff, B. L., Meyer, M. A., Nywening, T. M., West, B. L., Luo, J., . . . DeNardo, D. G. (2014). CSF1/CSF1R Blockade Reprograms Tumor-Infiltrating Macrophages and

Improves Response to T-cell Checkpoint Immunotherapy in Pancreatic Cancer Models. *Cancer Res*. doi:0008-5472.CAN-13-3723 [pii]
10.1158/0008-5472.CAN-13-3723
Zhu, Y., Knolhoff, B. L., Meyer, M. A., Nywening, T. M., West, B. L., Luo, J., . . . DeNardo, D. G. (2014). CSF1/CSF1R Blockade Reprograms Tumor-Infiltrating Macrophages and Improves Response to T-cell Checkpoint Immunotherapy in Pancreatic Cancer Models. *Cancer Research, 74*(18), 5057-5069. doi:10.1158/0008-5472.Can-13-3723